

**Faculty of Physics and Astronomy**  
**University of Heidelberg**

Diploma thesis  
in Physics

submitted by  
**Jens Philipp Ronzheimer**

born in Aurich

2008



# **Interactions of Dark Solitons in cigar shaped Bose-Einstein Condensates**

This diploma thesis has been carried out by Jens Philipp Ronzheimer at  
the  
Kirchhoff-Institut für Physik  
under the supervision of  
Prof. Markus K. Oberthaler



In dieser Arbeit wird die Wechselwirkung von dunklen Solitonen, die in zigarrenförmigen Bose-Einstein Kondensaten oszillieren, experimentell und theoretisch untersucht. Eine gerade Anzahl von Solitonen wird erzeugt indem zwei in einem Doppelmuldenpotential voneinander getrennte Kondensate in einer harmonischen Falle zur Kollision gebracht werden. Die Bewegung der Solitonen wird über mehrere ihrer Schwingungsperioden beobachtet und ihre Stabilität nach mehrfachen Kollisionen miteinander gezeigt. Die Oszillationsfrequenzen der Solitonen werden bestimmt. Sie sind deutlich höher als die numerisch bestimmten Oszillationsfrequenzen von einzelnen Solitonen in Kondensaten mit gleichen Eigenschaften. Zur Interpretation dieser Abweichungen wird die Wechselwirkung von Solitonen für den exakten Fall homogener eindimensionaler Systeme untersucht und ein effektives Potential zur Beschreibung der Wechselwirkung eingeführt. Dieses Potential wird verallgemeinert um die Dynamik zweier oszillierender Solitonen in zigarrenförmigen Kondensaten zu beschreiben und seine Anwendbarkeit wird im Vergleich mit numerischen Simulationen bestätigt. Unter Anwendung dieses Wechselwirkungspotentials kann gezeigt werden, dass die Abweichungen der Oszillationsfrequenzen zweier Solitonen tatsächlich durch ihre Wechselwirkung hervorgerufen werden. Die Methode zur Erzeugung von Solitonen wird erweitert um die Erzeugung einer ungeraden Zahl von Solitonen zu ermöglichen und in einem ersten Experiment erfolgreich genutzt. Das effektive Wechselwirkungspotential wird weiter verallgemeinert und seine Anwendbarkeit auf die Wechselwirkung von mehr als zwei Solitonen mit verschiedenen Geschwindigkeiten wird in numerischen Rechnungen bestätigt. Dieses kann in der Zukunft genutzt werden, um die Wechselwirkung von Solitonen in solch allgemeineren Situationen durch Messung ihrer Oszillationsfrequenzen zu identifizieren.

This thesis investigates experimentally as well as theoretically the interactions between dark solitons oscillating in cigar shaped Bose-Einstein condensates. Even numbers of dark solitons are created experimentally in the collisions of two condensates released from a double well potential into a harmonic trap. Their motion in the trap is recorded for several oscillation periods and they are shown to be stable while undergoing multiple collisions with each other. The oscillation frequencies of two dark solitons in the trapped condensates are determined and are significantly higher than the numerically determined oscillation frequencies of single solitons under the same conditions. To interpret these frequency deviations, the interactions of dark solitons are investigated for the exact case of homogeneous one-dimensional systems and an effective potential describing their interactions is introduced. This potential is generalized to describe the dynamics of two dark solitons oscillating in cigar shaped condensates and its validity is shown by comparison to numerical simulations. Using this potential, the observed frequency deviations of the two oscillating solitons can be attributed explicitly to their interaction. Furthermore, the soliton generation method is extended to allow the creation of odd numbers of solitons which is realized in a first experiment. The effective interaction potential is further generalized and numerically corroborated to allow for the treatment of more than two solitons with different velocities and can in the future be used to identify interaction effects on their oscillation frequencies in these more general cases.



# Contents

<b>1</b>	<b>Introduction</b>	<b>1</b>
<b>2</b>	<b>Dark Solitons - Dynamics and Interactions</b>	<b>5</b>
2.1	Solitons . . . . .	5
2.1.1	A Definition . . . . .	5
2.1.2	Bright and Dark Solitons . . . . .	6
2.2	Dark Solitons of the One-Dimensional Nonlinear Schrödinger Equation . . . . .	7
2.2.1	Single Dark Soliton Solutions . . . . .	7
2.2.2	Multiple Dark Soliton Solutions . . . . .	9
2.3	Interactions Between Dark Solitons . . . . .	10
2.3.1	Collisions of Dark Solitons . . . . .	10
2.3.2	Reflection or Transmission? . . . . .	12
2.3.3	Effective Interaction Potential for Dark Solitons . . . . .	17
2.3.4	Generalization to Asymmetric Collisions of Multiple Solitons . . . . .	20
2.3.5	Advantages of an Effective Potential Approach . . . . .	22
<b>3</b>	<b>Dark Solitons in Bose-Einstein Condensates</b>	<b>25</b>
3.1	Bose-Einstein Condensates as Nonlinear Systems . . . . .	25
3.1.1	The Gross-Pitaevskii Equation . . . . .	25
3.1.2	The One-Dimensional Gross-Pitaevskii Equation . . . . .	27
3.1.3	Effectively One-Dimensional Gross-Pitaevskii Equations . . . . .	29
3.2	Dark Solitons in Quasi One-Dimensional Bose-Einstein Condensates . . . . .	30
3.2.1	Soliton Like Excitations . . . . .	30
3.2.2	Stability of Dark Solitons . . . . .	33
3.3	Dynamics of Dark Solitons in Harmonically Confined Condensates . . . . .	35
3.3.1	Oscillating Dark Solitons in the asymptotic one-dimensional case . . . . .	35
3.3.2	Deviations of the Oscillation Frequency from the Asymptotic Prediction . . . . .	37
3.3.3	Multiple Oscillating Solitons . . . . .	39
<b>4</b>	<b>Creation and Observation of Oscillating Dark Solitons</b>	<b>47</b>
4.1	Creation of Dark Solitons in a Bose-Einstein Condensate . . . . .	47
4.1.1	Dark Soliton Production through Matter Wave Interference . . . . .	47
4.1.2	Experimental Realization . . . . .	50
4.1.3	Soliton Creation with Initial Phase Difference . . . . .	54
4.2	Observation of Oscillating Solitons . . . . .	57
<b>5</b>	<b>Oscillation Frequencies and Interaction</b>	<b>63</b>

*Contents*

5.1	Oscillation Frequencies . . . . .	63
5.2	Effects on the Oscillation Frequencies . . . . .	65
<b>6</b>	<b>Conclusion and Outlook</b>	<b>69</b>
<b>A</b>	<b>Published Paper: Experimental Observation of Oscillating and Interacting Matter Wave Dark Solitons</b>	<b>71</b>
	<b>Bibliography</b>	<b>77</b>

# 1 Introduction

The dynamics of nonlinear systems exhibit characteristic features which have been, in different forms, the subject of research for more than 150 years. The existence of solitons is one of these features. Solitons were first observed in the year 1834 by John Scott Russel at the Union Canal in Scotland as travelling water waves. He wrote about them [1]:

*"I was observing the motion of a boat which was rapidly drawn along a narrow channel by a pair of horses, when the boat suddenly stopped - not so the mass of water in the channel which it had put in motion; it accumulated round the prow of the vessel in a state of violent agitation, then suddenly leaving it behind, rolled forward with great velocity, assuming the form of a large solitary elevation, a rounded, smooth and well-defined heap of water, which continued its course along the channel apparently without change of form or diminution of speed. I followed it on horseback, and overtook it still rolling on at a rate of some eight or nine miles an hour, preserving its original figure some thirty feet long and a foot to a foot and a half in height. Its height gradually diminished, and after a chase of one or two miles I lost it in the windings of the channel. Such, in the month of August 1834, was my first chance interview with that singular and beautiful phenomenon which I have called the Wave of Translation"*

These “waves of translation”, or bright solitons, show some characteristics quite distinct from ordinary waves. They travel for long distances at constant velocities without a deformation of their shape. Their velocity is directly related to the height of the wave and instead of merging upon collision with each other, they pass through each other, only experiencing a shift of their position.

The solitons were later explained as solutions to the Korteweg-de Vries equation [2], which describes the behavior of waves in shallow water. Solitons were found to exist as solutions to many other nonlinear differential equations and in addition to the bright solitons, which constitute a local elevation of a constant background, dark solitons were found to exist. These are characterized by a localized dip travelling through a constant background. Aside from this obvious difference between the two kinds of solitons, they share the general characteristics mentioned above. Physical systems in which the dark solitons were experimentally observed include the surfaces of liquids [3], discrete mechanical systems [4] and thin magnetic films [5].

Dark solitons were also intensively investigated as solutions to the one-dimensional nonlinear Schrödinger equation [6, 7] which were experimentally created and investigated in the context of nonlinear fiber optics [8, 9, 10]. A special attention in the theoretical examination of the dark solitons was payed to the nature of their interaction with each other, which was found to be of a repulsive nature [7, 11, 12]. Evidence for this interaction has been experimentally observed for dark optical solitons [13, 14].

## 1 Introduction

With the first creation of Bose-Einstein condensates [15, 16, 17], a new system for the investigation of nonlinear dynamics became available. Dark Soliton have been created and observed in Bose-Einstein condensates with three dimensional geometries [18, 19, 20, 21], but they were found to be unstable in these systems and to decay rapidly [22].

This decay is inhibited for Bose-Einstein condensates with more one-dimensional geometries, where the condensate is strongly confined in two directions. In the completely one-dimensional case, the nonlinear equation governing the dynamics of the condensate is completely equivalent to the one-dimensional nonlinear Schrödinger equation describing the behavior of optical dark solitons.

Dark solitons have recently been created in so called cigar shaped geometries, which are in the crossover regime between one and three dimensions [23]. In these geometries, the solitons are stable for hundreds of milliseconds which allows for a detailed investigation of their dynamics. The dark solitons in these geometries oscillate along the axis of rotational symmetry of the cigar shaped condensate due to the harmonic confinement along this axis that traps the condensates[24]. This was observed experimentally in [23] for a single oscillation period. Also very recently, the collision of two dark solitons was observed in the same experiment, but no conclusions about the interaction of these solitons could be reached [25] because the effects of interaction in this case of a single collision were too small to be observed.

In our experiments, two dark solitons are created in the collision of two Bose-Einstein condensates released from a double well potential into a harmonic trap. Their subsequent oscillation in the cigar shaped condensate is observed for several oscillation periods.

During this oscillation, the two solitons collide with each other multiple times, which increases the total effect of the short ranged interaction between the solitons on their dynamics and facilitates the quantitative investigation of their interaction.

The influence of this interaction on the oscillation frequency of the dark solitons is identified using an effective interaction potential. For the first time, the theoretical predictions about the interaction between dark solitons can be quantitatively tested with experimental data.

### **Outline of this thesis**

Chapter 2 investigates the dynamics of dark solitons in the framework of the one-dimensional nonlinear Schrödinger equation. A special focus is put on the interaction between dark solitons and an effective interaction potential is introduced.

In chapter 3, the concept of dark solitons is extended to cigar shaped Bose-Einstein condensates. The soliton dynamics is shown to be oscillatory and the oscillation frequencies are investigated numerically and using a generalization of the effective interaction potential. The effects of the interaction are found to increase the oscillation frequencies of multiple oscillating solitons with respect to those of single solitons, which provides an approach for the experimental investigation of this interaction.

In chapter 4, a method to create multiple oscillating solitons in a  $^{87}\text{Rb}$  Bose-Einstein

condensate is discussed and the experimental results on the creation and subsequent oscillation of dark solitons are presented.

Chapter 5 discusses the observed soliton oscillation frequencies. In comparison to the theoretical predictions, the role and magnitude of the repulsive interaction between dark solitons is unambiguously identified.

Chapter 6 provides a short summary of the results of this thesis and an outlook on further experiments.



# 2 Dark Solitons - Dynamics and Interactions

Solitons, first observed by John Scott Russel as travelling, shape preserving water waves in a canal, were found to exist as stable solutions of various types of nonlinear partial differential equations and exhibit a set of common characteristics.

Solitons are localized wavepackets in nonlinear dispersive media. They can be either bright, constituting a localized elevation, or dark, as a localized dip, on a homogeneous background. They travel without deformation and at a constant velocity that is directly related to their height, in the case of bright solitons, or depth, in the case of dark solitons. When two or more solitons collide with each other, instead of merging to form larger wave packets, they leave the collisions without perturbation of their characteristic features, which are their shape and velocity. The only form of interaction with each other is a phase shift acquired during the collision.

In this chapter, the general characteristics of dark soliton solutions to the homogeneous one-dimensional nonlinear Schrödinger equation (NLS) are investigated, with a special attention being paid to their behavior upon collision with each other and the implications of their interactions.

## 2.1 Solitons

### 2.1.1 A Definition

Following the definition of Scott [26], a soliton is a solution of an integrable partial differential equation which satisfies the following criteria:

1. The solution is a travelling wave that travels with a constant velocity  $v$ , *i.e.* the solution  $\Phi(\xi)$  depends on the spatial variable  $z$  and the time variable  $t$ <sup>1</sup> only via the relation  $\xi = z - vt$ .
2. The solution is a solitary wave, *i.e.* it exhibits a transition between two asymptotic constant values of  $\Phi(\xi)$  for  $\xi \rightarrow \pm\infty$  that is localized in  $\xi$ .
3. The solution asymptotically preserves its shape and velocity upon collision with other solitary waves, *i.e.* a solution which, at  $t \rightarrow -\infty$ , is composed of a sum of

---

<sup>1</sup>Note that in some cases the time and space variables may be interchanged, e.g. for optical solitons in waveguides [27].

## 2 Dark Solitons - Dynamics and Interactions

solitary waves  $\sum_j \Phi_j(\xi_j)$  with  $\xi_j = (z - v_j t)$  will, after a collision between the separate solitary waves, for  $t \rightarrow +\infty$  be composed of the same solitary waves  $\sum_j \Phi_j(\tilde{\xi}'_j)$ , subjected only to a phase shift  $\tilde{\xi}'_j = (z - v_j t + \delta_j)$ .

This definition of a soliton is a rather mathematical one, being strictly applicable only to integrable systems. The properties of these types of soliton solutions will be discussed in this chapter but in an experimental realization the condition of integrability of the governing nonlinear equation will not be fulfilled. A more practical definition for “soliton-like” wave packets in the realistic case of near- or non-integrable systems will be given in chapter 3.2.1 and it will be investigated, how closely the characteristics of ideal solitons are reflected in more complex situations.

Criterion three, which Scott considers a “working definition”, entails some of the fascinating features solitons exhibit, namely their stability in collisions with each other and their interaction with each other, affecting them only via a phase shift.

In the way it is stated in [26], criterion three seems to presuppose that the solitons are identified by their velocities and thus a soliton leaving a collision with a certain velocity is identified with the soliton of that velocity entering the collision as being the same soliton preserving its shape. In section 2.3.1 a different viewpoint on these collisions will be taken to make way for a more particle like interpretation of soliton collisions in cases where it is physically counterintuitive to regard the solitons as being transmitted through each other. In this picture it will be possible for two solitons to exchange velocity during a collision and thus a single soliton will indeed change its shape and velocity. Nevertheless, criterion three will still hold since the final solution still contains the same number of solitons with the same velocities; it is simply the question of identification that will be treated differently.

### 2.1.2 Bright and Dark Solitons

There are numerous types of nonlinear partial differential equations that support soliton solutions. First discovered as solutions to the Korteweg-de Vries equation, they were later also found for the Sine-Gordon equation, nonlinear lattice equations, the Born-Infeld equation and many others [26], including the nonlinear Schrödinger equation which will be investigated within this thesis.

To illustrate the mechanism responsible for the stability of soliton solutions, it is instructive to look at the nonlinear Schrödinger equation as an example. The homogeneous one-dimensional nonlinear Schrödinger equation has the form:

$$i \frac{\partial}{\partial t} u(z, t) = \left[ -\frac{1}{2} \frac{\partial^2}{\partial z^2} \pm |u(z, t)|^2 \right] u(z, t) \quad (2.1)$$

The first term of the right hand side is the normal dispersion term for massive particles which, in the absence of the second, nonlinear term on the right hand side, leads to a broadening of a localized wave packet. This effect results from the fact that every wave packet solution can be decomposed into a series of different frequency Fourier components. In a system with normal dispersion and no counteracting effect, these components

## 2.2 Dark Solitons of the One-Dimensional Nonlinear Schrödinger Equation

propagate with different phase velocities and any localized structure smears out over time. Figure 2.1(a) illustrates this behavior.

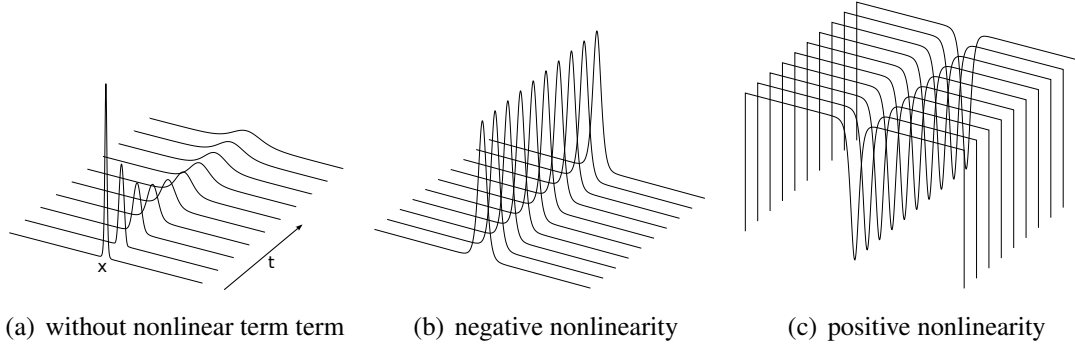


Figure 2.1: Numerical time evolution of wave packets using the nonlinear Schrödinger equation (Eq. 2.1) with different signs of the nonlinearity. In the presence of nonlinearity, solitonic, *i.e.* non-spreading solutions, are observed.

For a soliton solution of the nonlinear Schrödinger equation this dispersion effect is cancelled out by the effect of the nonlinear term. Depending on the sign of the nonlinear term, two different classes of solutions are allowed.

In the so called focusing case of a negative sign, the nonlinear term leads to a reduction of energy at points with high density and a bright soliton solution exists. This bright soliton corresponds to a localized peak of  $|u(z,t)|$  with  $|u(z,t)| \rightarrow \text{const.}$  for  $z \rightarrow \pm\infty$ . Figure 2.1(b) shows a stationary bright soliton solution and its time evolution. The shape of the solution remains completely unchanged over time since the dispersion is completely cancelled out by the nonlinearity.

In the defocusing case of a positive sign of the nonlinearity, the wavefunction experiences an effective repulsion, since the nonlinear term leads to an increase of energy at points of high density. In this case, a dark soliton solution exists, corresponding to a local minimum of  $|u(z,t)|$  with nonzero asymptotic values of  $|u(z,t)| \rightarrow \text{const.}$  for  $z \rightarrow \pm\infty$ . This case and its time evolution are shown in Figure 2.1(c) for a stationary solution. Again, the shape of the solution is stable over time.

## 2.2 Dark Solitons of the One-Dimensional Nonlinear Schrödinger Equation

### 2.2.1 Single Dark Soliton Solutions

Dark solitons exist as analytic solutions of the homogeneous one-dimensional nonlinear Schrödinger equation with a positive nonlinear term:

$$i \frac{\partial}{\partial t} u(z,t) = \left[ -\frac{1}{2} \frac{\partial^2}{\partial z^2} + |u(z,t)|^2 \right] u(z,t) \quad (2.2)$$

## 2 Dark Solitons - Dynamics and Interactions

Note that this equation is given in dimensionless units, and will be used in this form throughout this chapter. To apply it to different physical situations, it can be scaled by a transformation of the variables and the normalization of the wave function  $u(z, t)$ .

The first exact soliton solution to this equation was given by Tsuzuki [6] and later by Zakharov and Shabat [7] for the more general case of multiple solitons and is here given in the form of [27] for a single dark soliton in a homogeneous background:

$$u(z, t) = e^{it} (B \tanh[B(z - vt - z_0)] + iv). \quad (2.3)$$

This complex valued solution exhibits a local minimum of the modulus of the wavefunction  $|u(z, t)|$  which is accompanied by a phase change of the wavefunction. The local minimum is considered the soliton's position, which is at  $t = 0$  given by  $z_0$ . The asymptotic background value of  $|u(z, t)|$  is normalized to one and the global phase factor  $e^{it}$  describes the time evolution of this background but, without a fixed scale for the phase, bears no physical significance. The parameter  $B = \sqrt{1 - v^2}$  determines the darkness of

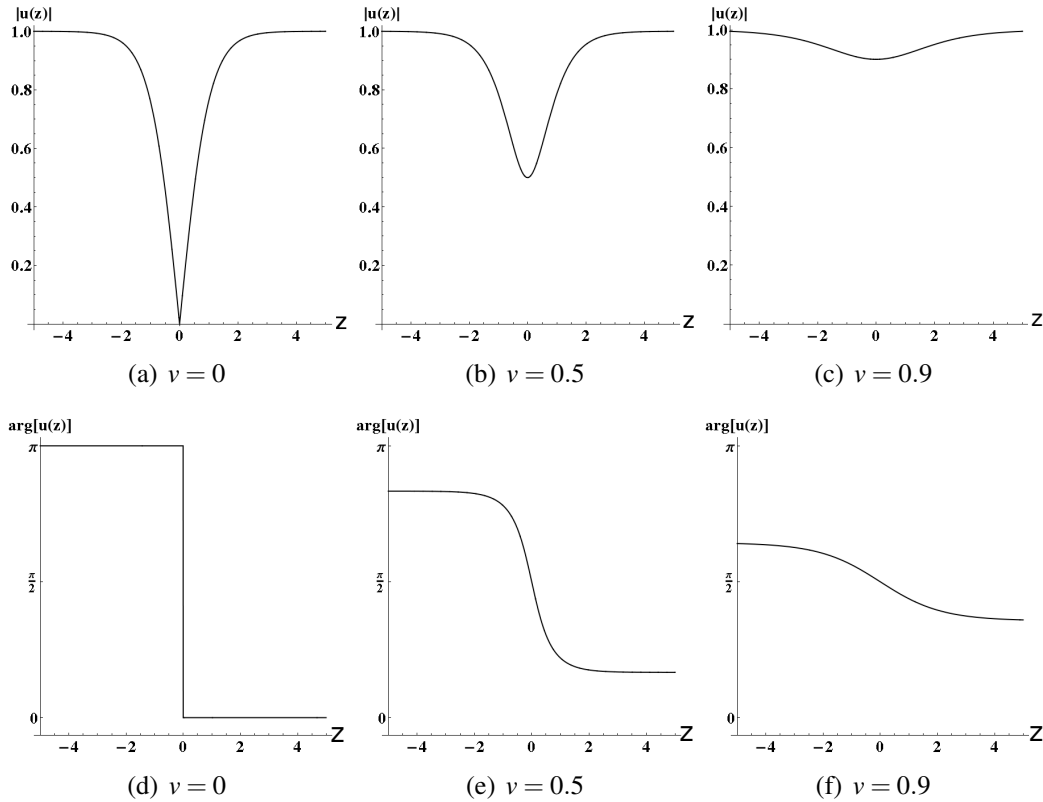


Figure 2.2: (a)-(c): The modulus of single soliton solutions (eq.2.3) for different soliton velocities  $v$ . The dip in the homogeneous background becomes shallower the faster the soliton moves. (d)-(f): The phase of the soliton wave functions for the same velocities. The phase jump at the position of the soliton becomes less sharp and smaller in magnitude for faster solitons.

the soliton. The value of  $|u(z, t)|$  at the local minimum is given by  $\sqrt{1 - B^2}$ . This parameter depends on the velocity  $v \in [0, 1]$  with which the local minimum moves. For the

## 2.2 Dark Solitons of the One-Dimensional Nonlinear Schrödinger Equation

limiting case of a stationary soliton ( $v = 0$ ) the modulus of  $|u(z, t)|$  at the minimum goes completely down to zero and  $B = 1$ . These solitons are referred to as black solitons, while solitons with velocities  $v > 0$  are commonly referred to as gray solitons.

The faster the soliton moves, the shallower the dip in the modulus of the wave function becomes, as exemplified in figure 2.2(a)-(c), which shows the modulus of the soliton wave function for different values of  $v$ . As the soliton's velocity approaches one,  $B$  goes to zero and the solitons vanishes, becoming identical to the homogeneous background.

The phase change of the wave function also depends on the soliton velocity. For a stationary soliton the phase has a sharp jump of  $\pi$  at the position of the minimum of the modulus of the wave function. For moving solitons this phase change gets smaller in magnitude and extends over a larger distance centered around the minimum as shown in figure 2.2(d)-(f).

This soliton solution satisfies the criteria one and two of the definition (section 2.1.1). The solution is a travelling wave solution with a constant velocity, since, aside from a global phase factor, it depends on the time and space variables only via the relation  $(z - vt - z_0)$ . As shown in figures 2.2(a)-(f) it is also a localized solution, since the transition between two asymptotic values of the wave function takes place within a small region.

To answer the question whether criterion three, regarding the interactions of solitons, is satisfied one has to turn to solutions containing more than one soliton.

### 2.2.2 Multiple Dark Soliton Solutions

The nonlinear Schrödinger equation also supports solutions of multiple dark solitons propagating with different velocities. The first solutions of this kind were obtained by Zakharov and Shabat by means of the inverse scattering transform [7]. The dynamics of multi soliton wavefunctions was later investigated by Blow and Doran [11] who obtained an analytic solution for two dark solitons travelling with different velocities that is given by:

$$u(z, t) = \left[ 1 - \frac{2i}{\Gamma} \left[ \frac{2}{B_1 + B_2} \left( \frac{1}{iB_1 + v_1} + \frac{1}{iB_2 + v_2} \right) + (iB_1 - v_1) \left( \frac{1}{B_1} + \frac{e^{2zB_1}}{\mu_1} \right) + (iB_2 - v_2) \left( \frac{1}{B_2} + \frac{e^{2zB_2}}{\mu_2} \right) \right] \right] e^{-2it} \quad (2.4)$$

with :

$$\Gamma = (v_1 - iB_1)(v_2 - iB_2) \left( \frac{e^{2zB_1}}{\mu_1} + \frac{1}{B_1} \right) \left( \frac{e^{2zB_2}}{\mu_2} + \frac{1}{B_2} \right) - \frac{1}{(B_1 + B_2)^2} \left( \frac{1}{v_1 + iB_1} + \frac{1}{v_2 + iB_2} \right)^2,$$

$$\mu_j = e^{2B_j(x_j^0 + v_j t)}$$

$$B_j = \sqrt{1 - v_j^2}, \quad j = 1, 2$$

## 2 Dark Solitons - Dynamics and Interactions

where  $v_1$  and  $v_2$  denote the velocities of the solitons, subject to the conditions  $-1 < v_{1,2} < 1$  and  $v_1 \neq v_2$ .  $B_1$  and  $B_2$  are measures for the darkness of the solitons analogous to  $B$  of equation 2.3. Again, for a stationary soliton the solution goes completely to zero at the local minimum of the dip that constitutes the soliton. For faster solitons the dip becomes shallower and vanishes for solitons approaching  $v_j \rightarrow \pm 1$ . The  $x_j^0$  are constants to adjust the initial positions of the two solitons.

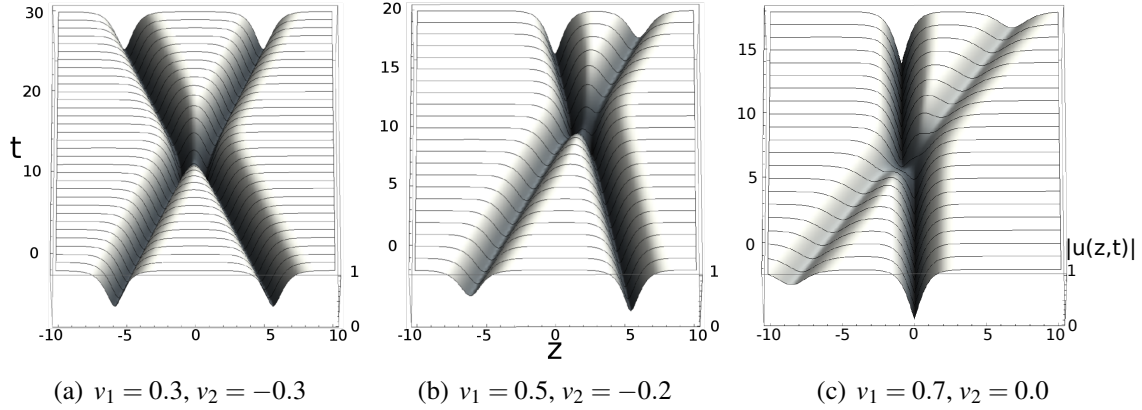


Figure 2.3: Time Evolution of the modulus of the two soliton solution (Eq.2.4) for different initial soliton velocities  $v_1, v_2$ .

This equation, its time evolution being visualized in Figure 2.3 for different initial soliton velocities, fulfills all three criteria demanded in the definition of the term soliton (see section 2.1.1). For  $t \rightarrow \pm\infty$  the solitons are well localized and travel with constant velocities. The solution for  $t \rightarrow +\infty$  consists of two solitons travelling with the same velocities as the solution for  $t \rightarrow -\infty$  and the shapes of the solitons are preserved. The only effect of the shown collision of the two solitons, as demanded in the third criterion, is a phase shift between the incoming and the outgoing solitons. This phase shift is visible as a shift between the trajectories of the solitons before and after the collision and is investigated in more detail in the next section.

## 2.3 Interactions Between Dark Solitons

### 2.3.1 Collisions of Dark Solitons

The interaction between dark solitons can be characterized by the phase shifts of their wavefunctions acquired upon collision, manifesting themselves in the displacement of the soliton trajectories. Following Zakharov and Shabat [28, 7], for  $t \rightarrow \pm\infty$  the two soliton solution can be decomposed into individual solitons:

$$\begin{aligned} u(z,t) &\rightarrow u_0(z - v_1 t, z_1^+) \text{ and } u_0(z - v_2 t, z_2^+), t \rightarrow +\infty \\ u(z,t) &\rightarrow u_0(z - v_1 t, z_1^-) \text{ and } u_0(z - v_2 t, z_2^-), t \rightarrow -\infty \end{aligned} \quad (2.5)$$

where

$$u_0(z - v_i t, z_i^\pm) = e^{it} (B_i \tanh [B_i(z - v_i t - z_i^\pm)] + i v_i). \quad (2.6)$$

The two separate soliton solutions are valid in regions far apart from each other and the wavefunction in the region between them is supposed to take the homogeneous background value of  $|u(z, t)| = 1$ .

The scattering of the two solitons leads to a phase shift of their center:

$$\delta z_1 = z_1^+ - z_1^-, \quad \delta z_2 = z_2^+ - z_2^- \quad (2.7)$$

This shift has been calculated in [7], assuming  $v_1 > v_2$ , to be

$$\begin{aligned} \delta z_1 &= \frac{1}{2B_1} \ln \frac{(v_1 - v_2)^2 + (B_1 + B_2)^2}{(v_1 - v_2)^2 + (B_1 - B_2)^2} \\ \delta z_2 &= -\frac{1}{2B_2} \ln \frac{(v_1 - v_2)^2 + (B_1 + B_2)^2}{(v_1 - v_2)^2 + (B_1 - B_2)^2}. \end{aligned} \quad (2.8)$$

In the case of  $v_1 > 0$  and  $v_2 < 0$ , in which the two solitons move in opposite directions, the signs of the phase shifts imply that both shifts act in the direction of motion of the individual solitons.

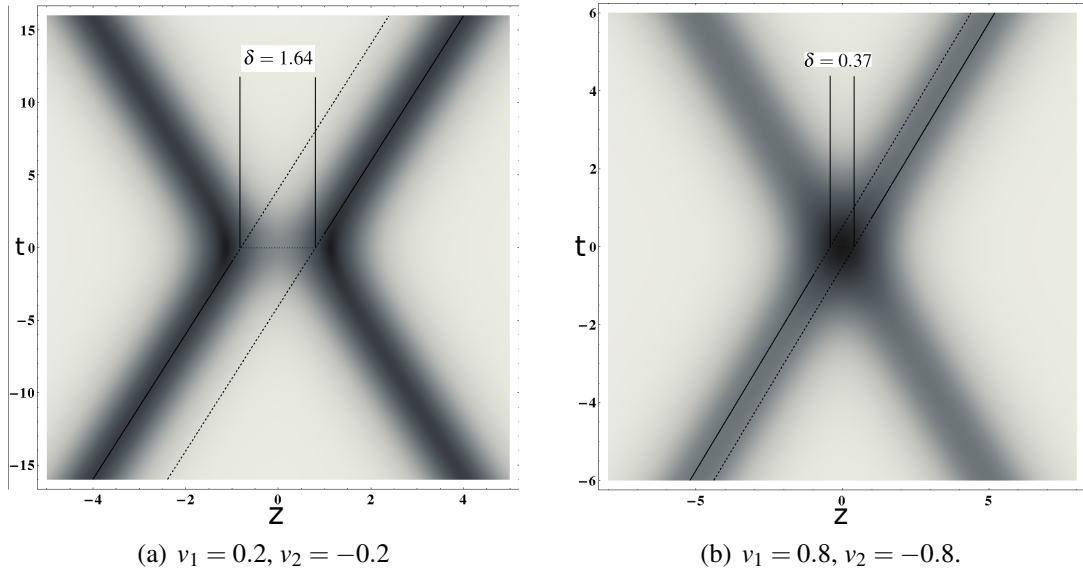


Figure 2.4: Symmetric two soliton collisions as given by eq. 2.4 for different initial soliton velocities  $v_1, v_2$ . The soliton trajectories before and after the collisions (full lines) and the acquired phase shifts are indicated.

Figure 2.4 shows these phase shifts of the trajectories of the soliton with  $v > 0$  for two different velocities. It can be clearly observed, that the soliton travels with the same constant velocity before and after the collision but the trajectories are displaced with regard to each other by the amount given by equation 2.8.

Figure 2.5 shows the phase shifts that a soliton moving with velocity  $v_1$  experiences in a collision with a second soliton for cases of particular interest in the scope of this thesis.

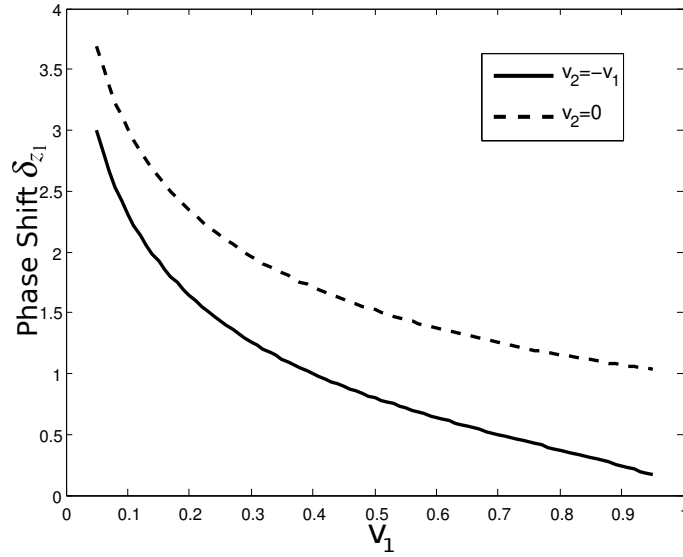


Figure 2.5: The phase shifts a soliton moving with velocity  $v_1$  experiences upon collision with a soliton moving with  $v_2 = -v_1$  (full line) and with a stationary soliton with  $v_2 = 0$  (dashed line)

The full line shows the phase shift for the case where the second soliton moves with the same velocity in the opposite direction ( $v_2 = -v_1$ ) and the dashed line for the case of a stationary second soliton ( $v_2 = 0$ ). In both cases, the phase shift increases with decreasing soliton velocity. The phase shifts for the collision with a stationary soliton are higher than the ones for the collision with the moving soliton.

In general, the phase shift, that determines the effect of the interaction on the trajectories of two colliding solitons, depends on their total velocity, having a much larger effect on slowly moving solitons than on very fast ones.

### 2.3.2 Reflection or Transmission?

So far the investigation of the nature of collisions between dark solitons has been conducted in the spirit of criterion three of the definition of a soliton (section 2.1.1), identifying the separate solitons by their velocities. This point of view implies that in every collision the solitons are transmitted through each other and afterwards continue to move in the same direction as they did while approaching each other. From a formal point of view, this assumption can always be justified by the fact, that the multi-soliton solutions, at times long before and after the collision, can be decomposed into the same single soliton wave functions being only affected through a phase shift. Nevertheless, when looking at the collisions directly, this picture is counterintuitive.

Figure 2.6 shows collisions in two different velocity regimes. In Fig 2.6(a) both solitons move fast. As they collide, the modulus of the wavefunction between the solitons decreases below the level it takes at the center of each individual soliton before and after the collision. This collision indeed looks like the solitons are transmitted through each

### 2.3 Interactions Between Dark Solitons

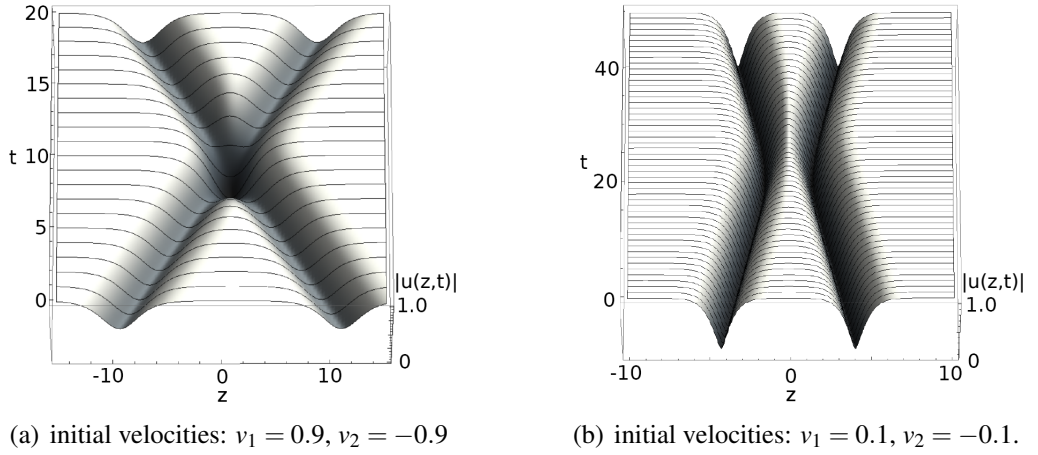


Figure 2.6: The collision dynamics of dark solitons (eq. 2.4) for slow and fast solitons show a qualitatively different behavior at the point of closest proximity of the two solitons.

other, for a short time being in the same place forming a deeper dip. On the other hand, Figure 2.6(b) shows a collision for two slow solitons. Here, the modulus of the wavefunction between the two solitons hardly changes from the asymptotic background level and, instead of forming a dip that is deeper than each individual soliton, the solitons seem to simply repel each other and change their direction of motion without being transmitted through each other.

To investigate these different regimes more quantitatively, a simpler form of equation 2.4 is employed, obtained by Akhmediev and Ankiewicz [12] for the case of two solitons moving with equal velocities  $v$  in opposite directions that is given by:

$$u(z,t) = \frac{(1 - 2v^2) \cosh[2tvB] - \sqrt{v^2} \cosh[2Bz] + 2ivB \sinh[2tvB]}{\cosh[2tvB] + \sqrt{v^2} \cosh[2Bz]} e^{it} \quad (2.9)$$

This solution has the advantage of being symmetric in time and the point of closest proximity of the two dark solitons is always at  $t = 0$ .

Figure 2.7 shows the behavior of this two soliton wavefunction at  $t = 0$  for different initial velocities. Three cases can be distinguished. For  $v < 0.5$ , the modulus of the solution at  $z = 0$ , which is the center between the two solitons at the point of closest approach during their time evolution, never goes down to zero. The solitons approach each other up to a certain distance but are always characterized by two separate minima. At  $t = 0$  the wave function at these minima takes the value  $u(z,t) = 0$ . For  $v = 0.5$ , the solution at  $z = 0$  goes exactly down to zero and the two solitons form, at the point of collision, a single dip. For  $v > 0.5$ , the solitons still form a single dip at  $t = 0$  but the modulus of the solution does not go completely down to zero at the minimum.

The behavior of the modulus of equation 2.9 at  $t = 0$  for the complete range of allowed velocities is shown in figure 2.8. It can be seen that for all velocities  $v < 0.5$  the solution entails two distinguishable minima with  $u = 0$  while the modulus of  $u(z = 0, t = 0)$  slowly

## 2 Dark Solitons - Dynamics and Interactions

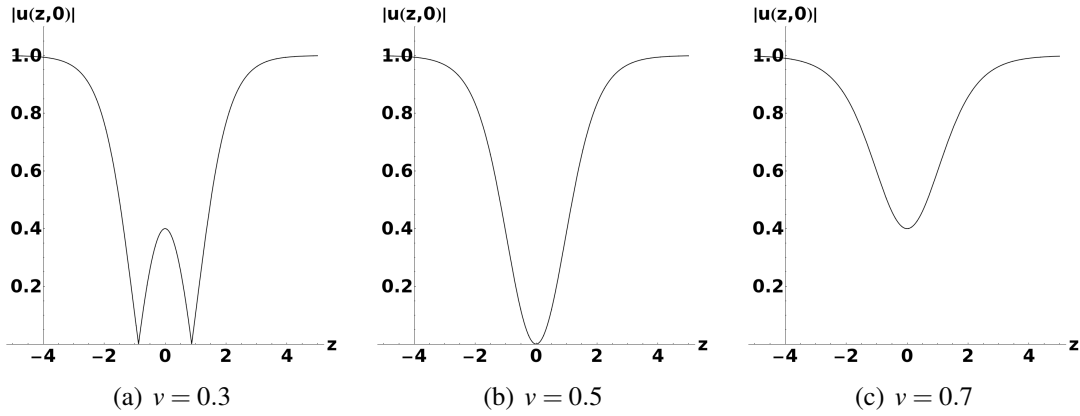


Figure 2.7: The modulus of the symmetric soliton solution (eq.2.9) at  $t = 0$ , the point of closest proximity, for different soliton velocities  $v$

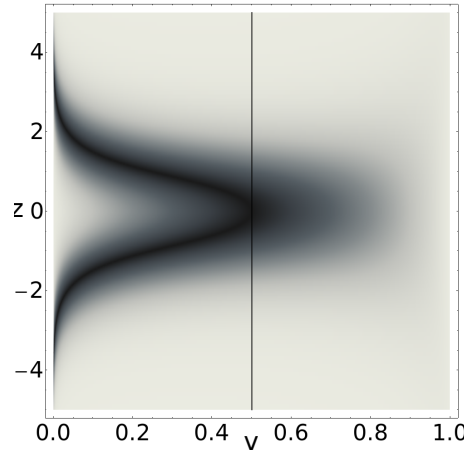


Figure 2.8: Dependence of the modulus of the symmetric two soliton solution (Eq.2.9) at  $t = 0$  on the velocity  $v$  of the solitons. The line at  $v = 0.5$  indicates the transition where the two separate minima merge into a single one

decreases with increasing  $v$ . At  $v = 0.5$ , the two separate minima merge into a single one at  $z = 0$  and for larger velocities, the solution maintains a single minimum. From there on, the modulus of the solution at  $z = 0$  increases with increasing velocities and reaches  $|u(z = 0, t = 0)| = 1$  at  $v = 1$ , for which the two solitons completely vanish, since  $B = \sqrt{1 - v^2} \rightarrow 0$  for  $v \rightarrow 1$ .

Regarding the question whether the two solitons pass through each other or are reflected by each other upon collision, the different behavior for  $v < 0.5$  and  $v > 0.5$  can serve as a distinction between these two cases. For  $v < 0.5$  it seems physically more intuitive to regard the behavior of colliding solitons as a repulsion of slowly moving particles (as already stated in [12]). During their complete time evolution, they can be characterized by two separate minima which, as they approach each other, become deeper, suggesting a slowdown of the solitons. When the modulus of the solution at the two minima reaches

the value 0, which happens at the point of closest proximity, the solitons have completely stopped and change their direction of motion.

For the case of  $v > 0.5$ , it is not immediately clear, which point of view is the physically more convincing. This point marks the border between the two regimes. Since for increasing velocities in the regime  $v < 0.5$  the centers of the two solitons approach each other with closer and closer proximity at  $t = 0$  and merge at  $v = 0.5$ , it seems suggestive to assume, that for velocities larger than  $v = 0.5$  the repulsion between the two solitons is not sufficient to lead to a reflection and the solitons are transmitted through each other. When investigated more closely, it turns out that, in contrast to the repulsive interaction in the case  $v < 0.5$ , the interaction would actually change its sign and become attractive in the case of  $v > 0.5$  if the solitons were considered to be passing through each other.

This can be seen by looking at the phase shifts the solitons acquire during a collision, as given by equation 2.8 for  $v_1 = -v_2 = v$ . The magnitude of the phase shift for the first soliton travelling with velocity  $v_1 > 0$  is in the reflected and transmitted case given by

$$|\delta_{z_1}| = \frac{1}{2B} \ln \left( 1 + \frac{B^2}{v^2} \right) \quad (2.10)$$

but the sign of the phase shift and of the final velocity changes. If the solitons are considered as being transmitted through each other, the single soliton wave function of soliton one before and after the collision will be

$$u_0(z - v_1 t) = e^{it} (B \tanh [B(z - v_1 t)] + iv_1) \rightarrow e^{it} (B \tanh [B(z - v_1 t - \delta_{z_1})] + iv_1) \quad (2.11)$$

If instead the solitons are considered as being reflected by each other and their direction of motion is inverted, the single soliton wave functions before and after the collision are given by

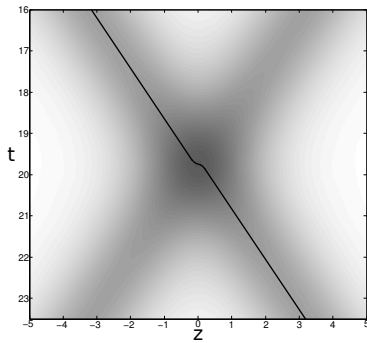
$$u_0(z - v_1 t) = e^{it} (B \tanh [B(z - v_1 t)] + iv_1) \rightarrow e^{it} (B \tanh [B(z + v_1 t + \delta_{z_1})] + iv_1) \quad (2.12)$$

In the first approach, the behavior of the wavefunction before and after the collision indicates that during the collision the soliton has actually advanced faster than it would have, had it been travelling with its constant asymptotic speed, since the shift is in the direction of the solitons movement (see also figure 2.4). The interaction between the solitons in this approach is of an attractive nature. If one were to attribute classical trajectories to the solitons while they are undergoing a collision this would mean that the solitons are accelerated by their interaction up to the point where their trajectories cross each other and afterwards decelerated to their asymptotic constant velocities, travelling in the same directions as before the collision. This is indicated in figure 2.9(a) for one of the solitons.

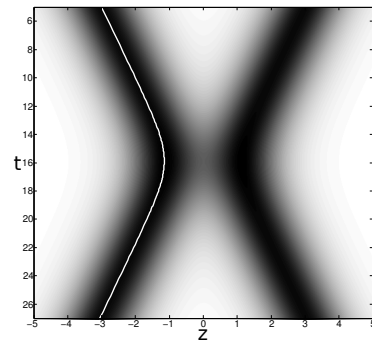
In the second approach, the nature of the interaction is obviously repulsive, since the soliton changes its direction of motion. If one were to attribute classical trajectories in this case, the solitons would first be decelerated until they come to a full stop and then be accelerated again to their asymptotic constant velocities with inverted directions of motion. The full line in figure 2.9(b) shows this trajectory for one of the solitons.

To summarize, there are three different points of view which can be taken regarding the question of whether two solitons pass through each other or are reflected by each other.

## 2 Dark Solitons - Dynamics and Interactions



(a) If the collision is regarded as a transmission, the soliton is first accelerated and then slowed down during the collision



(b) If the collision is regarded as a reflection, the soliton is slowed down first and then accelerated again

Figure 2.9: Exemplary classical trajectories for the dark solitons in collisions considered transmissive (a) or reflective (b)

The first point of view is to always consider the solitons as being transmitted through each other. This has the advantage of a clear criterion of identification, mathematical clarity and a well described interaction via the phase shifts of equation 2.8. The disadvantage is, that the assumption of a transmission seems very arbitrary and counter intuitive for slow solitons which exhibit separate minima throughout the whole collision process.

The second point of view is to consider the solitons as reflected by each other for the case  $|v_{1,2}| < 0.5$  and transmitted through each other for the case  $|v_{1,2}| > 0.5$ . The investigated symmetric two soliton solution suggests this point of view but the interaction between the solitons then has to be described as repulsive in the first and attractive in the second case.

The third point of view is to consider the solitons as always being reflected by each other. This point of view explains the behavior of slow solitons very well. If the collision is regarded as that of two particles with an interaction potential that becomes more and more like that of hard spheres the faster the solitons move, the behavior over the whole range of allowed velocities can qualitatively be explained. Nevertheless, one would expect the central dip to be deeper, considering that in this picture the two solitons are always decelerated to  $v = 0$  at some point during their evolution where their minima should go down to zero.

In the following, the solitons will be regarded as repulsively interacting, being reflected by each other upon collision. This allows for treating the soliton interaction as that of simple repelling particles, albeit with a velocity dependent interaction potential that is investigated in the next section, and satisfies the intuitive picture of repulsion for the case of slow solitons. Since in the situation relevant for the experiment the solitons have velocities smaller than 0.5, this point of view is the most intuitive and turns out to be helpful in the analysis of soliton collisions.

### 2.3.3 Effective Interaction Potential for Dark Solitons

In cases without a homogeneous background, the asymptotic velocities of the solitons are not defined, and the phase shifts that result from collisions between them can not be calculated using the exact equation 2.8. In these cases it is useful to consider the two solitons as repelling particles and model their interaction by an effective potential, that depends on their momentary velocity.

Assuming a particle like nature of the solitons and repulsive interaction between them, equation 2.9 can be used to derive such an effective interaction potential for the collision of two equally dark solitons of the one-dimensional nonlinear Schrödinger equation, as done by Kivshar and Królikowski [29]. Under the assumption that the solitons are always well separated from each other, *i.e.* that their initial velocities are smaller than  $|v| < 0.5$ , they derive an equation of motion for the two minima constituting the solitons and deduce an interaction potential from this equation of motion. This repulsive interaction potential in the symmetric case is given by <sup>2</sup>:

$$V(z, v) = \frac{1}{2} \frac{B^2}{\sinh^2(2zB)}, \quad B = \sqrt{1 - v^2} \quad (2.13)$$

where  $z = z_1$  denotes the position of the local minimum of one of the dark solitons.

The equation of motion for the dark soliton is then given by the Lagrange equation:

$$\frac{d}{dt} \left( \frac{\partial L}{\partial \dot{z}} \right) = \frac{\partial L}{\partial z}, \quad (2.14)$$

$$\text{with: } L = T - V = \frac{\dot{z}^2}{2} - V(z, v) \quad (2.15)$$

$$\Rightarrow \ddot{z} - \frac{d}{dt} \left( \frac{\partial V}{\partial \dot{z}} \right) = -\frac{\partial V}{\partial z}, \quad (2.16)$$

$$\text{with: } \frac{d}{dt} \left( \frac{\partial V}{\partial \dot{z}} \right) = \frac{d}{dt} F = \frac{\partial F}{\partial z} \dot{z} + \frac{\partial F}{\partial \dot{z}} \ddot{z}, \quad F = \frac{\partial V}{\partial \dot{z}} \quad (2.17)$$

$$\Rightarrow \ddot{z} \left( 1 - \frac{\partial F}{\partial \dot{z}} \right) - \frac{\partial F}{\partial z} \dot{z} + \frac{\partial V}{\partial z} = 0 \quad (2.18)$$

Since the collision between the solitons is symmetric, the equation of motion for the soliton at  $z_2 = -z_1$  is simply given by  $\ddot{z}_2 = -\ddot{z}_1$ . This allows for describing the solitons as classical particles moving in a velocity dependent potential. The potential depends on the darkness  $B$  of the solitons, being stronger for darker solitons in accordance with the exact phase shifts given by equation 2.8.

Figure 2.10 shows the repulsive potential during a soliton collision. Note that the velocities indicated on the graph are the initial velocities of the soliton. Since the potential

<sup>2</sup>Note that this potential differs from the one used in [29], where the sinh term in the denominator is replaced by a cosh term. The correct form used here has been determined by Kevrekidis et al. [30] and confirmed by the authors of [29]. The potential used in [29] also gives correct results, since the derivation requires  $|v| < 0.5$  and thus the solitons are always so far apart from each other (see figure 2.10) in their collisions, that only the asymptotic behavior of the potentials is relevant, which does not deviate significantly.

## 2 Dark Solitons - Dynamics and Interactions

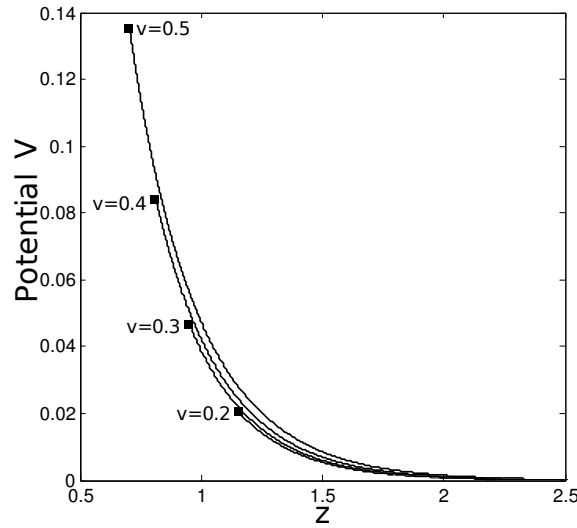


Figure 2.10: The strength of the repulsive potential given by equation 2.13 for different initial velocities  $v$ . The potential is only plotted down to the turning points of the solitons, indicated by the squares.

depends on the darkness  $B$  and thus on the velocity of the soliton, which is slowed down and turns its direction of motion during collision, the spatial behavior that is plotted includes the changing velocity during the collision. The potentials are plotted only down to the turning points indicated by the squares.

The different behavior for different velocities agrees with the picture of solitons always being reflected by each other with a potential that corresponds closer to that of a hard sphere the faster the solitons move. For  $v = 0.2$ , the solitons always move in a potential with a rather gentle slope. For  $v = 0.5$  the potential starts out steeper to begin with and, since the solitons come much closer to each other, at the turning point it exhibits a very steep slope.

The potential was derived under the assumption that the solitons are well separated. As discussed in section 2.3.2, this is only the case for solitons with velocities  $|v| < 0.5$ . Thus, the behavior of  $V(z, v) \rightarrow \infty$  for  $z \rightarrow 0$ , given by the  $1/\sinh^2$  dependence on the soliton distance  $2z$ , is irrelevant, since the solitons in the velocity regime of applicability never come closer to each other than indicated in figure 2.10.

Figure 2.11 shows the phase shifts the soliton with velocity  $v_1 > 0$  experiences in a symmetric collision with a soliton with  $v_2 = -v_1$ . The dots indicate the exact phase shifts calculated from equation 2.8 and the crosses those determined from a numerical solution of the differential equation for the soliton coordinate using the effective interaction potential (equation 2.18). The potential approximates the behavior of the solitons very well for velocities smaller than 0.5. For velocities larger than 0.5, the phase shifts obtained from the effective potential start to deviate from those given by equation 2.8 and for very large velocities the phase shifts from the potential even start to increase again, while the phase shifts given by equation 2.8 are monotonically decreasing.

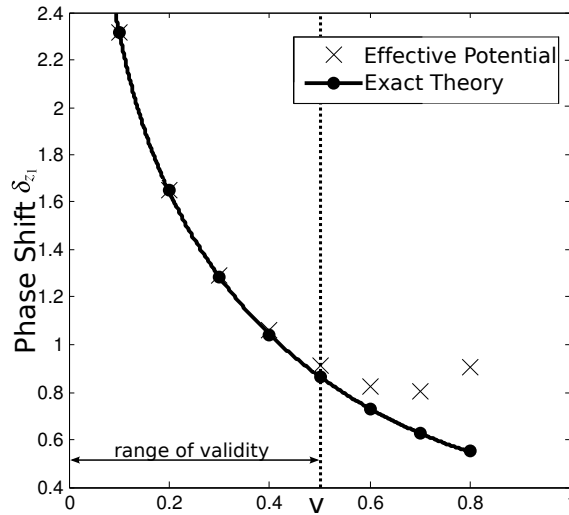


Figure 2.11: Comparison between the exact phase shifts the solitons experience in symmetric collisions with velocities  $v$  given by equation 2.8 and the phase shifts determined using the effective interaction potential

Figure 2.12 shows the comparison between soliton trajectories given by a numerical time evolution of a solution of the nonlinear Schrödinger equation containing separate solitons (density plot in the background) and those of particles subjected to the repulsive potential of equation 2.13 (bright lines). Once again, for velocities  $|v| \leq 0.5$  (figures 2.12(a) and 2.12(b)) the agreement between the trajectories is very good. For  $v > 0.5$  (figure 2.12(c)), the difference between the trajectories after the collision becomes larger.

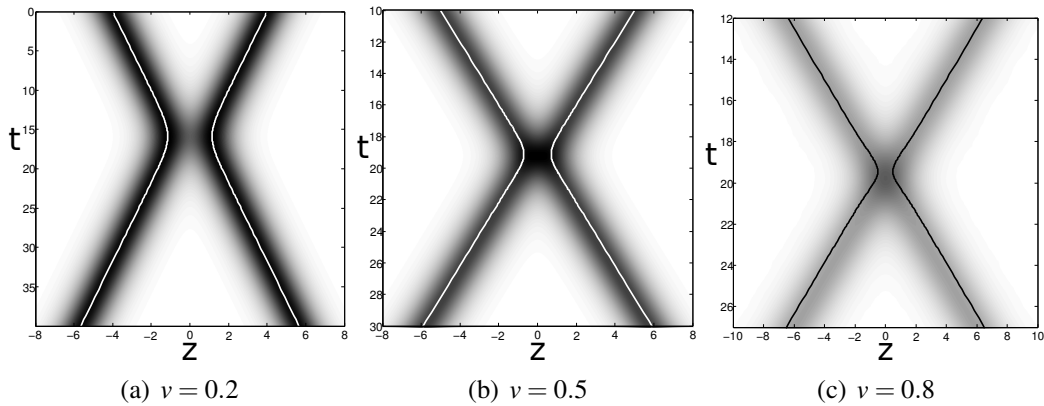


Figure 2.12: Soliton trajectories for symmetric collisions, calculated with the effective potential (full lines) and with a numerical time evolution of the 1D homogeneous NLS (density plot in the background), for different initial velocities

The trajectories still show qualitative agreement and the effective potential might be used to investigate qualitatively the behavior of faster solitons, but quantitative agreement to a satisfactory degree is only reached if the criteria for the derivation of the potential are

met, *i.e.* the solitons are always identifiable by two separate minima which is the case if their initial velocity in a symmetric collision is smaller than  $\pm 0.5$ .

### 2.3.4 Generalization to Asymmetric Collisions of Multiple Solitons

The effective potential of equation 2.13, being derived from equation 2.9, is only applicable to symmetric collisions, *i.e.* collisions of two solitons moving with equal velocities in opposite directions. A derivation directly from 2.4, which would incorporate cases with arbitrary velocities, is more complicated and does not lead to such a simple form as in the symmetric case. A generalization of the symmetric potential can instead be attempted using an average darkness for two colliding solitons. This preserves the form of the potential but takes into account the two different velocities of the solitons. It is not obvious how to define this average darkness. The definition that is used here has to be justified *a posteriori* by a comparison of the results to those of the analytic theory of interactions.

The following definition for the average darkness is considered.  $B_{ij} = (B_i + B_j)/2$ , where  $B_i$  is the darkness given by velocity  $v_i$  of soliton  $i$ , and the coordinate  $z$  of the symmetric case is replaced by relative coordinates  $z \rightarrow (z_i - z_j)/2$ . With these substitutions the interaction potential for soliton  $i$  in the presence of other solitons is

$$V_i = \sum_{j \neq i} \frac{B_{ij}^2}{2 \sinh^2 B_{ij}(z_i - z_j)}, \quad B_{ij} = \frac{B_i + B_j}{2} \quad (2.19)$$

This interaction potential reduces to equation 2.13 in the case of two solitons with  $v_i = -v_j$  and  $x_i = -x_j$ .

Using this potential, it is now possible to obtain equations of motion for an arbitrary number of solitons. The total Lagrangian for  $n$  solitons is given by

$$L = T - V = \sum_{i=1}^n T_i - \sum_{i=1}^n V_i = \sum_{i=1}^n \frac{\dot{z}_i^2}{2} - \sum_{i,j=1, i \neq j}^n \frac{B_{ij}^2}{2 \sinh^2 B_{ij}(z_i - z_j)} \quad (2.20)$$

The Lagrange equations are

$$\frac{d}{dt} \left( \frac{\partial L}{\partial \dot{z}_i} \right) = \frac{\partial L}{\partial z_i}, \quad i = 1, 2, \dots, n \quad (2.21)$$

$$\Rightarrow \ddot{z}_i - \frac{d}{dt} \left( \frac{\partial V}{\partial \dot{z}_i} \right) = -\frac{\partial V}{\partial z_i} \quad (2.22)$$

Expressing the total time differential as partial differentials with respect to all variables

$$\frac{d}{dt} \left( \frac{\partial V}{\partial \dot{z}_i} \right) = \frac{d}{dt} F_i = \sum_{j=1}^n \frac{\partial F_i}{\partial z_j} \dot{z}_j + \sum_{j=1}^n \frac{\partial F_i}{\partial \dot{z}_j} \ddot{z}_j, \quad F_i = \frac{\partial V}{\partial \dot{z}_i} \quad (2.23)$$

leads to a set of  $n$  coupled differential equations:

$$\ddot{z}_i - \left( \sum_{j=1}^n \frac{\partial F_i}{\partial z_j} \dot{z}_j + \sum_{j=1}^n \frac{\partial F_i}{\partial \dot{z}_j} \ddot{z}_j \right) = -\frac{\partial V}{\partial z_i}, \quad i = 1, 2, \dots, n \quad (2.24)$$

which can be solved for the  $\dot{z}_i$  and integrated numerically to obtain the time evolution of the solitons.

It is not immediately clear what the range of validity with respect to the initial soliton velocities for this potential is. In the scope of this thesis it will be applied to collisions of a moving soliton with another initially stationary soliton and the range of validity is investigated for this situation.

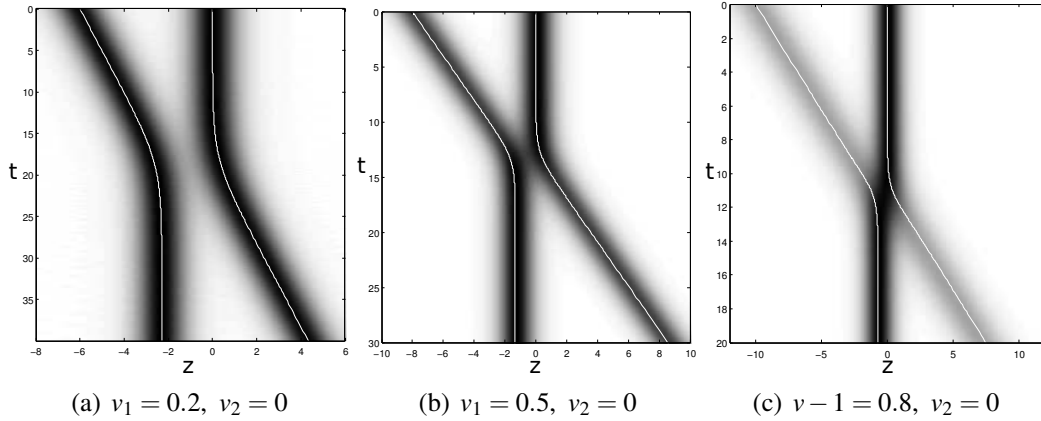


Figure 2.13: Soliton trajectories for asymmetric collisions, calculated with the generalized effective potential (full lines) and with a numerical time evolution of the 1D homogeneous NLS (density plot in the background), for different initial velocities  $v_1, v_2$

Figure 2.13 shows a comparison between the soliton trajectories obtained from the equations of motion using this generalized effective potential (bright lines) and the time evolution of the nonlinear Schrödinger equation for a wavefunction containing two solitons with different initial velocities (density plots in the background). The collisional dynamics are qualitatively well reproduced by the asymmetric effective potential.

In Figure 2.14 the phase shifts in this situation, obtained from the generalized effective potential, are compared to the exact ones given by equation 2.8 for different initial velocities of the moving soliton. It can be seen, that the agreement between the asymmetric potential and the results of equation 2.8 are good for initial velocities  $v < 0.5$  of the moving soliton. For larger velocities the deviations become more significant and again the phase shifts obtained from the effective potential show a different trend for high velocities than the exact ones derived from equation 2.8.

This generalization of the interaction potential, as shown in the derivation of the equations of motion, allows for the application of the interaction potential to collisions involving more than two solitons.

This is shown in figure 2.15 for the case of three solitons, where one is initially stationary and the other two collide with it at the same time from both sides with equal velocities. The bright lines indicate the soliton trajectories obtained from the generalized effective potential and the density plot in the background shows a numerical time evolution of the homogeneous one-dimensional nonlinear Schrödinger equation for three solitons.

## 2 Dark Solitons - Dynamics and Interactions

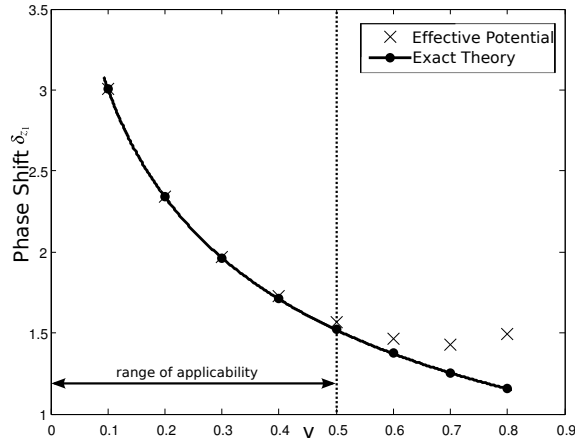


Figure 2.14: Comparison between the exact phase shifts the soliton with velocity  $v$  experience in an asymmetric collisions with a stationary soliton given by equation 2.8 (dots, full line) and the phase shifts determined using the effective interaction potential (crosses)

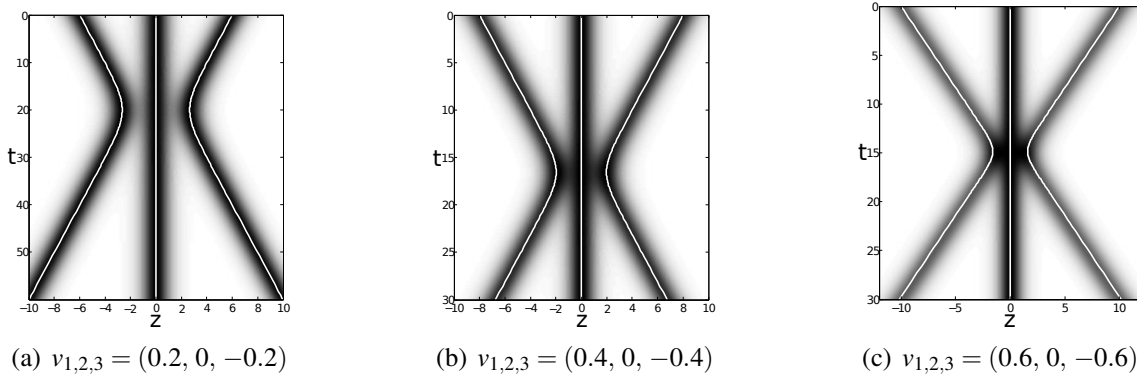


Figure 2.15: Soliton trajectories for collisions of three solitons, calculated with the generalized effective potential (full lines) and with a numerical time evolution of the 1D homogeneous NLS (density plot in the background), for different initial velocities  $(v_1, v_2, v_3)$

### 2.3.5 Advantages of an Effective Potential Approach

The interaction between two solitons is well defined in the homogeneous one-dimensional situation. Given the initial velocities of the two colliding solitons, the phase shift they acquire can be directly obtained from equation 2.8. The effective potential approach becomes useful when considering less ideal situations or collisions with more than two solitons.

The effective interaction potential has two advantages. Firstly, it describes only the interaction of solitons in arbitrary collisions. The exact phase shift of equation 2.8 requires knowledge about the asymptotic constant velocities. In cases where the solitons are not as well defined as in the framework of the homogeneous one-dimensional nonlinear Schrödinger, these asymptotic values are also not defined. The effective potential

circumvents this problem by depending on the momentary velocity of the solitons. As it will be seen in the next chapter, other effects on the dynamics of the solitons that do not stem from their interaction can be incorporated as additional effective potentials added to the interaction potential. Their separate effects on the soliton motion can then be distinguished, given that the effective potential accurately approximates these nonideal situations.

Secondly, the effective interaction potential is applicable to collisions of arbitrary numbers of solitons. To obtain the effects of interactions between more than two solitons one has to do a numerical time evolution of their wavefunction using the governing nonlinear equation, which is in general a lot more time consuming than a numerical solution of the equations of motion given by the interaction potential.



# 3 Dark Solitons in Bose-Einstein Condensates

Bose-Einstein condensates are a new system for the experimental investigation of nonlinear dynamics. They are well described by the nonlinear equation governing their dynamics, the Gross-Pitaevskii equation, given that their temperature is well below the critical temperature of condensation. They are usually three dimensional systems and the questions arise whether solitons can exist in Bose-Einstein condensates and how their properties differ from those of solitons in the ideal, homogeneous and one-dimensional case. These questions are addressed in this chapter.

## 3.1 Bose-Einstein Condensates as Nonlinear Systems

### 3.1.1 The Gross-Pitaevskii Equation

For a realistic description of a dilute Bose gas, as realized in cold atom experiments, interactions between the atoms and the effects of an external confining potential have to be taken into account. The many body Hamiltonian in second quantization for this problem reads

$$\hat{H} = \int d\mathbf{r} \hat{\Psi}^\dagger(\mathbf{r}) \left[ -\frac{\hbar^2}{2m} \nabla^2 + V_{\text{ext}} \right] \hat{\Psi}(\mathbf{r}) + \frac{1}{2} \int d\mathbf{r} d\mathbf{r}' g \hat{\Psi}^\dagger(\mathbf{r}) \hat{\Psi}^\dagger(\mathbf{r}') \hat{\Psi}(\mathbf{r}) \hat{\Psi}(\mathbf{r}') \quad (3.1)$$

where  $\hat{\Psi}^\dagger(\mathbf{r})$  and  $\hat{\Psi}(\mathbf{r})$  are the boson field operators,  $V_{\text{ext}}$  is the confining external potential,  $m$  is the mass of the atoms and

$$g = \frac{4\pi\hbar^2 a_s}{m}. \quad (3.2)$$

describes the interaction between the atoms. Here, the fact has been used that for dilute atomic gases, where almost every collision process is a two-body process at low energies, the interaction is governed by the s-wave scattering potential which can be described by a delta distribution with a single parameter  $g$  that depends on the s-wave scattering length  $a_s$ [31].

Solving the complete many body problem for large numbers of atoms is analytically impossible and numerically very demanding. The problem can be greatly simplified by

### 3 Dark Solitons in Bose-Einstein Condensates

employing a mean field approximation to avoid having to treat all interatomic interactions individually. The field operator is approximated by a complex valued function

$$\hat{\Psi}(\mathbf{r}) \approx \Phi(\mathbf{r}) \quad (3.3)$$

$\Phi(\mathbf{r})$  is generally referred to as the wave function of the condensate. At temperatures well below the critical temperature for condensation ( $T_c$ ) essentially all atoms are in the macroscopically occupied ground state and the condensate can be adequately described by the complex wave function  $\Phi(\mathbf{r})$  and the fact that  $\hat{\Psi}(\mathbf{r})$  is actually an operator can be neglected [32]. The wave function  $\Phi(\mathbf{r})$  is taken to fulfill the normalization condition

$$N = \int |\Phi(\mathbf{r}, t)|^2. \quad (3.4)$$

where  $N$  is the total number of atoms in the Bose-Einstein condensate.

Applying this substitution to the equation of motion for the Hamiltonian 3.1 leads to [33]

$$i\hbar \frac{\partial}{\partial t} \Phi(\mathbf{r}, t) = \left[ -\frac{\hbar^2}{2m} \nabla^2 + V(\mathbf{r}) + g |\Phi(\mathbf{r}, t)|^2 \right] \Phi(\mathbf{r}, t). \quad (3.5)$$

This equation was originally derived independently by Gross and Pitaevskii [33, 34] and is known as the three dimensional Gross-Pitaevskii equation (3D GPE).

In the following the external potential that confines the Bose-Einstein condensates will be considered as harmonic, given by

$$V_{\text{ext}} = \frac{m}{2} (\omega_x^2 x^2 + \omega_y^2 y^2 + \omega_z^2 z^2) \quad (3.6)$$

In the case of cigar shaped trap geometries, where the trapping frequencies in two directions are equal and much larger than in the third one, the  $x$  and  $y$  directions will always be considered the transverse directions with stronger confinement and the  $z$  direction is considered the longitudinal direction with weaker confinement.

The chemical potential  $\mu$  of the condensate is for the ground state given by the relation

$$N\mu = E_{\text{kin}} + E_{\text{pot}} + 2E_{\text{int}} = \int d\mathbf{r} \Psi^*(\mathbf{r}) \left[ -\frac{\hbar^2}{2m} \frac{\partial^2}{\partial x^2} + V(\mathbf{r}) + 2g |\Psi(\mathbf{r}, t)|^2 \right] \Psi(\mathbf{r}) \quad (3.7)$$

The separate energy contributions are the kinetic energy  $E_{\text{kin}}$ , the potential energy  $E_{\text{pot}}$  and the nonlinear interaction energy  $E_{\text{int}}$  and correspond to the respective parts of the Hamiltonian.

The chemical potential has an associated length scale, the so called healing length  $\xi$  of the condensate. This is the length scale over which the condensate density grows from zero to  $n$  if subjected to an infinite potential barrier. It is given by

$$\xi = \sqrt{\frac{\hbar}{ngm}} \quad (3.8)$$

For the case of a homogeneous condensate with density  $n_0$  the chemical potential is given by  $\mu = n_0 g$  and the healing length can be written as:

$$\xi = \sqrt{\hbar/\mu m} \quad (3.9)$$

In the case of a non-homogeneous harmonically confined condensate, this expression of the healing length can be used to get an approximate value for the healing length close to the center of the condensate. In the following, whenever a healing length is attributed to the whole condensate, this is the quantity referred to.

### 3.1.2 The One-Dimensional Gross-Pitaevskii Equation

If the harmonic confinement of a BEC is much stronger in two directions and the harmonic oscillator length  $a_{\perp} = \sqrt{\hbar/m\omega_{\perp}}$  of the confinement in these perpendicular directions is smaller than the healing length  $\xi$  of the condensate<sup>1</sup> the Gross-Pitaevskii equation can be simplified by integration over these axes, leading to a one dimensional Gross Pitaevskii equation (1DGPE) for the remaining longitudinal direction with weaker confinement[35]:

$$i\hbar \frac{\partial}{\partial t} \Psi(z, t) = \left[ -\frac{\hbar^2}{2m} \frac{\partial^2}{\partial z^2} + \frac{1}{2} m \omega_z^2 z^2 + g_{1D} |\Psi(z, t)|^2 \right] \Psi(z, t) \quad (3.10)$$

Here  $g_{1D}$  is the effective one dimensional interaction strength given by

$$g_{1D} = \frac{g}{2\pi a_{\perp}^2}. \quad (3.11)$$

If the confining potential is set to zero, the homogeneous form of the one dimensional Gross-Pitaevskii equation is obtained:

$$i\hbar \frac{\partial}{\partial t} \Psi(z, t) = \left[ -\frac{\hbar^2}{2m} \frac{\partial^2}{\partial z^2} + g_{1D} |\Psi(z, t)|^2 \right] \Psi(z, t) \quad (3.12)$$

This equation has the same form as the nonlinear Schrödinger equation

$$i \frac{\partial}{\partial \tau} u(\tilde{z}, \tau) = \left[ -\frac{1}{2} \frac{\partial^2}{\partial \tilde{z}^2} + |u(\tilde{z}, \tau)|^2 \right] u(\tilde{z}, \tau) \quad (3.13)$$

which was considered in chapter 2 as the description of a medium supporting dark soliton solutions. They are connected through the following scaling of the variables and normalization of the wavefunction:

$$\begin{aligned} t &\rightarrow \frac{\hbar}{g_{1D} n} \cdot \tau \\ z &\rightarrow \frac{\hbar}{\sqrt{g_{1D} n m}} \cdot \tilde{z} \\ \Psi(z, t) &\rightarrow \sqrt{n} \cdot u(z, t) = \Psi(z, t) \end{aligned} \quad (3.14)$$

<sup>1</sup>This can also be expressed by the relation  $\mu \ll \hbar\omega_{\perp}$

### 3 Dark Solitons in Bose-Einstein Condensates

where  $n$  is the homogeneous one-dimensional atom density in the condensate.

The wave function of a single dark soliton solution of the homogeneous one-dimensional Gross-Pitaevskii equation, which for the homogeneous one-dimensional nonlinear Schrödinger equation is given by equation 2.3, takes the form [36]

$$\sqrt{n} \left[ B \tanh \left( B \frac{(z - vt - z_0)}{\xi} \right) + i \frac{v}{c} \right] e^{-\frac{i\mu t}{\hbar}} \quad (3.15)$$

where  $\mu$  is the one-dimensional chemical potential  $\mu = g_{1D}n$  and  $B$  is the darkness of the soliton, in this case defined as  $B = \sqrt{1 - v^2/c^2}$  with the Bogoliubov speed of sound  $c = \sqrt{\mu/m}$  and  $\xi$  is the healing length  $\xi = \hbar/\sqrt{\mu m}$ .

For a Bose-Einstein condensate that can be described by the homogeneous one dimensional Gross-Pitaevskii equation all considerations that were taken in chapter 2 about the nature of dark solitons and their interactions apply as well.

### Applicability of the One-Dimensional Gross-Pitaevskii Equation

In realistic experimental situations, the conditions for the applicability of the homogeneous one-dimensional Gross-Pitaevskii equation are hard to fulfill. Firstly, in most cases the condensate is confined by an external potential in the longitudinal direction<sup>2</sup>, so the equation is not completely homogeneous and secondly the confinement in the perpendicular direction has to be very strong to achieve the ideal one dimensional regime.

Menotti and Stringari derived the following criterion for a harmonically confined Bose-Einstein Condensate to be in the one dimensional regime [38, 39]:

$$N\Omega \frac{a_s}{a_{\perp}} \ll 1 \quad (3.16)$$

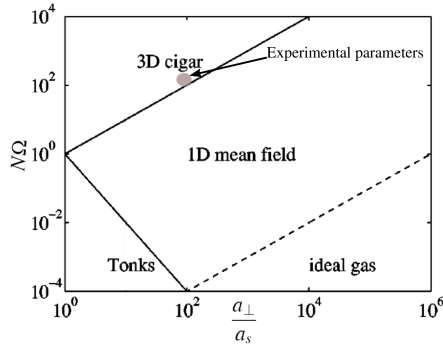
where  $\Omega = \omega_z/\omega_{\perp}$  is the aspect ratio of the confining trap. For their derivation a local density approximation is used which also requires

$$\left( \frac{N}{\sqrt{\Omega}} \frac{a_s}{a_{\perp}} \right)^{1/3} \gg 1. \quad (3.17)$$

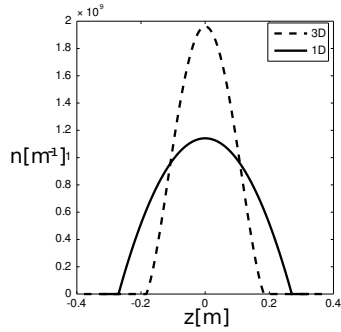
Figure 3.1(a) shows a phase diagram indicating the conditions for the different dimensionality regimes and figures 3.1 (c)-(e) show a comparison between the ground states of Bose-Einstein condensates determined with the three dimensional and the one dimensional Gross-Pitaevskii Equations. For parameters in the regime indicated by “3D cigar” in figure 3.1(a), the wavefunctions obtained from the one-dimensional Gross-Pitaevskii equation deviate substantially from those of the three-dimensional Gross-Pitaevskii equation and an accurate description of the dynamics of such condensates can not be expected from the one-dimensional equation.

<sup>2</sup>Note that recent advances in the creation of ring shaped traps overcome this need for a confinement in the longitudinal direction, see e.g. [37]

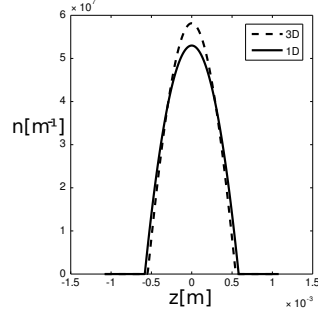
### 3.1 Bose-Einstein Condensates as Nonlinear Systems



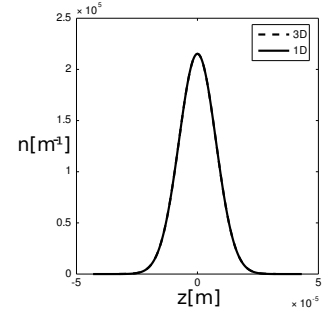
(a) The different regimes of dimensionality of a Bose-Einstein condensate (taken from [38]). The regime investigated experimentally is indicated by the gray shaded area.



(b)  $N\Omega = 100, \frac{a_{\perp}}{a_s} = 1$



(c)  $N\Omega = 100, \frac{a_{\perp}}{a_s} = 100$



(d)  $N\Omega = 100, \frac{a_{\perp}}{a_s} = 10000$

Figure 3.1: Comparison between BEC Groundstates determined with three- and one-dimensional Gross-Pitaevskii equations

Our experiments will be performed for parameters in the region indicated by the grey shaded area in figure 3.1(a). Our experimental parameters are not in the fully one dimensional regime but rather in the dimensionality crossover regime between the three-dimensional cigar shape and one-dimensionality. Thus the one-dimensional Gross-Pitaevskii equation cannot yield a precise description of the systems investigated. Furthermore, the Bose-Einstein condensates under experimental investigation are subjected to a harmonic confinement in the longitudinal direction and thus the condensates will not be homogeneous in this direction. The question has to be raised whether solitonic excitations of such a system can exist, how they can be characterized, how stable they are and how much of the theoretical aspects lined out in chapter 2 can be applied to them.

#### 3.1.3 Effectively One-Dimensional Gross-Pitaevskii Equations

As mentioned above, the one dimensional Gross-Pitaevskii equation does not accurately describe a Bose-Einstein condensate for the parameters accessible in our experimental realization. The three dimensional Gross-Pitaevskii equation does give an almost accurate

### 3 Dark Solitons in Bose-Einstein Condensates

description of our experiment (neglecting finite temperature effects), but is in general non-integrable and thus its time evolution has to be computed numerically. Numerical methods for the integration of (3.5) provide in principle the possibility to obtain  $\Psi(\mathbf{r}, t)$  at any point in time with arbitrary precision, given adequate computational resources. Since all three spatial dimensions have to be incorporated into the computations, this is numerically very demanding and time consuming. In the cases relevant to the performed experiments, one can still take advantage of the elongated shape of the condensate. In these cases it is more efficient to use effectively one-dimensional equations that take the transverse structure of the Bose-Einstein condensate into account without the need to extend the calculations over the whole space. These equations still rely on the fact, that the extension of the condensates in two transverse directions is much smaller than in the third, longitudinal one, but not as strictly as equation 3.10 does.

#### The Non-Polynomial Schrödinger Equation

In [40], Salasnich et al. derive a so called nonpolynomial nonlinear Schrödinger equation (NPSE). Assuming a gaussian shape of the Bose-Einstein condensate in the transverse direction that is slowly varying along the longitudinal direction and employing a variational ansatz for this gaussian profile, they arrive at

$$i\hbar \frac{\partial}{\partial t} f(z, t) = \left[ -\frac{\hbar^2}{2m} \frac{\partial^2}{\partial z^2} + V_{ext} + \frac{gN}{2\pi a_{\perp}^2} \frac{|f(z, t)|^2}{C} + \frac{\hbar\omega_{\perp}}{2} \left( \frac{1}{C} + C \right) \right] f(z, t) \quad (3.18)$$

$$\text{with : } C = \sqrt{1 + 2a_s N |f(z, t)|^2} \quad (3.19)$$

This equation will be employed to do the numerical time evolution of the wave functions of cigar shaped Bose-Einstein condensates in the most cases throughout this thesis. In the dimensionality crossover regime (see 3.1.2) it gives an excellent approximation of the dynamics[41]. The numerical time evolutions will be carried out using the split-step fast Fourier transform method [42] which is a common tool for the numerical integration of the Gross-Pitaevskii equation and related Schrödinger equations [43].

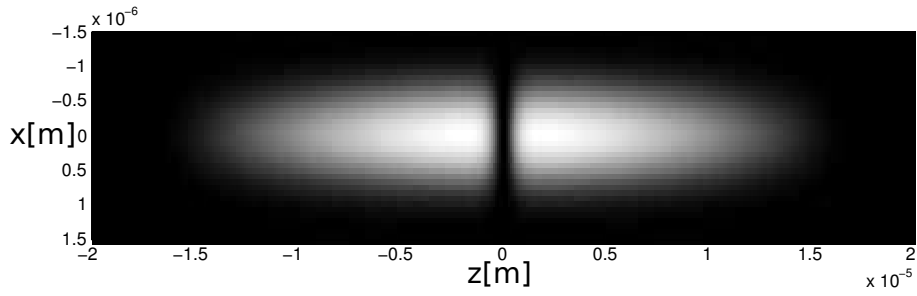
## 3.2 Dark Solitons in Quasi One-Dimensional Bose-Einstein Condensates

### 3.2.1 Soliton Like Excitations

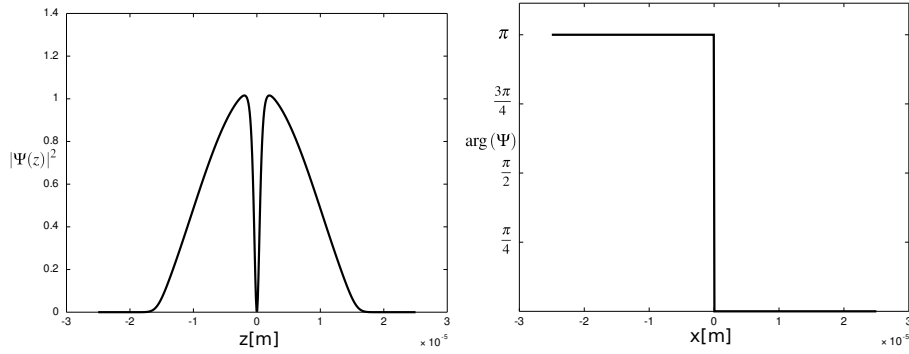
As discussed at the beginning of chapter 2, dark solitons of the nonlinear Schrödinger equation are only well defined in the one-dimensional homogeneous case, where they exist as exact analytic solutions.

To obtain a notion of a dark soliton that can be applied to realistic experimental situations, the concept of a dark soliton has to be extended to three dimensional condensates

### 3.2 Dark Solitons in Quasi One-Dimensional Bose-Einstein Condensates



(a) Density of the first excited state of a cigar shaped Bose-Einstein condensate



(b) Density of the first excited state, integrated over the transverse directions (c) Phase of the first excited state along the longitudinal axis

Figure 3.2: The first excited state of a cigar shaped BEC, numerically determined using the 3D GPE

subjected to external confining potentials.

Since the three-dimensional Gross-Pitaevskii equation reduces to a one-dimensional nonlinear Schrödinger equation in the limit of tight radial confinement, dark soliton like states can be expected for condensates in cigar shaped traps [44]. When looking at Bose-Einstein condensates in such geometries, the simplest structure that features dark soliton like characteristics is the first excited state of the condensate. This state has a macroscopic wave function that exhibits a nodal plane perpendicular to the symmetry axis of the trap (longitudinal axis).

Figure 3.2(a) shows the density of a cigar shaped condensate (summed over one of the transverse directions) in its first excited state. The density of the condensate in the nodal plane at  $z = 0$  goes down to zero (see also figure 3.2(b), which shows the longitudinal density distribution, summed over both transverse directions) and the first excited state is analogous to a completely black, stationary dark soliton. The similarity becomes obvious when looking at figure 3.2(c), which shows the phase of the condensate along its symmetry axis. The phase experiences a sharp jump of  $\pi$  at the local density minimum, as the phase of a completely dark soliton in the one dimensional homogeneous case does.

To generalize this concept to nonstationary solitons, one can turn to the effectively one-dimensional non-polynomial Schrödinger equation (Eq. 3.19). This equation incorporates the transverse structure of the condensate while still being defined one-dimensionally.

### 3 Dark Solitons in Bose-Einstein Condensates

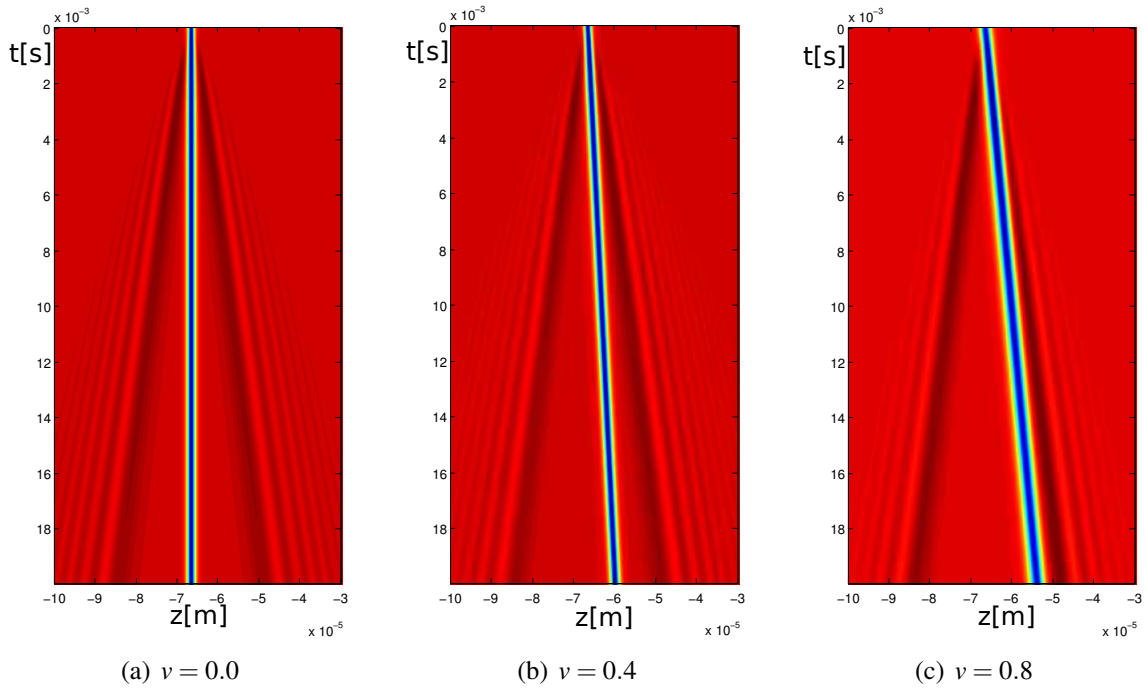


Figure 3.3: The time evolution of analytic soliton solutions of the homogeneous 1DGPE with different velocities  $v$ , in units of the speed of sound  $c$ , conducted with the homogeneous NPSE. After some initial radiation, the density dips are stable and propagate through the condensate.

To approximate a dark soliton in the non-polynomial Schrödinger equation a homogeneous background density of the condensate in the longitudinal direction is assumed. The condensate is only confined in the transverse directions. The analytic soliton solution to the homogeneous one-dimensional Gross-Pitaevskii equation 3.15 is multiplied to this background. Obviously, this soliton solution is not an exact solution to the non-polynomial Schrödinger equation, but it can be seen in figure 3.3, which shows the time evolution of such a wave packet for different initial velocities, that after some initial radiation leaves the soliton a stable dip maintains that is stationary or moves through the homogeneous background density with a constant velocity. This shows the general stability of dark solitons. The soliton itself constitutes a local energy minimum of the total energy of the condensate. If, like in this case, an initial density or phase modulation is close enough to the shape of a dark soliton, it is energetically favorable for the wavefunction to develop into such a soliton. The energy and density difference between the initial shape and the dark soliton is radiated into the condensate. This mechanism is of great use for the experimental creation of dark solitons that will be discussed in section 4.1.

Figure 3.4 shows a comparison between the initial shape of the wave packet and the final shape after a time evolution of 30ms for the case of a stationary soliton as shown in figure 3.3(a). The shapes correspond very closely, but the soliton of the non-polynomial Schrödinger equation has a slightly larger spatial extension than the initial solution to the homogeneous one-dimensional Gross-Pitaevskii equation.

### 3.2 Dark Solitons in Quasi One-Dimensional Bose-Einstein Condensates

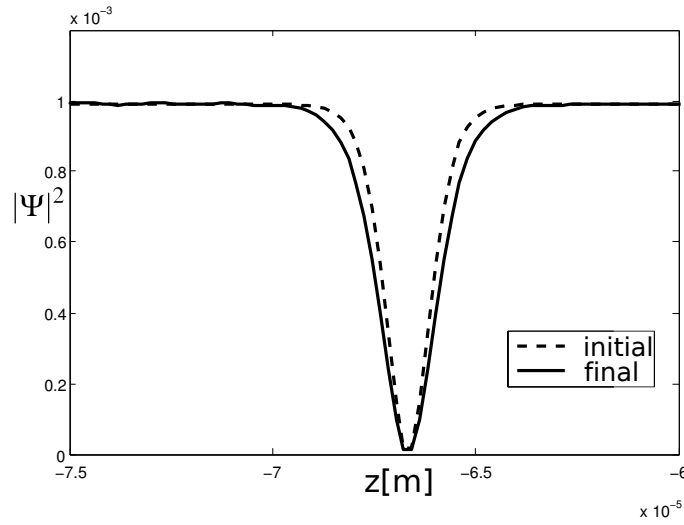


Figure 3.4: The shape of the initial dark soliton solution (dashed line) and the final shape after a time evolution of 30ms (full line) for the stationary case shown in figure 3.3(a)

This approach to a definition of a soliton entails in principle that the soliton in a three-dimensional setting is approximatively considered as being a one-dimensional structure modifying a three-dimensional stationary condensate:

$$\Psi_s(x, y, z, t) \approx \Psi_{BG}(x, y, z) \cdot \Phi_s(z, t) \quad (3.20)$$

The complete wavefunction of the soliton and the background  $\Psi_s$  is seen as the product of a stationary three dimensional cloud  $\Psi_{BG}$  and a one-dimensional time dependent soliton  $\Phi_s$ .

The effect of a confinement in the longitudinal direction on the dynamics of a soliton will be discussed in detail in section 3.3. As far as the characterization of a soliton in such an inhomogeneous situation is concerned one can resort to the local density approximation. The soliton's extension is on the scale of the healing length. As long as the condensate density does not vary strongly on this scale it can be approximated as homogeneous in the direct vicinity of the soliton and thus the above considerations are locally valid in such a condensate.

Thus, a dark soliton in a cigar shaped condensate shall be defined as a travelling or stationary depletion of the condensate density over a plane transverse to the longitudinal axis and can be regarded as the realization of a one dimensional soliton-like excitation in a three dimensional system.

#### 3.2.2 Stability of Dark Solitons

Dark solitons of the one-dimensional nonlinear Schrödinger equation are exact solutions of the integrable system and stable. The situation is more complex in nonintegrable systems like the three dimensional Gross-Pitaevskii equation where the properties of the

### 3 Dark Solitons in Bose-Einstein Condensates

stable solutions only apply approximately. Since the soliton corresponds to an excited state of the Bose-Einstein condensate, which only experiences a local energy minimum, it can be expected that the system eventually decays into the energetically lower ground state, given appropriate decay channels.

The phenomenon of soliton decay was first investigated by Kuznetsov and Turitsyn [22] who showed that one-dimensional solitons in three-dimensional systems are unstable against transverse perturbations. These perturbations lead to a snake-wise bending of the dark soliton [45], which is initially flat in the perpendicular direction, and finally a decay of the soliton into pairs of vortex solitons, as experimentally observed in [20]. Due to the bending of the soliton along the transverse plane, this decay channel is referred to as the snaking-instability. Muryshev et al. [46] investigated this transversal instability for the case of cigar shaped Bose-Einstein condensates. They derived a parameter

$$\gamma = \frac{n_{0m}g}{\hbar\omega_{\perp}}, \quad (3.21)$$

where  $n_{0m}$  is the maximum density of the condensate, which determines the stability of the dark soliton. If  $\gamma$  is below a critical value  $\gamma_c$  the dark soliton is stable against transverse decay. This value depends on the aspect ratio  $\Omega = v_z/v_{\perp}$  and for our experimental parameters it can be obtained from [46] to be  $\gamma_c > 2.2$ .

Typical densities for our experiment are  $n_{m0} \approx 1 \cdot 10^{14} \text{ cm}^{-3}$  and typical transversal trapping frequencies are on the order of  $\omega_{\perp} \approx 400 - 800 \text{ Hz}$ . Thus in our experiments the value for  $\gamma$  ranges from 1.2 to 1.7 and a stationary soliton is stable against the snaking instability.

A similar transverse instability exists for moving dark solitons. In this case, the transverse structure of the dark soliton is modified due to the inhomogeneity of the condensate density in radial direction, which results in different soliton velocities at the center of the soliton and at its edges, and leads to a bending of the soliton. This instability is referred to as the inhomogeneity induced dynamical instability.

The stability against this form of decay is also characterized by the parameter  $\gamma$  but the critical value  $\gamma_c(v)$  is velocity dependent. For velocities between  $v = 0$  and  $v = 0.5 \cdot c$  the critical value ranges from  $\gamma_c \approx 2.2$  in the stationary case to  $\gamma_c \approx 3$  for  $v = 0.5c_s$ , where  $c_s$  is the speed of sound at maximum density given by  $\sqrt{n_{0m}g/2m}$ . [47] Thus for a moving dark soliton the criterion for stability against transverse decay is even more relaxed.

Another possibility of decay is due to a thermodynamic instability which originates from the scattering of thermal particles on the dark soliton at finite temperatures [48, 18, 47]. This scattering leads to an increase of the soliton's velocity over time until it reaches the velocity of sound and, keeping in mind the relation between velocity and darkness of a dark soliton, becomes essentially indistinguishable from the background. At low temperatures  $T \ll \mu$  the time  $\tau$  at which the soliton acquires sound velocity is given by

[48]:

$$\tau^{-1} = 2\tau_D^{-1} \ln^{-1} \left( \frac{M}{m} \right) \quad (3.22)$$

$$\tau_D^{-1} \sim 24\zeta(4)\omega_{\perp}(\pi n_0 a_s^3)^{1/2} \left( \frac{T}{\mu} \right)^4 \quad (3.23)$$

where  $M = 4n_0 a_{\perp} \xi m$  and the Riemann  $\zeta$ -function takes the value  $\zeta(4) \approx 1.08$ . For our experimental parameters, assuming a temperature of the condensate of  $T \approx 20$  nK, this corresponds to a lifetime of the dark soliton between 350ms and 6s.

In conclusion, for our experimental conditions the cigar shaped Bose-Einstein condensate allows the existence of dark solitons that are stable over a time scale long enough to observe their dynamics, which in our experiment is done for times on the order of 100ms. The question how the fact that the condensate is subject to a longitudinally varying, harmonic potential is expected to alter these dynamics still remains.

## 3.3 Dynamics of Dark Solitons in Harmonically Confined Condensates

### 3.3.1 Oscillating Dark Solitons in the asymptotic one-dimensional case

The confining potential in the longitudinal direction leads to a drastic alteration of the soliton dynamics. The difference between this situation and the one for the homogeneous case is that the potential significantly changes the boundary conditions for the allowed solutions. For dark soliton solutions in the homogeneous case, the boundary conditions demand that the modulus of the wave function approaches a constant value larger than zero for  $z \rightarrow \pm\infty$ . In the case of harmonic confinement, this can obviously not be fulfilled and instead it has to be demanded that  $|\Psi(z, t)| \rightarrow 0$  for  $z \rightarrow \pm\infty$ . The background density of the BEC cloud will be high in the center of the trap and vanish at the edges of the cloud.

The behavior of dark solitons in confined Bose-Einstein condensates was investigated by Busch and Anglin [24] for slowly varying potentials in the framework of the one-dimensional Gross-Pitaevskii equation. Slowly varying in this case means that the background density of the confined condensate is varying slowly on the healing length scale and its associated time scale so that spatial and temporal derivatives of the background cloud can be neglected. This is usually referred to as the Thomas-Fermi approximation.

Using this assumption, the dynamics of a dark soliton in such a cloud is described by

$$\ddot{z} = -\frac{1}{2} \frac{\partial}{\partial z} V_{\text{ext}}(z) \quad (3.24)$$

where  $V_{\text{ext}}$  is the confining potential and  $z$  denotes the position of the dark soliton. In the case of harmonic confinement with a potential  $V_{\text{ext}} = m\pi v_z^2 z^2$  this will lead to an

### 3 Dark Solitons in Bose-Einstein Condensates

oscillation of the soliton described by

$$z(t) = z_0 \sin\left(\sqrt{2}2\pi\nu_z t\right). \quad (3.25)$$

Thus, the frequency of a soliton oscillating in a harmonically confined one-dimensional Bose-Einstein condensate in the Thomas-Fermi approximation is

$$\nu_{DS} = \frac{1}{\sqrt{2}}\nu_z. \quad (3.26)$$

The frequency of the oscillating soliton and the frequency of the dipole oscillation of the Bose-Einstein condensate in the trap differ by a factor  $\sqrt{2}$ . This result for the case of harmonic confinement had already been obtained by Muryshv et al. [46] for small oscillations and will be referred to in the following as the asymptotic prediction for the oscillation frequency of a dark soliton.

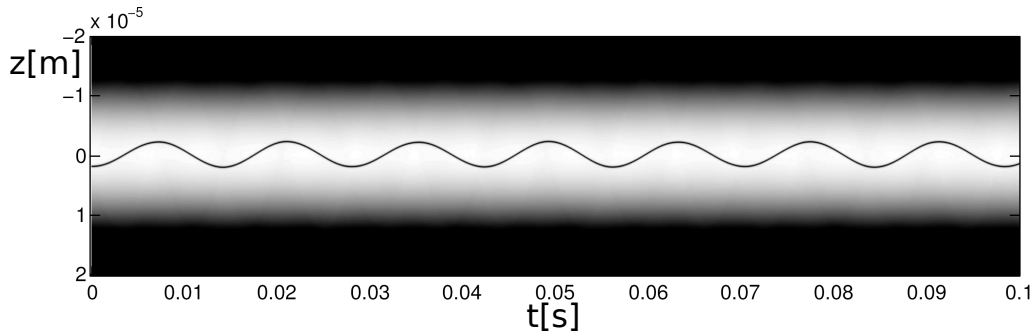


Figure 3.5: A dark soliton oscillating in a Bose-Einstein condensate in the Thomas-Fermi regime, calculated using a numerical time evolution of the 1D GPE.

Figure 3.5 shows the oscillation of a single dark soliton in a Bose-Einstein condensate determined with the numerical time evolution of the one-dimensional Gross-Pitaevskii equation. The frequency of the oscillating dark soliton is  $\nu_{DS} = 71.13$  Hz. With a longitudinal trap frequency of  $\nu_z = 100$  Hz the ratio  $\nu_z/\nu_{DS}$  is 1.406 which is very close to  $\sqrt{2} = 1.414$ . The parameter for the Thomas-Fermi criterion (see equation 3.27) in this case is  $(N/\sqrt{(\Omega)a_s/a_\perp})^{1/3} = 7.9$ , the atom number is  $N = 10000$  and  $\nu_\perp = 1000$  Hz.

The dynamical properties of the dark soliton correspond closely to the basic features discussed in chapter 2. At the turning points of the oscillatory motion the density at the center of the soliton goes completely down to zero as it is expected for a soliton with velocity  $v = 0$ . During its motion through the trap the soliton becomes less dark with respect to the background density the faster it gets. This can be seen in figure 3.6, which shows the longitudinal density of a condensate cloud with one oscillating soliton at its turning point (figure 3.6(a)) and in the center of the trap, where its velocity is highest (figure 3.6(b)).

To obtain these graphs of a single oscillating soliton, the soliton wave function has been approximated in the following way: The split-step fast Fourier method[42] in imaginary time is used to calculate the ground state of the Bose-Einstein condensate for the given

### 3.3 Dynamics of Dark Solitons in Harmonically Confined Condensates

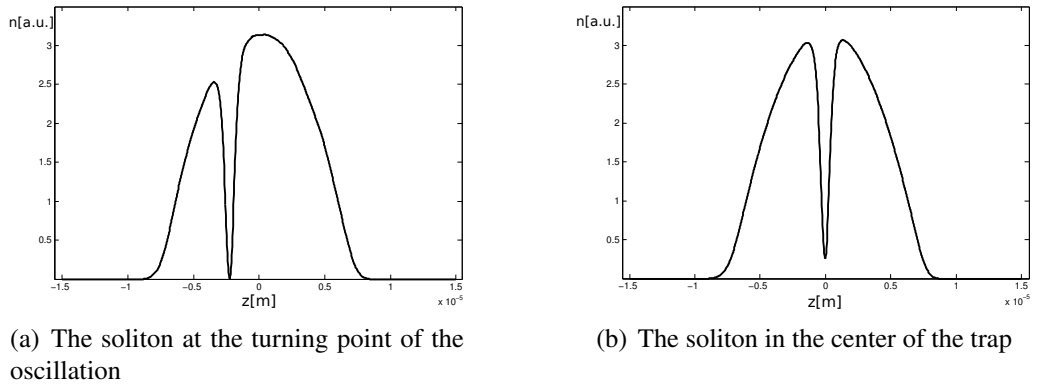


Figure 3.6: The longitudinal density distribution of a Bose-Einstein condensate in a harmonic trap with a single oscillating soliton at different points in the evolution

parameters ( $N, v_{\perp}$  and  $v_z$ ). Then, the single soliton solution for a stationary soliton of the homogeneous one-dimensional Gross-Pitaevskii equation is multiplied to the condensate wave function such that the minimum of the soliton is located at the center of the trap. Another numerical evolution in imaginary time is conducted which leads to an evolution of the condensate cloud into its first excited state with a density depletion in the center of the trap. This first excited state is divided pointwise by the ground state wavefunction to obtain the pure shape of a stationary single soliton in the center of the trap that goes asymptotically to  $\pm 1$  far away from the center of the trap. This soliton shape is now multiplied back to the ground state of the condensate, but displaced by the desired oscillation amplitude. The obtained wavefunction corresponds closely enough to that of an oscillating dark soliton at its turning point, where the soliton has a velocity of  $v = 0$ . This method will be used throughout this thesis to numerically investigate the dynamics of dark solitons.

#### 3.3.2 Deviations of the Oscillation Frequency from the Asymptotic Prediction

The result above was obtained assuming that the one dimensional Gross-Pitaevskii equation (eq. 3.10) correctly describes the condensate dynamics and that the background cloud can be described in the Thomas-Fermi limit, i.e. that the spatial and temporal derivatives of the background cloud can be neglected.

As indicated in figure 3.1(a), our experimental parameters are in a regime where the conditions for the applicability of the one dimensional Gross-Pitaevskii equation are not completely fulfilled.

A condition for the cloud to be in the longitudinal direction accurately described by the Thomas-Fermi approximation can be given by [38]

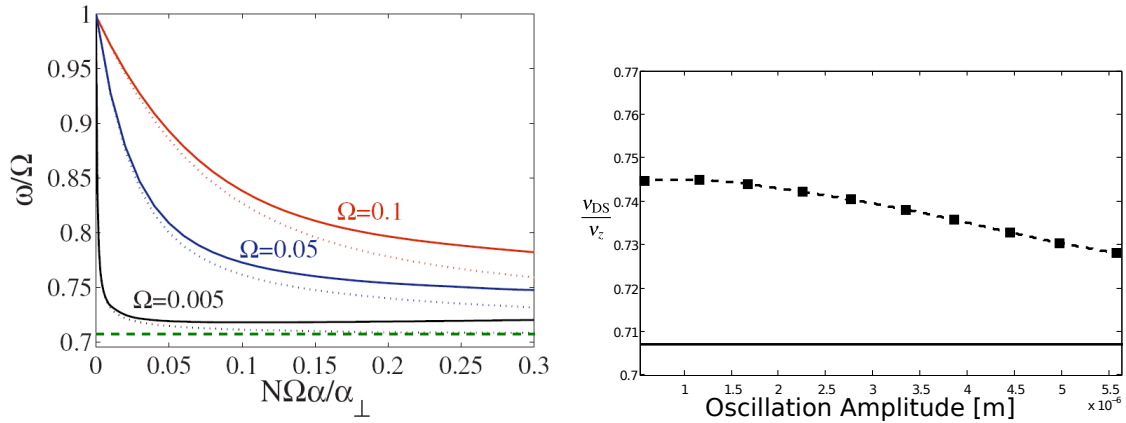
$$\left( \frac{N}{\sqrt{\Omega}} \frac{a_s}{a_{\perp}} \right)^{1/3} \gg 1 \quad (3.27)$$

### 3 Dark Solitons in Bose-Einstein Condensates

In our case, the values for this parameter range from 1.5 to 2.5 which is not sufficiently high to assume the validity of the Thomas-Fermi approximation. Thus, deviations from the asymptotic prediction have to be expected.

As pointed out by Brazhnyi and Konotop [49], the deviations from the Thomas-Fermi limit will lead to an increase of the soliton oscillation frequency on the order of a few percent.

Another change of the oscillation frequency of the dark solitons arises if the condensate can not be described by the one dimensional Gross-Pitaevskii equation. This was investigated by Theocharis et al. [41] who showed that in the crossover regime between condensates that can be described one-dimensionally and those that require a full three-dimensional description, the oscillation frequencies of dark solitons can be increased with respect to the prediction of  $v_z/\sqrt{2}$  by up to 10 %.



(a) Single Soliton oscillation frequencies in cigar shaped BECs for different dimensionalities of the condensates. Full lines are calculated via a Bogoliubov-de Gennes analysis, dotted lines via the 1D GPE. The dashed line indicates the asymptotic prediction  $1/\sqrt{2}$ . Taken from [41]

(b) Single Soliton frequencies for typical experimental parameters and different oscillation amplitudes (squares, dashed line). The asymptotic prediction is indicated by the full line.

Figure 3.7: Oscillation frequencies of single dark solitons in cigar shaped Bose-Einstein condensates

This is shown in figure 3.7(a), taken from [41], which shows soliton oscillation frequencies, normalized to the longitudinal trap frequency  $v_z$ , for different dimensionality parameters. It can be seen, that for a constant dimensionality parameter  $N\Omega\alpha_s/a_\perp$ , the oscillation frequency also depends on the aspect ratio  $\Omega$  alone.

To demonstrate the magnitude of deviations of the single soliton oscillation frequencies from the asymptotic prediction that are expected in the case of our experiment, figure 3.7(b) shows the oscillation frequencies of a single soliton with typical parameters used in our experiments for different oscillation amplitudes. The trap frequencies are  $v_z = 50$  Hz and  $v_\perp = 500$  Hz and the atom number is  $N = 1000$ . The asymptotic prediction of  $v_z/\sqrt{2}$  is indicated by the full line and the deviations in this case are on the order of 5%.

### 3.3 Dynamics of Dark Solitons in Harmonically Confined Condensates

It should be noted, that the oscillation frequency of single dark solitons, as can be observed in figure 3.7(b), not only depends on the dimensionality parameters of the condensate but also on the amplitude of the oscillation. This dependence can be attributed to the fact that for large amplitudes the soliton reaches the low density tail of the condensate density distribution where its dynamics are altered compared to the more or less flat central regions of the condensate [49, 50].

Thus, when investigating the question how the presence of more than one soliton in the condensate alters their oscillation frequencies, which will be done in the next section, it has to be kept in mind that the frequencies of multiple solitons have to be compared to those of the corresponding single soliton oscillations, which deviate significantly from the asymptotic prediction, depending on amplitude and dimensionality.

#### 3.3.3 Multiple Oscillating Solitons

As discussed in chapter 2.3, two dark solitons interact repulsively with each other. Assuming now a situation, where two dark solitons oscillate symmetrically in a trapped Bose-Einstein condensate, this interaction will modify their oscillation frequencies. Since the strength of interaction between the two solitons depends on their velocities, which in turn depend on the oscillation amplitude, it can be expected that the modification of the soliton oscillation frequencies depends on their oscillation amplitude.

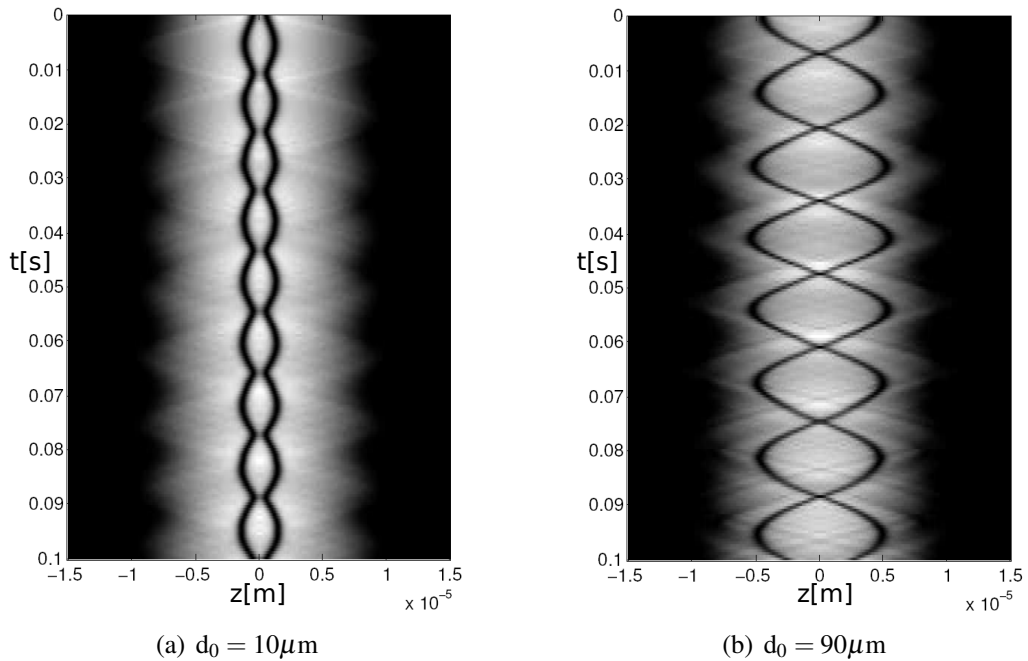


Figure 3.8: Two dark solitons with different initial distances  $d_0$  oscillating in a harmonically confined Bose-Einstein condensate, calculated using the NPSE

Figure 3.8 shows the oscillation of two dark solitons in a harmonically confined Bose-Einstein condensate for different initial distances of the solitons, obtained from a nu-

### 3 Dark Solitons in Bose-Einstein Condensates

merical time evolution of the non-polynomial Schrödinger equation. The trapping frequency of the confining potential is  $\nu_z = 50$  Hz,  $\nu_{\perp} = 1000$  Hz and the number of atoms is  $N = 1000$ . These parameters will be exemplarily used throughout this section.

The initial wave function containing the two solitons was determined as described in section 3.3 but in this case, the soliton wave function was multiplied twice to the ground state of the condensate. The wave functions of the two solitons are not ideal and some radiation is produced during the first milliseconds (see section 3.2.1), that also oscillates in the cloud. After this initial radiation, the two solitons are stable and their oscillation frequencies can be investigated.

As expected, the oscillation frequencies differ for the two different oscillation amplitudes. In figure 3.8(a), the effect of the repulsion between the two solitons is also observable. The solitons start at  $t = 0$  very close to each other and are repelled away from the center of trap before they turn around in the effective harmonic potential and approach each other again. This can not be observed in 3.8(b) where the solitons start so far away from each other that they are first accelerated by the effective harmonic potential towards the center where they are repelled by each other and move outwards again.

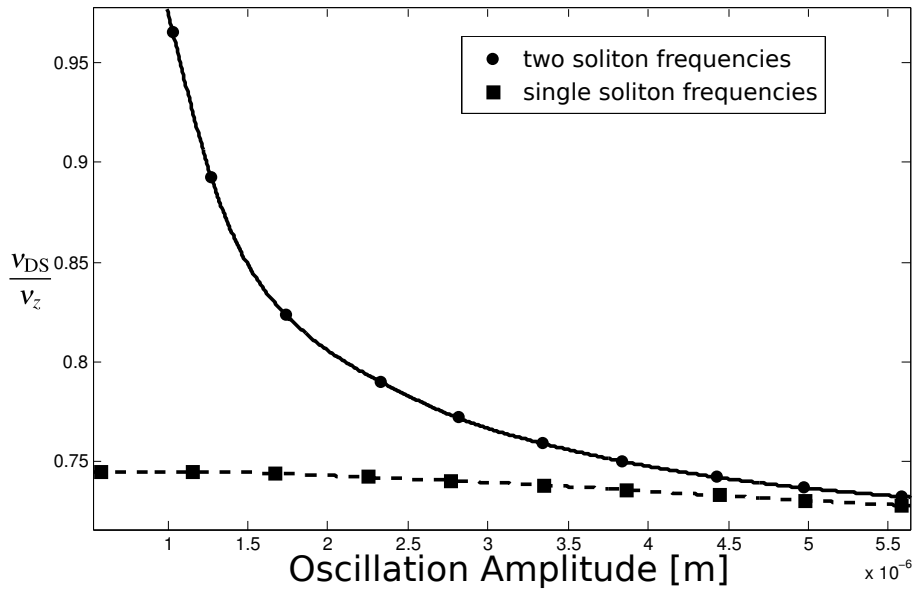


Figure 3.9: The normalized oscillation frequencies of two dark solitons as a function of their oscillation amplitude (dots, full line) compared to those of single dark solitons (squares, dashed line)

To investigate the effect the oscillation amplitude has on the frequency of the solitons figure 3.9 shows the oscillation frequencies of two dark solitons oscillating in the condensate for different oscillation amplitudes. The frequencies are normalized to the trap frequency. The oscillation frequencies for a single soliton under the same conditions are also shown in the graph.

Note, that the frequency of the two soliton oscillation has been obtained by applying a fit function  $d|\sin(2\pi\nu_z t)| + d_0$  to the soliton trajectories which describes the oscillation

### 3.3 Dynamics of Dark Solitons in Harmonically Confined Condensates

of their distance from each other. This avoids having to answer the question whether the solitons are transmitted or reflected at the collision point. The maximum distance that the two solitons assume is  $d + d_0$ . The offset  $d_0$  is introduced because for small oscillation amplitudes, the minima that constitute the solitons do not meet at the center of the trap (see figure 3.8(a)) and the solitons always maintain a minimum distance. In order to compare the amplitude dependence of the two soliton frequencies with the single soliton frequencies, the amplitude, which is well defined in the single soliton case, is in the two soliton case taken to be  $(d + d_0)/2$  which amounts to the maximum distance the solitons move from the center of the trap.

The effect of the different oscillation amplitudes on the oscillation frequencies is clearly visible. For large oscillation amplitudes the oscillation frequencies differ only very slightly from those of single solitons oscillating in the trap. The smaller the amplitude gets the higher is the oscillation frequency and the larger the deviation from the single soliton frequency.

This behavior is qualitatively explained by considering that for smaller oscillation amplitudes, the velocities of the solitons upon collision with each other are also smaller than the velocities for large amplitudes. Looking at figure 2.4, which shows the phase shifts two solitons acquire upon collision with each other depending on their velocities, it is obvious that for smaller velocities the effect of the interaction is much stronger, leading to a larger increase of the oscillation frequency since the phase shifts always act in the direction of motion of the solitons.

#### Application of the Effective Interaction Potential

To investigate the contributions of the interaction to the oscillation frequencies more closely the effective interaction potential of section 2.3.3 can be employed. The repulsive potential between two solitons given by equation 2.13, scaled to the physical units of the homogeneous one-dimensional Gross Pitaevskii equation, reads:

$$V_{\text{int}}(z, v) = \frac{\mu B^2}{2m \sinh(2B \frac{z}{\xi})} \quad B = \sqrt{1 - \frac{v^2 \hbar^2}{c^2 \mu^2}} \quad (3.28)$$

Considering now that the harmonic confinement of the Bose-Einstein Condensate leads to an effective external harmonic potential, the total potential determining the evolution of a soliton in the trapped condensate can be written down as

$$V(z, v) = V_{\text{int}}(z, v) + V_{\text{ext}}(z) = \frac{\mu B^2}{2m \sinh(2B \frac{z}{\xi})} + (2\pi v_{\text{eff}})^2 \frac{z^2}{2} \quad (3.29)$$

The frequency  $v_{\text{eff}}$  of the effective harmonic potential for the dark solitons is taken to be the frequency of a single soliton oscillating in a Bose-Einstein Condensate. As seen in section 3.3.2, this oscillation frequency deviates from the asymptotic prediction  $v_{1s} = v_z/\sqrt{2}$  depending on the oscillation amplitude and the dimensionality of the system. In order to apply this potential to a certain physical situation, the single soliton frequency

### 3 Dark Solitons in Bose-Einstein Condensates

is obtained from numerical time evolutions of the non-polynomial Schrödinger equation for a condensate with a single oscillating soliton.

The parameters  $\mu$  and  $\xi$  are the one-dimensional chemical potential and healing length, since the potential was derived from the homogeneous one-dimensional nonlinear Schrödinger equation and rescaled to the units of the homogeneous one-dimensional Gross-Pitaevskii equation. For the adaption of the potential to the three-dimensional case,  $\mu$  is taken to be the chemical potential obtained from the three-dimensional Gross-Pitaevskii equation and  $\xi$  is taken to be the associated healing length  $\xi = \sqrt{\hbar/(m\mu)}$ . This choice is not obvious, since these quantities for the three dimensional case are not in general applicable to the homogeneous one-dimensional situation. It will be justified a posteriori by a comparison of the results given by the potential with those of the evolutions of the non-polynomial Schrödinger equation.

The potential can now be used to derive the Lagrangian equations of motion for the two oscillating solitons (equation 2.18) and the resulting differential equations can be solved numerically to obtain the trajectories of the two solitons. Figure 3.10 shows the comparison between these trajectories and the density evolution plot for two oscillating solitons determined with the non-polynomial Schrödinger equation. It can be seen that even though the effective potential was derived for the purely one dimensional, homogeneous case the oscillation pattern of two solitons in a harmonic trap is very well reproduced if the effective harmonic potential is adjusted to the frequency of a single oscillating soliton and  $\mu$  and  $\xi$  in the effective interaction potential are taken from the three-dimensional Gross-Pitaevskii equation.

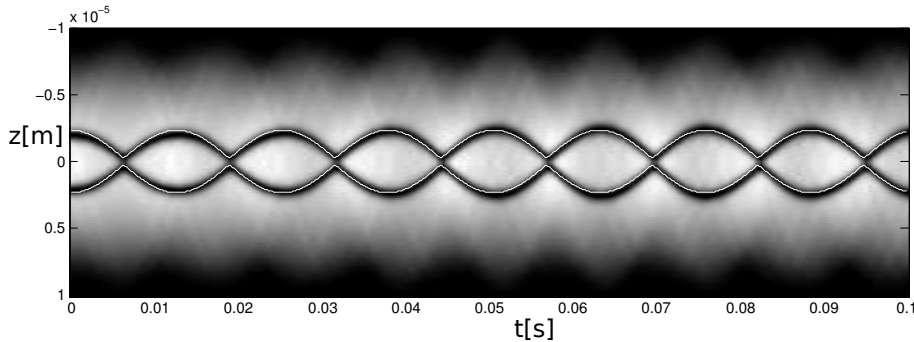


Figure 3.10: The oscillation of two dark solitons calculated with the NPSE (density plot in the background) and the soliton trajectories obtained from the effective potential (full lines)

To investigate this more quantitatively, Figure 3.11 shows a comparison between the oscillation frequencies of two solitons oscillating with different amplitudes obtained from the effective potential with those obtained from the non-polynomial Schrödinger equation.

The overall agreement of the frequencies obtained from the effective potential with those from the non-polynomial Schrödinger equation is very good, considering the idealizations contained in the effective interaction potential. For large amplitudes, the effective potential slightly overestimates the frequencies while for small amplitudes, it underestimates them. The deviations for the parameters used are at most 4%.

### 3.3 Dynamics of Dark Solitons in Harmonically Confined Condensates

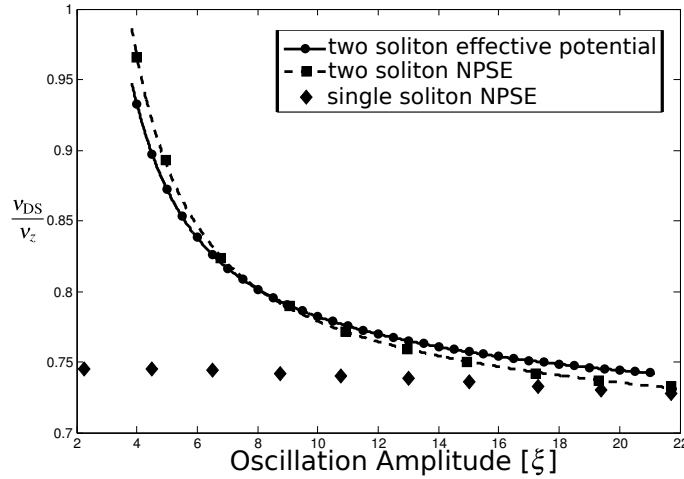


Figure 3.11: The oscillation frequencies of two dark solitons as a function of their oscillation amplitude determined with the NPSE (squares, dashed line) and with the effective potential (dots, full line) and the corresponding frequencies of single oscillating dark solitons (diamonds)

The effective potential provides a direct insight into the different contributions to the deviations from the asymptotic prediction. Since it incorporates the effects due to dimensionality directly via the frequencies of the oscillations of single solitons, the upshift from these frequencies seen in figure 3.11 can be attributed solely to the interaction of dark solitons.

As mentioned in chapter 2.3.3, the second advantage of the effective interaction potential is, that it can be applied to arbitrary numbers of solitons. To see this, it is applied to another experimentally relevant case of three solitons in a Bose-Einstein condensate of which one is stationary at the center of the trap and the other two oscillate to the left and right of the stationary soliton.

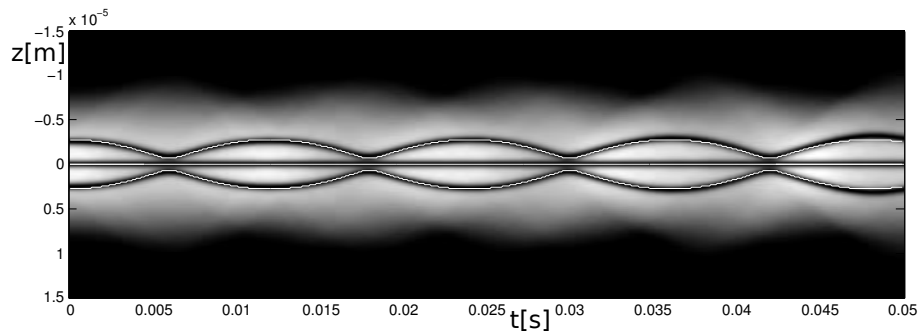


Figure 3.12: The oscillation of three dark solitons determined with the NPSE (density plot in the background) and the soliton trajectories obtained from the effective potential (white lines)

Figure 3.12 shows such an oscillation. The density plot in the background of the picture is calculated using the non-polynomial Schrödinger equation. The white lines indicate the

### 3 Dark Solitons in Bose-Einstein Condensates

trajectories obtained from the effective interaction picture which are in good agreement with the soliton trajectories of the non-polynomial Schrödinger equation. In this case the generalization of the potential for asymmetric collisions (equation 2.19) has to be used, since the collisions between the solitons are not symmetric anymore and more than two solitons are involved in the collisions.

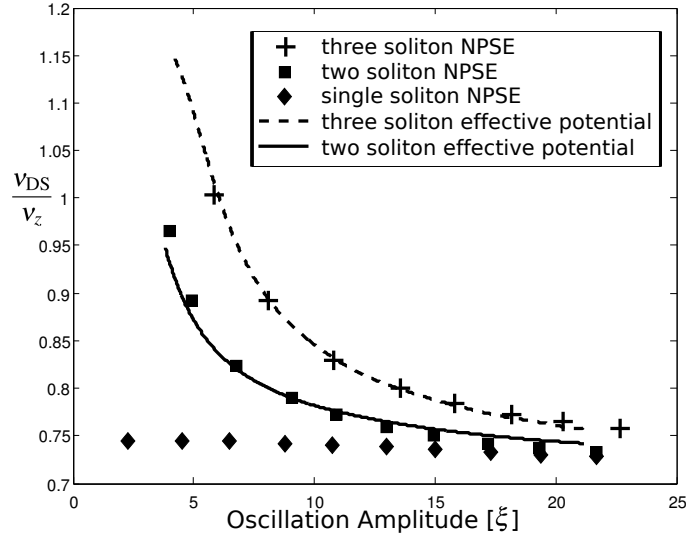


Figure 3.13: The oscillation frequencies of dark solitons as a function of their oscillation amplitude determined with the NPSE for one soliton (diamonds), two solitons (squares) and three solitons (crosses) and the frequencies determined with the effective interaction potential for two solitons (full line) and three solitons (dashed line)

The effect of the interaction on the oscillation frequencies is even stronger in the case of three solitons, as shown in figure 3.13. The deviations of the frequencies from the single soliton oscillations are significantly higher for the three soliton case than for the two soliton case. This is easily explained by considering that the oscillating solitons in the three soliton case always collide with the stationary soliton and not with another moving soliton. Thus, the total velocity of the solitons involved in the collision is lower for the three soliton case, which, as shown in figure 2.4, leads to larger phase shifts and thus higher oscillation frequencies.

The relation between the oscillation frequencies of dark solitons and their oscillation amplitudes can now be used to experimentally investigate the interactions of dark solitons (see chapters 4 and 5). Solitons with different oscillation amplitudes are produced experimentally and their oscillation frequency is recorded to reproduce this amplitude dependence of their oscillation frequency. The effective potential can then be used to clearly distinguish between effects stemming from the dimensionality of the condensate and effects stemming from the interaction of the solitons to show that observed deviations of the frequency from the asymptotic value of  $v_z/\sqrt{2}$  indeed result from both effects and how large the different contributions are.

Note that the distinction between effects stemming from the dimensionality and those stemming from the interaction between the solitons is slightly misleading. Obviously, the

### *3.3 Dynamics of Dark Solitons in Harmonically Confined Condensates*

effective potential incorporates the effects the dimensionality has on the single solitons directly via an effective harmonic potential. But, as it can be seen in equation 3.28, the interaction potential itself depends on the chemical potential  $\mu$  of the condensate. This chemical potential is directly influenced by the dimensionality of the system and thus, the interaction strength between the two solitons depends as well on the dimensionality.

The distinction between the effects of dimensionality and the effects of interaction in the following means to distinguished between effects that are always present for dark solitons in Bose-Einstein condensates resulting from the dimensionality of the system and effects that only appear when two or more solitons interact with each other, even though the latter are also influenced by the dimensionality.



# 4 Creation and Observation of Oscillating Dark Solitons

As explained in the previous chapter, the interaction between dark solitons can be investigated experimentally by measuring their oscillation frequencies and amplitudes in harmonically confined Bose-Einstein condensates. Since the interaction can only be observed if two or more solitons oscillate in the condensate, a method to produce different numbers of solitons oscillating with different amplitudes is required.

## 4.1 Creation of Dark Solitons in a Bose-Einstein Condensate

Different methods to create dark solitons in Bose-Einstein condensates have been suggested. Methods that rely on the direct manipulation of the condensate wavefunction imprint a local phase change to the condensate wave function, locally modify its density distribution or use a combination of both techniques [51].

For phase imprinting, an additional potential is introduced to one part of the condensate which leads to a different time evolution of its phase. If this additional potential is spatially well localized, a localized phase difference at the interface between the two regions of the condensate develops. This technique has been used to create dark solitons in elongated Bose-Einstein condensates [18, 19] and very recently a collision of two dark solitons created this way has been observed [25].

A density modification technique can also rely on the manipulation of the condensate wave function via an additionally introduced potential [52]. A different approach has been taken by Dutton et al. [21], who created a density depletion in a Bose-Einstein condensate by shining in an ultra-slow light pulse, creating quantum shock waves that shed dark solitons.

### 4.1.1 Dark Soliton Production through Matter Wave Interference

Another approach to the creation of dark solitons takes advantage of interference phenomena in collisions between two separate Bose-Einstein condensates. As first demonstrated by Andrews et al. [53], two condensates that collide with each other produce a pattern of interference fringes. For the description of this interference pattern, that deviates from a

#### 4 Creation and Observation of Oscillating Dark Solitons

simple linear superposition of the two wavefunctions of the separate condensates, the nonlinear interaction of Bose-Einstein condensates has to be taken into account [54] which can lead to the formation of dark solitons [55].

Scott et al.[56] investigated these nonlinear interference patterns theoretically by considering two Bose-Einstein condensate ground states, displaced equal and opposite amounts from the center of a harmonic trap, which are released and collide in the center. In the collisional dynamics, they found two different regimes to be distinguished, depending on the relation between the kinetic energy the condensates acquire before colliding and the nonlinear interaction energy.

If the kinetic energy of the two condensates exceeds the nonlinear interaction energy, the clouds will essentially pass through each other while exhibiting an interference pattern that closely corresponds to the one expected for linear superposition of the individual wavefunctions of the condensates. A critical initial distance of the condensates to be in this regime is shown to be

$$d > \pi \left( \frac{6N\hbar a_s}{v_z m} \right)^{1/3} \quad (4.1)$$

If the initial distance between the condensates is smaller than  $d$ , the nonlinear interaction energy dominates the kinetic energy. The interference pattern experiences nonlinear features and some of the central interference fringes develop into dark solitons. This happens because a dark soliton, as mentioned in chapter 3.2.2, is stable, constituting a local energy minimum of the governing nonlinear equation, and a deformation towards the filling of a dark soliton would be energetically unfavorable. Thus, once the shape and phase distribution of an interference fringe are close enough to that of a dark soliton, the nonlinear dynamics, approaching the minimalization of energy, lead to a stabilization of this fringe as a dark soliton.

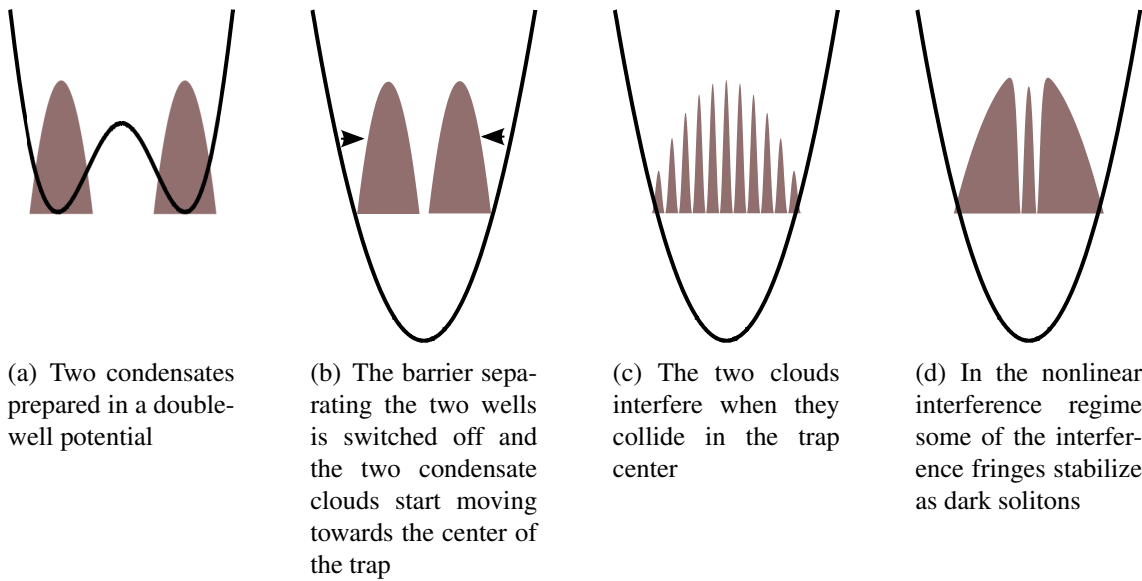


Figure 4.1: Schematic depiction of the dark soliton creation process

#### 4.1 Creation of Dark Solitons in a Bose-Einstein Condensate

A schematic depiction of this production process is shown in figure 4.1 for two condensates initially prepared in a double well potential.

The two colliding condensates are considered to have the same phase and as a result, the interference fringe pattern will be symmetric about the center of the trap with a density peak exactly at the trap center. Thus, the number of formed solitons will always be even. The total number of solitons formed in the collision of the condensates depends on the kinetic energy the condensates acquire while moving down the harmonic potential. This can be seen in figure 4.2 where the numerical time evolution of two condensate clouds in the situation described above is shown for different speeds with which the separating barrier is removed.

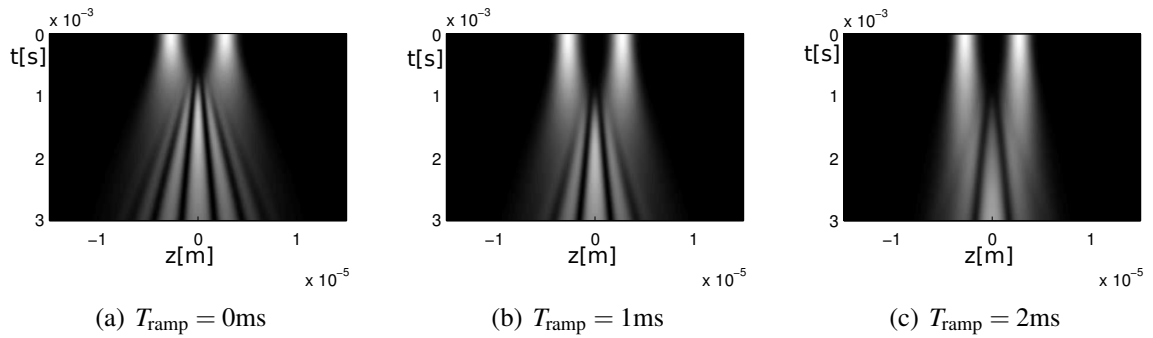


Figure 4.2: The condensate evolution during and after the soliton creation process for different ramping times  $T_{\text{ramp}}$  of the barrier

In figure 4.2(a), the barrier is instantaneously removed. The condensates acquire a high kinetic energy while they are accelerated by the harmonic potential. After the collision three pairs of solitons are formed, which travel outwards from the center of the trap. In figure 4.2(b), the height of the barrier is linearly ramped down over 1ms. The condensates are slowed down in their evolution, acquire less kinetic energy and only two pairs of solitons are formed. For a ramping time of 2ms, as seen in figure 4.2(c), only one pair of solitons is formed. The trapping frequencies in this case are  $\nu_z = 50$  Hz and  $\nu_{\perp} = 500$  Hz, the number of atoms is  $N = 1000$  and the initial barrier height is  $V_0 = 1000$  Hz (see section 4.1.2).

The same effect can also be achieved by choosing a different trapping frequency of the harmonic confinement, which lowers or raises the potential energy of the two wells. This is limited in practice by the fact that for a weaker harmonic confinement the difference between the potential energy of two adjacent wells is also lowered which can lead to the initial population of more than two wells. In the collision of more than two condensates, solitons will still be created but since they originate from several points their dynamics will be more complicated, with multiple solitons moving in different directions, colliding very frequently.

Another way to influence the number and distance of the created solitons is by adjusting the initial barrier height. For a higher barrier, the distance between the two wells increases slightly, and the kinetic energy of the condensates is higher. Experimentally, this is limited

#### 4 Creation and Observation of Oscillating Dark Solitons

for high barriers by the fact, that a sufficient coupling for the two clouds has to be given in order to prevent a dephasing due to the finite temperature [57] and thus the barrier can not be chosen too high.

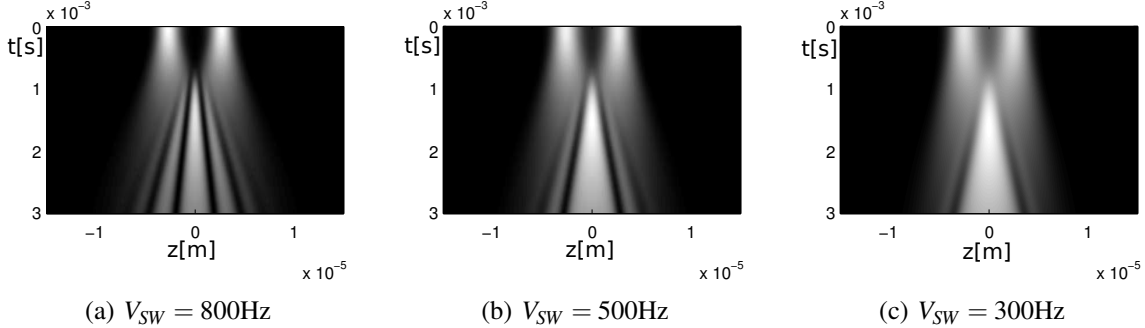


Figure 4.3: The condensate evolution during and after the soliton creation process for different heights of the standing wave potential separating the two wells

Figure 4.3 shows the condensate evolution for different initial barrier heights. In this case, the barrier is removed instantaneously, the trapping frequencies are again  $\nu_z = 50$  Hz and  $\nu_{\perp} = 500$  Hz and the number of atoms is  $N = 1000$ . Again, for an initially higher barrier, which increases the initial well distance and thus the kinetic energy upon collision, more solitons are formed. For lower barriers less solitons are formed and their initial velocity increases, which can be seen very well in 4.3(c), where the solitons are only faintly visible, due to their high velocity and low darkness.

The transverse trapping frequency  $\nu_{\perp}$ , varied over our experimentally possible range, and the total atom number both have only a very slight effect on the number and distance of the produced solitons.

Using the initial barrier height and the ramping time of the barrier it is thus possible to create different numbers of solitons with different initial velocities in a harmonically confined Bose-Einstein condensate, which is done experimentally as detailed in the next section.

#### 4.1.2 Experimental Realization

For the experimental realization of the creation of dark solitons a Bose-Einstein condensate of  $^{87}\text{Rb}$  is prepared in a double well potential. The  $^{87}\text{Rb}$  atoms from a heated dispenser are gathered in a  $2\text{D}^+$  magneto-optical trap (MOT)[58] that confines and cools them in two spatial directions and creates a collimated beam of atoms that is subsequently captured by a three dimensional MOT [59]. After cooling in the MOT, all atoms are optically pumped to the  $|F = 2, m_F = 2\rangle$  state in which they are trapped by a magnetic quadrupole trap with a time-orbiting potential [60]. In this trap, the atoms are evaporatively cooled to temperatures slightly above the critical temperature of condensation. Afterwards, the atoms are transferred into an optical dipole trap, where they are further

#### 4.1 Creation of Dark Solitons in a Bose-Einstein Condensate

evaporatively cooled below  $T_c \approx 110\text{nK}$  and condense into a Bose-Einstein condensate. For more details about the condensation of  $^{87}\text{Rb}$  in our experimental setup, see [61].

The optical dipole trap is created by a laser beam at  $\lambda = 1064\text{nm}$  which is far red detuned from the optical resonance at  $780\text{ nm}$  of the  $|F = 2\rangle \rightarrow |F' = 3\rangle$  transition of the  $D_2$  line. The  $^{87}\text{Rb}$  atoms are high field seeking in this case and the gaussian intensity distribution of the beam creates an effective potential with a minimum at the point of highest intensity. The gaussian waist of the beam is approximately  $5\ \mu\text{m}$  and creates a strong confinement in the transverse direction. The Rayleigh range is about  $70\ \mu\text{m}$  which creates a weaker confinement in the longitudinal direction. The strength of the confinement can be adjusted by varying the intensity of the laser beam. The ratio between the transverse and the longitudinal confinement is  $v_{\perp}/v_z \approx 20$ . This optical dipole trap is called the charger. [62]

To increase the confinement along the longitudinal direction another laser beam is superimposed. This beam orthogonally crosses the charger and has an elliptic shape with waists of  $60\ \mu\text{m}$  in the longitudinal direction and  $120\ \mu\text{m}$  in the transverse direction of the charger.

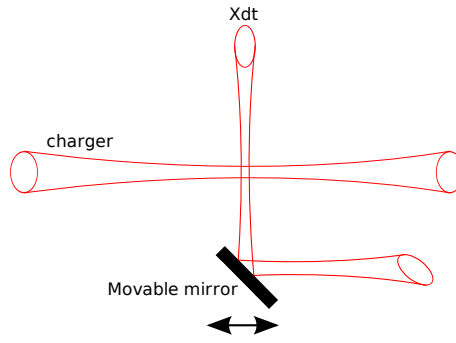


Figure 4.4: The setup of the crossed optical dipole trap

This crossed beam, which in the following will be referred to as the Xdt, leads to an additional confinement mainly in the longitudinal direction of the charger. The Xdt can be moved along this direction using a mirror mounted to a high precision piezo stage and the strength of the longitudinal confinement can be adjusted by varying the laser intensity. The combined crossed optical dipole trap is used in our experiments with transverse trapping frequencies of  $\nu_{\perp} = 408\text{ Hz}$  or  $\nu_{\perp} = 890\text{ Hz}$  and longitudinal trapping frequencies between  $\nu_z = 25\text{ Hz}$  and  $\nu_z = 58\text{ Hz}$ . A schematic depiction of the layout of the crossed optical dipole trap is shown in figure 4.4

To create the double well potential, a one-dimensional optical lattice, created by two laser beams with  $\lambda = 843\text{ nm}$  crossed in the region of the dipole trap under an angle of  $8^\circ$ , is superimposed on the crossed optical dipole trap. This creates a standing wave lattice potential with a lattice spacing of  $l = 5.7\ \mu\text{m}$ . The superposition of the lattice potential with the optical dipole trap leads to a modulation of the harmonic potential as shown in figure 4.5.

The total external potential created by the superposition of the harmonic potential and

#### 4 Creation and Observation of Oscillating Dark Solitons

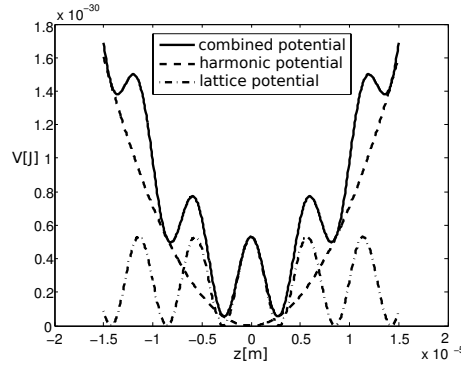


Figure 4.5: The sum of the lattice potential and the harmonic potential create a symmetric double well potential.

the lattice potential is given by

$$V(x, y, z) = \frac{m}{2}(\omega_x^2 x^2 + \omega_y^2 y^2 + \omega_z^2 z^2) + \frac{V_0}{2} 2\pi(1 + \cos(2\pi \frac{z}{l} + z_0)) \quad (4.2)$$

where the strength of the lattice potential  $V_0$  is given in Hz.

By adjusting the longitudinal position of the Xdt, the relative position  $z_0$  between the center of the harmonic trap and one of the maxima of the lattice potential can be made zero. The minima of the lattice to the left and right of the center of the harmonic trap form a symmetric double well potential. The other wells created by the lattice potential are shifted up in energy because they are situated further away from the center of the harmonic trap. If the atom number of the condensate is low enough or the longitudinal confinement high enough so that no other wells of the lattice can be populated with atoms, a symmetric double well potential with one Bose-Einstein condensate in each well is obtained. For more details about the creation of the double well potential see [63].

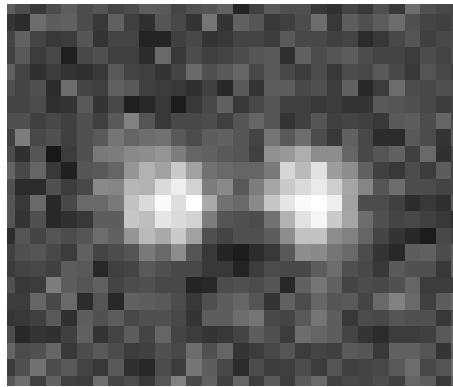


Figure 4.6: Absorption image of two condensates, containing a total of about 910 atoms, in the double well potential

Figure 4.6 shows the two condensates in a symmetric double well potential with a total of about 910 atoms, trapping frequencies of  $\nu_z \approx 63$  Hz and  $\nu_{\perp} \approx 408$  Hz and a barrier

## 4.1 Creation of Dark Solitons in a Bose-Einstein Condensate

height between the two wells of  $V_0 \approx 1050$  Hz.

The images of the condensate density as seen in figure 4.6 are obtained by absorption imaging of the condensate. A laser beam resonant to the  $|F = 2\rangle \rightarrow |F' = 3\rangle$  transition of the  $D_2$  line with a  $\sigma^+$  polarization is shined in. The atoms are kept spin polarized by a constant magnetic field so that all atoms absorb the imaging light. An objective images the beam on a CCD chip with a magnification of about 11.2. The pixel size of the CCD chip is  $6.45 \mu\text{m}$  so that the length of one pixel of the absorption image corresponds to  $0.58 \mu\text{m}$ . The resolution of the imaging system is approximately  $1 \mu\text{m}$ . Since the condensate absorbs the resonant imaging light, the atoms gain energy and after the imaging process, the Bose-Einstein condensate is destroyed. Thus, to observe a time evolution using this imaging technique, one has to repeat the experiment for every time step and take an image at a different point in time of the condensate evolution. For more details on the imaging system see [64].

The initial trap configuration used for the creation of dark solitons is that of  $\nu_z = 63$  Hz and  $\nu_{\perp} = 408$  Hz. The barrier height is experimentally adjusted to be low enough to allow enough coupling between the two condensates in order to prevent a dephasing [57], ensuring that the relative phase of the two clouds is always close to 0. In our experiments, the height of the initial barrier is always around 1000 Hz and the total number of atoms ranges from 860 to 2080. The phase fluctuations for smaller barrier heights can be used to determine the temperature of the Bose-Einstein condensate [65]. In our case, the temperature is on the order of 10 – 20 nK.

The barrier between the two condensates is then instantaneously removed and the two condensates collide in the center of the trap. The critical distance for the formation of solitons (equation 4.1) in our experiments is on the order of  $25 \mu\text{m}$ , which is much larger than the well distance of  $5.4 \mu\text{m}$  and thus, dark solitons develop from the interference of the two condensate clouds.

The evolution of the solitons in the condensate is investigated for different longitudinal trapping frequencies  $\nu_z$ . Thus, during the first few milliseconds after switching off the barrier, the longitudinal trapping frequency is ramped down to the desired final value for  $\nu_z$ . The duration of the ramp is experimentally adjusted to prevent excitations of quadrupole oscillations of the whole cloud after merging, which naturally arise when two condensates collide.

Figure 4.7 shows a time evolution of the longitudinal density of the condensate during such a soliton formation process. At each time step longitudinal density distributions from nine realizations of the condensate, obtained from absorption images, are averaged. At  $t = 1$  ms, the two condensates initially in the double well can be seen. At  $t = 2$  ms the condensates have already collided and the central maximum has formed. Close to the maximum, two dark solitons are recognizable. At  $t = 3$  ms and thereafter, two additional solitons can be observed that move further out in the trap

This production method is used for all experiments conducted to determine the oscillation frequencies of two solitons in harmonically confined Bose-Einstein condensates. Special attention is paid to the visibility of the solitons during their further evolution and the initial barrier height as well as the ramping time of the trap frequency are determined

## 4 Creation and Observation of Oscillating Dark Solitons

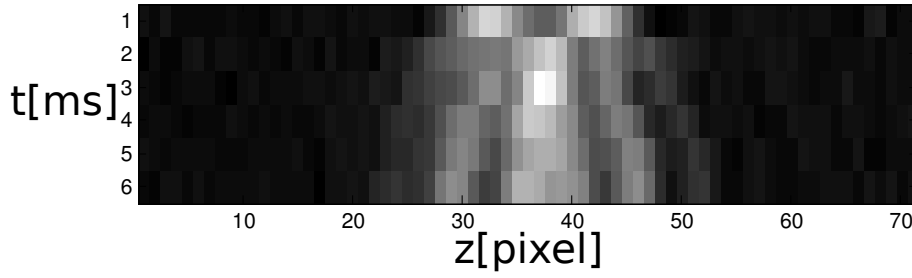


Figure 4.7: Time evolution of the experimentally observed longitudinal density profile for the first six milliseconds of the creation process. Each horizontal line is the average over nine realizations of the experiment.

experimentally to maximize the reproducibility of the soliton evolution. In section 4.2 the observed soliton oscillations will be shown and chapter 5 will discuss the experimental results on the oscillation frequencies of the solitons created in this way and how conclusions about their interactions can be drawn.

### 4.1.3 Soliton Creation with Initial Phase Difference

The initial position of dark solitons formed in the collision of Bose-Einstein condensates depends on the phase difference between the two condensates. In the previous section, the phase difference was always taken to be zero, leading to an even number of solitons symmetric about the center of the trap. If the condensates instead have a phase difference of  $\pi$  before the collision, one interference fringe forms in the center of the trap and as a result, the total number of solitons is odd and one soliton is stationary in the center of the trap.

This phase difference has been applied to the ground state wave function of a double well potential and the subsequent collision of the condensates and the creation of solitons in numerical a numerical time evolution is shown in figure 4.8.

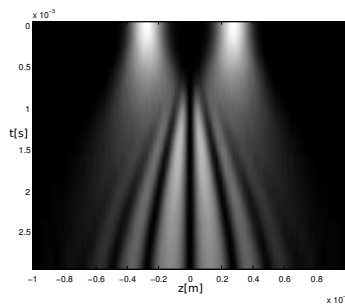


Figure 4.8: A phase difference of  $\pi$  between the condensates in the double well leads to the creation of one stationary soliton in the center of the trap during the collision of the two condensates

As expected, as the clouds collide one stationary soliton is created in the center of the

#### 4.1 Creation of Dark Solitons in a Bose-Einstein Condensate

trap and an equal amount of additional solitons to the left and right of the stationary one.

The experimental realization of such a phase modification of the condensate would best be achieved by employing an additional potential acting only on one of the wells, much like the phase imprinting methods [18, 19] mentioned above.

With our experimental setup, the only way to manipulate the relative phase of two condensates in the double well potential is to use the possibility of moving the harmonic trap along the longitudinal axis, which can be done by moving the Xdt beam. Moving the harmonic potential with respect to the standing wave creating the double well barrier results in an asymmetric double well, since the two wells created by the standing wave have their minima at different heights of the harmonic potential (see fig 4.9).

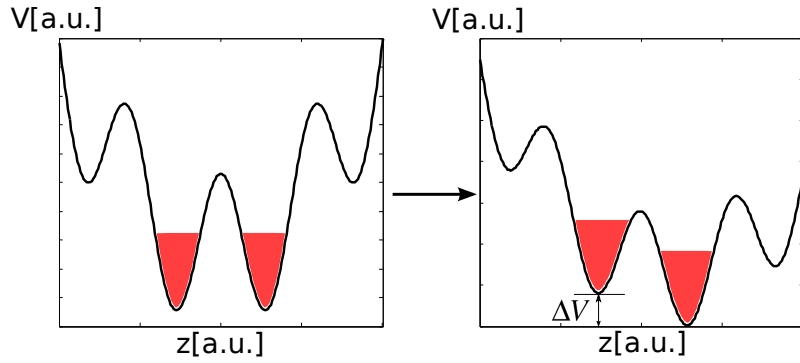


Figure 4.9: Moving the harmonic potential along the longitudinal direction creates an asymmetry in the double well potential which leads to a potential difference between the two wells

The different potential energy of the condensates in the two wells leads to a differently fast time evolution of their global phases and over time they acquire a phase difference.

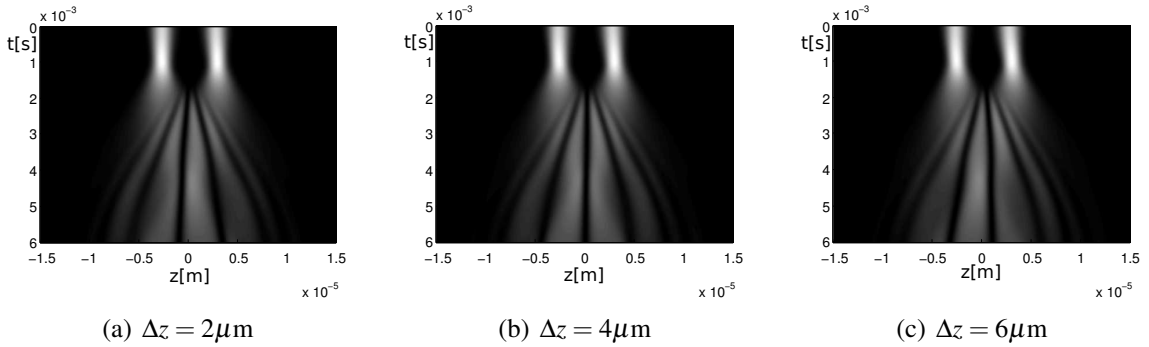
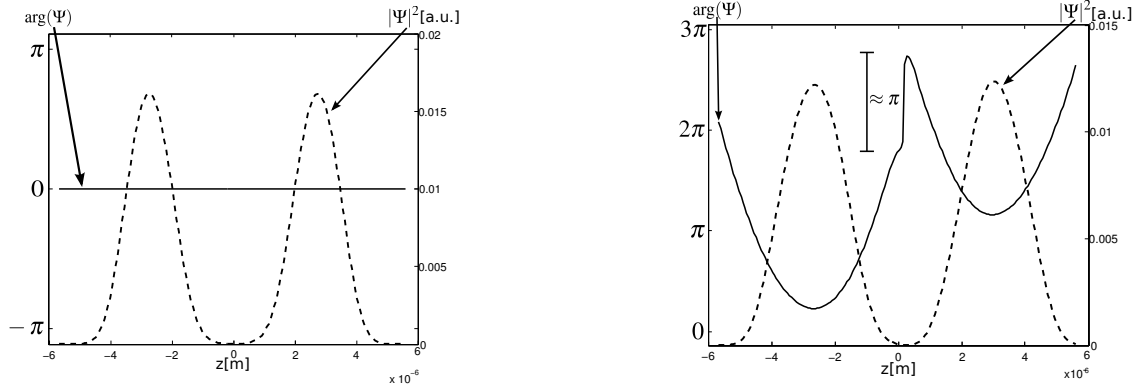


Figure 4.10: The condensate evolution during and after 1 ms of phase accumulation for different displacements  $\Delta z$  of the longitudinal harmonic potential

Figure (4.10) shows the numerical time evolution of the condensate during and after the modification of the relative phase. In this case, the parameters are  $v_z = 50$  Hz,  $v_\perp = 500$  Hz and  $N = 1000$ . The initial barrier height for the ground state determination is  $V_0 = 1000$  Hz. The barrier height is then set to  $V_0 = 2000$  Hz and the longitudinal

#### 4 Creation and Observation of Oscillating Dark Solitons

trapping potential is displaced along the longitudinal axis by different amounts  $\Delta z$  for one millisecond. During this time, the accumulation of the phase difference takes place. After 1 ms, the harmonic trap is shifted back to its original position and the barrier height is set back to  $V_0 = 1000$  Hz and from there on ramped down over 3 ms. It can be seen how the accumulated phase over a fixed time depends on the displacement  $\Delta z$ . For  $\Delta z = 4 \mu\text{m}$ , the accumulated phase is very close to  $\pi$  and the desired soliton pattern with one stationary soliton in the center forms. The height of the potential barrier is increased during the phase accumulation process in order to reduce tunneling of the atoms between the wells, which would lead to a relative atom number difference between them.



(a) The ground state density distribution in the double well potential at  $t = 0$  (dashed line) and the phase of the wavefunction, which is flat over the two condensates (full line)

(b) The density distribution at  $t = 1.6$  ms, after the phase accumulation process (dashed line). The phase of the wavefunction (full line) exhibits a phase jump of  $\pi$  between the two condensates

Figure 4.11: The density distributions and phase of the wave functions before and after the phase accumulation process

Figure 4.11 shows the density distributions and the phase of the wave functions before the phase accumulation process (figure 4.11(a)) and at  $t = 1.6$  ms (figure 4.11(b)), shortly before the two condensate clouds merge during the ramping down of the barrier. At  $t = 0$ , the phase of the wavefunction is flat over the extension of the two condensates. This is the ground state wavefunction of the double well potential. At  $t = 1.6$  ms, after the double well potential has been asymmetric for 1 ms and while the barrier is being ramped down, the phase of the two condensates is not flat anymore over the extension of the condensates but instead exhibits a parabolic shape, which is due to the different phase evolutions at points in the separate wells with different potential energies. More importantly, at the center between the two condensates, the phase of the wave function shows a sharp jump of  $\pi$ . This is the desired feature that leads to the formation of the stationary soliton in the center of the trap.

This phase accumulation process is the general procedure that is used in the experiment to create three oscillating dark solitons. The displacement and the barrier height during the phase accumulation time are experimentally adjusted to result in a stable pattern of three solitons being created. To investigate the oscillations for different aspect ratios, the

trap frequency in the longitudinal direction is again ramped from its start value of 63Hz to the desired final values and the ramping time is experimentally adjusted to minimize quadrupole oscillations of the condensate cloud after the collision.

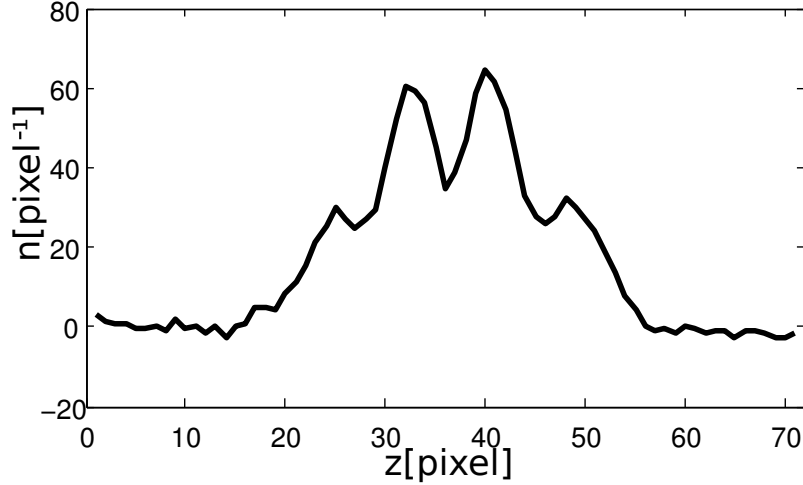


Figure 4.12: The longitudinal density of the condensate 4ms after the creation process with phase manipulation, averaged over 16 realizations of the experiment. The stationary soliton in the center of the trap and the two solitons to the left and right of the stationary one can be observed.

Figure 4.12 shows the first result on the creation of three solitons. The graph shows an average over 16 longitudinal density profiles of the condensate cloud 4ms after the ramping of the longitudinal trap frequency. The fact that the solitons are still visible after averaging over so many realizations shows that the phase difference accumulation process is stable enough to reproducibly create three dark solitons in a Bose-Einstein condensate.

## 4.2 Observation of Oscillating Solitons

For the measurements of the two soliton frequencies, solitons are created with the production method explained in section 4.1.1 for twelve different parameter sets. The parameters are in the ranges:  $v_z$  between 25 Hz and 60 Hz,  $v_\perp$  either 407.5 Hz or 890 Hz and the Atom number of the condensate  $N$  is between 860 and 2080.

For each data point, a Bose-Einstein condensate is produced, the solitons are created and the confining potential is ramped to the desired values. The end of the ramping process marks the start of the evolution time of the solitons, which now oscillate in the harmonically confined condensate. After a certain evolution time an absorption image of the condensate is taken, which destroys the Bose-Einstein condensate. Then, a new Bose-Einstein condensate is produced, the solitons are created and the confining potential is set using the same parameters. After a slightly longer evolution time, an absorption image is taken again. This process is repeated for a certain number of different points in time during the desired total evolution time. Typically, the spacing between two points in time

#### 4 Creation and Observation of Oscillating Dark Solitons

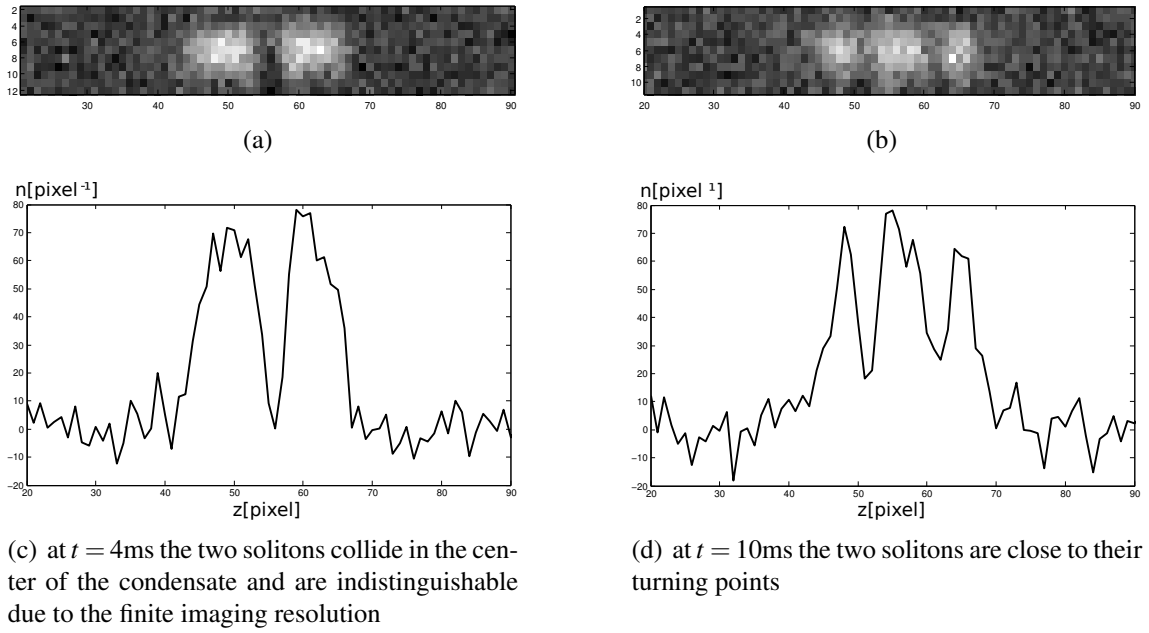


Figure 4.13: Absorption images of the condensate cloud with the dark solitons at different times  $t$

is 1 ms or 2 ms and the total evolution time ranges from 60 ms to 120 ms. After the image at the last point of the evolution time is taken, the whole process is repeated between 3 and 7 times.

At the end of the measurement for one parameter set, at each point in time during the evolution of the wave function between 3 and 7 images of the condensate density have been taken, which amounts to a total of 90 to 490 images per parameter set.

Figures 4.13(a) and 4.13(b) show exemplary absorption images of the condensate at different points in time for  $v_z = 53\text{ Hz}$ ,  $v_\perp = 407.5\text{ Hz}$  and an average atom number of  $N = 1710$ . The images are then summed over the transverse axis of the condensate to obtain their one-dimensional longitudinal density distribution.

Figures 4.13(c) and 4.13(d) show the density distributions corresponding to the two-dimensional absorption images above. In figure 4.13(d), the two dips in the condensate density are two dark solitons very close to their outer turning points. One would expect from the theory that for these solitons with  $v \approx 0$  the condensate density at the minimum of the dip would be depleted down to zero. It has to be assumed that this is the case but the imaging resolution is not high enough to resolve this.

Figure 4.13(c) exhibits only one large dip at the center of the density distribution. At this time the solitons are very close to the point of closest proximity during their oscillation and due to the finite imaging resolution appear as one very deep dip. This does not mean that the two solitons necessarily pass through each other, since the resolution does not allow to distinguish between the characteristic structures for transmission and reflection at the collision points (see chapter 2.3.2). As it will be seen in chapter 5.2, a numerical investigation of the experimental situation suggests, that the solitons move

slowly enough to be considered as being reflected upon collision.

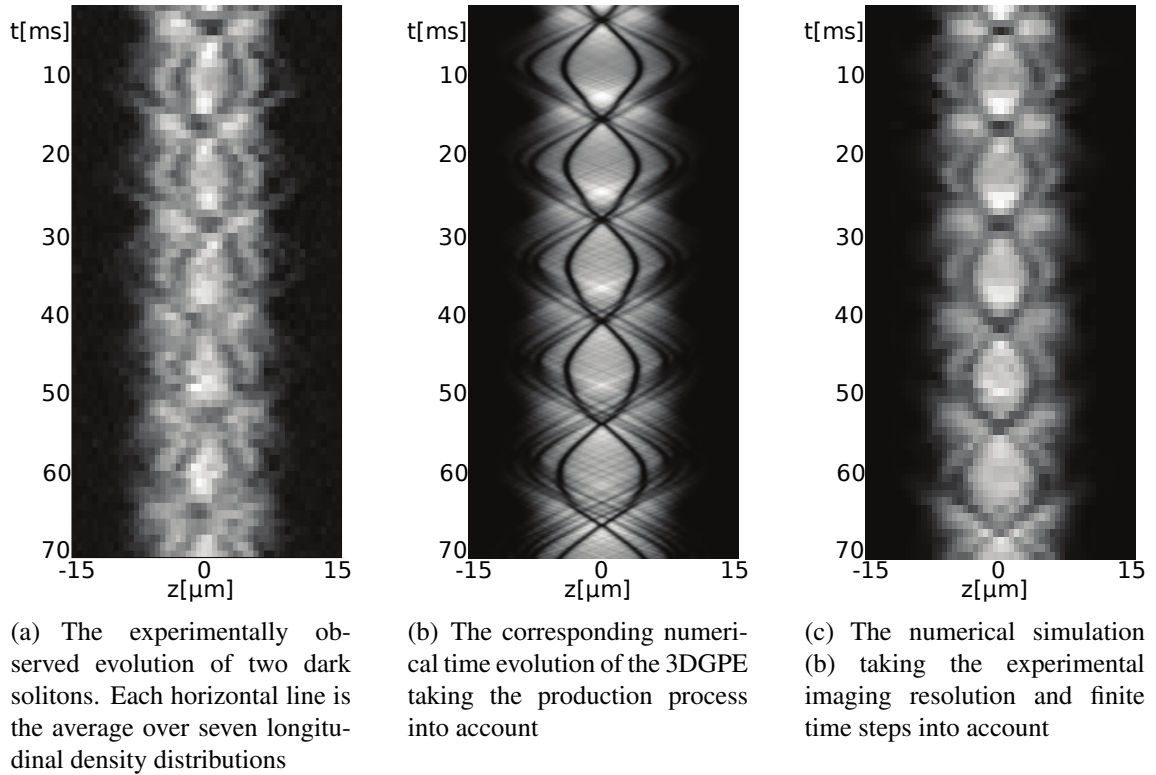


Figure 4.14: The time evolution of two dark solitons in a harmonically confined BEC, experimentally and numerically

To illustrate the complete oscillatory time evolution of the solitons, the one-dimensional density profiles of the cloud at consecutive moments during the evolution have been combined in figure 4.14(a). Each horizontal line corresponds to the average over seven one-dimensional density profiles at the given time step. In this case, the trap frequencies are  $\nu_z = 53\text{Hz}$  and  $\nu_{\perp} = 890\text{Hz}$  and the average atom number is  $N \approx 1710$ .

The oscillations of the solitons in the trap are clearly visible and six collisions between them are observed. This shows, that the solitons indeed oscillate in a trapped Bose-Einstein condensate and that they are stable over a timespan long enough to observe their oscillation and stable during collisions with each other.

Figure 4.14(b) shows the numerical simulation of the solitons conducted using the three-dimensional Gross-Pitaevskii equation. The simulation includes the full production process of the solitons, which is not shown in the figure since  $t = 0$  marks the end of the ramping time for the confining potential. It can be seen that two dark solitons oscillate close to the center of the trap and their oscillation dynamics shows good agreement with the one experimentally observed. Additionally, some solitons with a larger oscillation amplitude and smaller darkness are created in the production process. These solitons are only faintly visible in the experimental pictures due to their high velocity and lower contrast and their oscillation frequencies will not be investigated.

#### 4 Creation and Observation of Oscillating Dark Solitons

To compare the numerical simulation with the experimental data, in figure 4.14(c) the density evolution of the simulation is convolved along the longitudinal axis of the condensate (vertical axes in the figure) with a pointspread function with a width of 630 nm to take into account the resolution of the imaging system. Additionally, the time resolution is set to one density plot per millisecond as it is in the experiment.

As mentioned, the total observed evolution time ranges from 60 ms to 120 ms. This does not mean that all the solitons decay after this timespan. In fact, solitons are still observable after more than one second of evolution time but in general are less clearly identifiable after long evolutions. This is probably due to the thermodynamical instability discussed in chapter 3.2.2. The observation time for the soliton oscillation is limited by a dephasing of the soliton oscillations from realization to realization. This originates from variations in the experimental conditions, which in our case means mainly variations of the number of atoms in the condensate, for which the solitons experience slightly different oscillation frequencies. Thus, over longer evolution times the oscillations of the separate experimental realizations dephase and the trajectories of the solitons, that can be obtained by determining the positions of the solitons at each time step, smear out. Also, if the thermodynamical instability is the limiting factor for the visibility of the solitons, it will lead to an acceleration of the solitons and their oscillation amplitude will change over time. Thus, obtaining an oscillatory trajectory from the single soliton pictures is easier for more pictures at shorter evolution times than by increasing the evolution time.

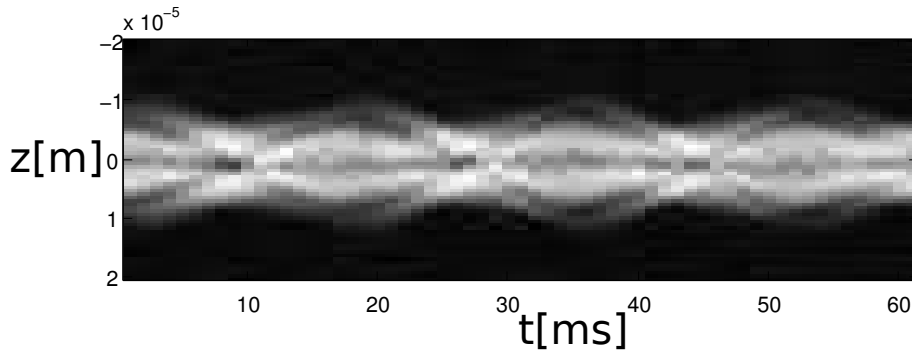


Figure 4.15: The experimentally observed time evolution of the longitudinal density of a condensate with three dark soliton. Each vertical line is the average over sixteen realizations of the experiment and the stationary soliton as well as the two oscillating solitons can be observed.

As explained in section 4.1.3, it is possible to modify the phase between the two condensate clouds in the double well potential before their collision and the production of solitons. This has been done experimentally to create three dark solitons of which two oscillate to the left and right of a third, stationary soliton situated in the center of the trap. Figure 4.15 shows the experimentally observed time evolution of the longitudinal density distribution for such a case. Each vertical line is the average over 16 longitudinal density distributions obtained from absorption imaging pictures of the condensate at the given point in time. The solitons behave exactly as expected. The central soliton remains stationary and the two outer ones oscillate and coincidentally collide with the central one.

## 4.2 *Observation of Oscillating Solitons*

The oscillation amplitude of the two outer solitons is very large and also a quadrupole oscillation of the cloud is present, both limiting the conclusions about interactions that can be drawn from this result.



# 5 Oscillation Frequencies and Interaction

To investigate the interaction of dark solitons, the oscillation frequencies of two dark solitons with different oscillation amplitudes are determined from the experimentally observed soliton oscillations. These oscillation frequencies can then be compared with the predictions from the effective interaction potential to identify the effects of the interaction.

## 5.1 Oscillation Frequencies

The oscillation frequencies of the dark solitons are extracted manually from the experimental data. The absorption images of the condensate representing its time evolution (see chapter 4.2) are summed over the transverse axis to obtain one-dimensional density distributions. These density distributions are then investigated one by one and the positions of the most prominent density dips (or, in the case of two solitons colliding in the center of the trap, the central dip) are recorded manually. In cases where it is not clear which of the observed minima have to be identified as the relevant solitons the density profile is discarded and no positions are recorded. Afterwards, the distance between the two solitons at each time step is determined and averaged over all distances recorded for this time step. This leads to a plot of the distance between the two solitons versus time. The plot is then fitted by the function  $2z_0|\sin(2\pi\nu_{DS}t + \phi)|$ . Figure 5.1 shows two of the oscillation plots that were obtained from the absorption images together with the corresponding fitting functions.

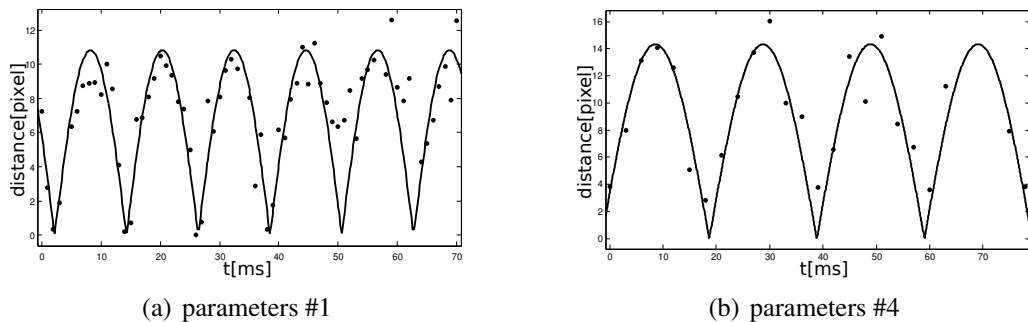


Figure 5.1: The experimentally determined time evolution of the soliton distance (dots) and the corresponding fits to the data (full lines) for two different parameter sets (see table 5.1)

## 5 Oscillation Frequencies and Interaction

#	$v_z$ [Hz]	$v_\perp$ [Hz]	$N$	$v_{DS}$	$z_{\max}$ [ $\mu\text{m}$ ]
1	$53.85 \pm 0.27$	$890 \pm 89$	$1372 \pm 93$	$41.32 \pm 0.26$	$3.12 \pm 0.20$
2	$53.0 \pm 0.25$	$890 \pm 89$	$1708 \pm 81$	$40.32 \pm 0.20$	$3.23 \pm 0.15$
3	$25.7 \pm 0.17$	$407.5 \pm 40.8$	$2079 \pm 106$	$19.67 \pm 0.13$	$5.06 \pm 0.25$
4	$32.9 \pm 0.7$	$407.5 \pm 40.8$	$1763 \pm 116$	$24.77 \pm 0.26$	$4.13 \pm 0.34$
5	$37.0 \pm 0.85$	$407.5 \pm 40.8$	$1603 \pm 132$	$29.49 \pm 0.34$	$3.27 \pm 0.29$
6	$37.0 \pm 0.85$	$407.5 \pm 40.8$	$1438 \pm 132$	$29.55 \pm 0.19$	$3.07 \pm 0.18$
7	$38.9 \pm 0.19$	$407.5 \pm 40.8$	$1536 \pm 126$	$30.25 \pm 0.24$	$3.51 \pm 0.15$
8	$54.0 \pm 0.82$	$407.5 \pm 40.8$	$1375 \pm 124$	$42.37 \pm 0.35$	$2.67 \pm 0.17$
9	$57.65 \pm 0.29$	$407.5 \pm 40.8$	$863 \pm 134$	$47.56 \pm 0.29$	$2.30 \pm 0.12$
10	$57.65 \pm 0.29$	$407.5 \pm 40.8$	$945 \pm 120$	$46.70 \pm 0.28$	$2.44 \pm 0.14$
11	$57.97 \pm 0.31$	$407.5 \pm 40.8$	$1055 \pm 105$	$46.35 \pm 0.6$	$2.07 \pm 0.23$
12	$57.0 \pm 0.3$	$407.5 \pm 40.8$	$870 \pm 120$	$48.12 \pm 0.48$	$2.22 \pm 0.20$

Table 5.1: The experimental parameters and the observed soliton oscillation frequencies

The fits allow to determine the two relevant variables for the oscillation of dark solitons, namely the oscillation amplitude  $z_0$  and the oscillation frequency  $v_{DS}$ .

As mentioned in chapter 3.3.3, the oscillation amplitude of the solitons is taken to be half of their maximum distance, in order to be able to compare them to the oscillation frequencies of single dark solitons.

In table 5.1, the recorded soliton oscillation frequencies  $v_{DS}$  and amplitudes  $z_{\max}$  are listed together with the corresponding experimental parameters. This is the main experimental result of this thesis.

The healing length  $\xi$  is the natural length scale of a Bose-Einstein condensate and also the relevant parameter for the extension of a soliton and the length scale for the interaction between them. To plot all the experimentally determined oscillation frequencies for different experimental parameters consistently and compare their amplitude dependence, the healing lengths for all experimental situations have been obtained from simulations using the three-dimensional Gross-Pitaevskii equation and are given in table 5.2 together with the oscillation amplitudes scaled in units of  $\xi$ . This allows for plotting the experimental oscillation frequencies depending on their oscillation amplitudes measured in  $\xi$  which is shown in figure 5.2.

The predictions for the oscillation frequencies, which can be determined by numerical time evolutions of the non-polynomial Schrödinger equation for the given experimental situations and observed oscillation amplitudes, are also shown in the graph. The agreement between the numerical predictions and the experimental results is good, all predictions fall within the experimental error margins of the observed frequencies.

Two things can be observed immediately. All oscillation frequencies are higher than the asymptotic prediction of  $1/\sqrt{2}$  and they show a clear amplitude dependence, being higher for smaller oscillation amplitudes. Both observations are expected because of the interaction of the two solitons with each other as discussed in chapter 3.3.3 and the influence of the dimensionality of the system as discussed in chapter 3.3.2.

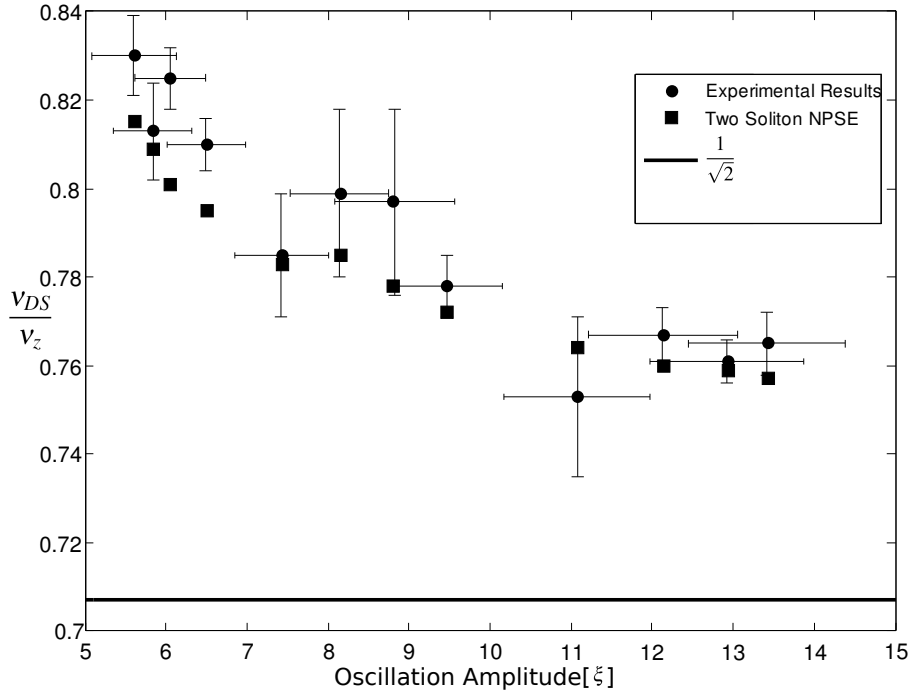


Figure 5.2: The experimentally observed Oscillation frequencies (dots with error bars), the corresponding oscillation frequencies obtained from the NPSE (squares) and the asymptotic prediction  $1/\sqrt{2}$  (full line)

## 5.2 Effects on the Oscillation Frequencies

To analyze the effects that influence the two soliton oscillation frequencies and extract the different contributions to the deviations from the one-dimensional Thomas-Fermi prediction of  $v_{DS} = v_z/\sqrt{2}$ , it is necessary to calculate some further quantities from the experimental results.

The first column of table 5.2 lists the oscillation frequencies of the solitons  $v_{DS}$  scaled to the respective longitudinal trapping frequencies. The second column lists the healing length  $\xi$  of the condensates determined from the ground states of numerical simulations using the three-dimensional Gross-Pitaevskii equation and the third column the oscillation amplitudes scaled in the respective healing lengths.

The fourth column of table 5.2 lists the different aspect ratios  $\Omega = v_z/v_{\perp}$  of the confining trap. As seen in figure 3.7(b), these aspect ratios influence the oscillation frequencies of the oscillating solitons.

As mentioned in section 3.1.2, one of the criteria for the applicability of the one-dimensional Gross-Pitaevskii equation is

$$N\Omega \frac{a_s}{a_{\perp}} \ll 1. \quad (5.1)$$

In the fifth column, the determined values for this quantity are given. They range from 1.21 to 1.81, which is close to one and can be considered a dimensionality crossover

## 5 Oscillation Frequencies and Interaction

#	$\frac{v_{DS}}{v_z}$	$\xi [\mu\text{m}]$	$z_{\text{max}} [\xi]$	$\Omega$	$N\Omega \frac{a_s}{a_{\perp}}$	$v_{1S} [\text{Hz}]$
1	$0.767 \pm 0.006$	0.2568	$12.15 \pm 0.78$	$0.061 \pm 0.006$	$1.22 \pm 0.15$	39.68
2	$0.761 \pm 0.005$	0.2496	$12.94 \pm 0.60$	$0.060 \pm 0.006$	$1.50 \pm 0.15$	39.03
3	$0.765 \pm 0.007$	0.3768	$13.43 \pm 0.66$	$0.063 \pm 0.006$	$1.30 \pm 0.15$	18.91
4	$0.753 \pm 0.018$	0.3724	$11.09 \pm 0.91$	$0.081 \pm 0.008$	$1.42 \pm 0.17$	24.32
5	$0.797 \pm 0.021$	0.3712	$8.81 \pm 0.78$	$0.091 \pm 0.009$	$1.45 \pm 0.19$	27.57
6	$0.799 \pm 0.019$	0.3769	$8.15 \pm 0.48$	$0.091 \pm 0.009$	$1.30 \pm 0.16$	27.63
7	$0.778 \pm 0.007$	0.3708	$9.47 \pm 0.40$	$0.096 \pm 0.010$	$1.46 \pm 0.19$	28.91
8	$0.785 \pm 0.014$	0.3590	$7.44 \pm 0.47$	$0.133 \pm 0.0146$	$1.81 \pm 0.25$	40.49
9	$0.825 \pm 0.007$	0.3802	$6.05 \pm 0.32$	$0.142 \pm 0.014$	$1.21 \pm 0.22$	43.95
10	$0.810 \pm 0.006$	0.3754	$6.50 \pm 0.37$	$0.142 \pm 0.014$	$1.33 \pm 0.22$	43.78
11	$0.830 \pm 0.009$	0.3693	$5.61 \pm 0.62$	$0.142 \pm 0.014$	$1.49 \pm 0.21$	44.03
12	$0.813 \pm 0.011$	0.3804	$5.84 \pm 0.53$	$0.140 \pm 0.014$	$1.21 \pm 0.21$	43.33

Table 5.2: additional quantities determined from the experimental parameters and results

regime, but already points out that deviations of the oscillation frequencies from  $v_z/\sqrt{2}$  have to be expected even for a single soliton oscillating in the trap.

The sixth column lists the oscillation frequencies of single dark solitons oscillating in condensates with the respective experimental parameters and the given amplitudes. These values have been determined in numerical time evolutions of the non-polynomial Schrödinger equation.

To show the effect the dimensionality of the system has on the oscillation frequency, figure 5.3(a) shows the experimentally observed oscillation frequencies together with the oscillation frequencies for single solitons oscillating under the corresponding experimental parameters.

It can be seen, that the experimentally observed oscillation frequencies differ significantly from the numerically determined single soliton oscillation frequencies and that the deviations are larger for smaller amplitudes of the oscillation. It can also be seen, that the single soliton frequencies themselves show an apparently strong amplitude dependence.

To see that this is not only an amplitude dependence, it is instructive to take a look at the behavior of the single soliton frequencies for their whole amplitude range. This is shown in figure 5.3(b). The single soliton frequency curves are grouped together by the aspect ratios of the harmonic trap  $\Omega = v_z/v_{\perp}$  and it can be seen that they show an amplitude dependence as well as a dependence on the aspect ratio. Additional deviations between the curves with different aspect ratios could be explained by taking also into account how close the different experimental situations are to the Thomas-Fermi approximation, as noted in chapter 3.3.2, but to systematically investigate all deviations for the single soliton frequencies is beyond the scope of this thesis.

Suffice it to note that the single soliton frequencies show a dependence on the oscillation amplitude as well as a dependence on the dimensionality of the system, both of which will be taken into account in the course of investigating the interactions between dark solitons in the following.

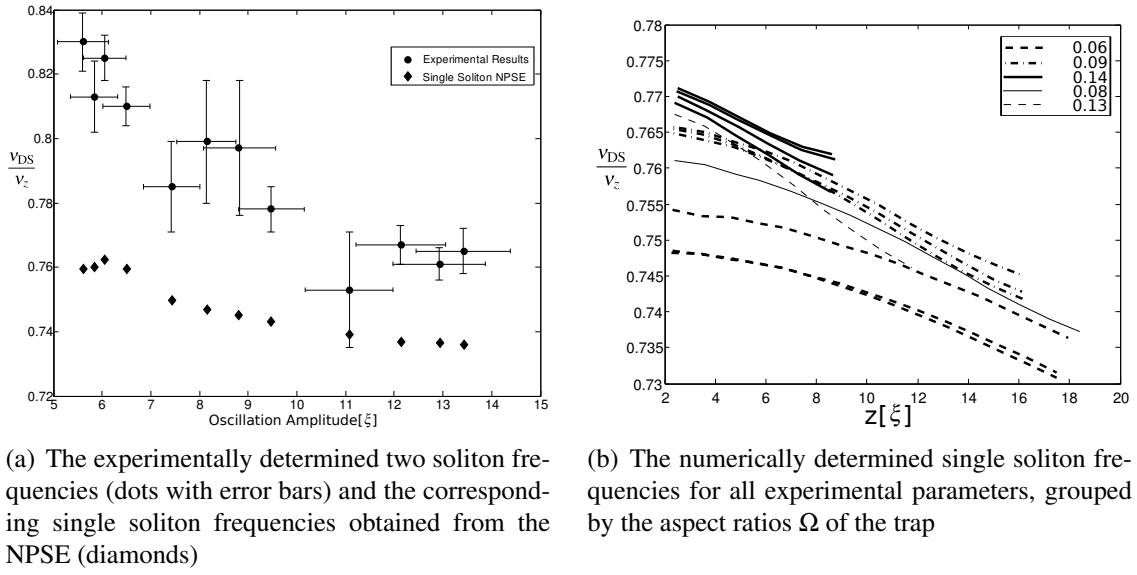


Figure 5.3: Comparison between the experimental results and the numerically determined single soliton oscillation frequencies

As mentioned in chapter 4.2, the dynamics of three solitons, of which one is stationary in the center of the trap and the other two oscillate to the left and right of it, has also been recorded. The oscillation frequency of the three oscillating solitons is determined as described in section 4.2. The oscillation frequency of the two outer solitons has been determined in the same way as for the two soliton cases and is  $\nu_{3S} = (28.0 \pm 0.2)$  Hz with a trap frequency of  $\nu_z = (36.1 \pm 0.1)$  Hz and  $\nu_{\perp} = 407.5$  Hz and a mean atom number of  $N = 1170 \pm 110$ . The amplitude of the oscillation scaled in the healing length  $\xi = 0.389 \mu\text{m}$  of the condensate is 20.59. This amplitude is very large compared to the ones of the two soliton oscillations. It can not be expected that the interaction will significantly alter the dynamics in this case and it also proves to be difficult to obtain the corresponding single soliton frequency, due to a problem with the initialization of the single soliton wave function for such high amplitudes. Additionally, the cloud experienced a large quadrupole oscillation, which affects the dynamics of the solitons since the cloud experiences a density modulation. Thus, the interaction effect can not be determined for the recorded case and in the following only the two soliton cases are investigated.

As detailed in chapter 3.3.3, to clearly separate the effects the dimensionality has on the oscillation frequencies from those stemming from the interactions of the solitons the effective potential (see section 3.3.3) can be used, since it incorporates the single soliton frequencies directly as an effective harmonic potential. Thus, using the effective potential to determine the oscillation frequencies of two solitons returns the effect of the interaction directly, as the difference between the calculated two soliton frequency and the numerically determined single soliton frequency.

Figure 5.4 shows the experimentally observed frequencies and the frequencies determined using the effective potential together with the single soliton frequencies from the numerical time evolution of the non-polynomial Schrödinger equation, which were used

## 5 Oscillation Frequencies and Interaction

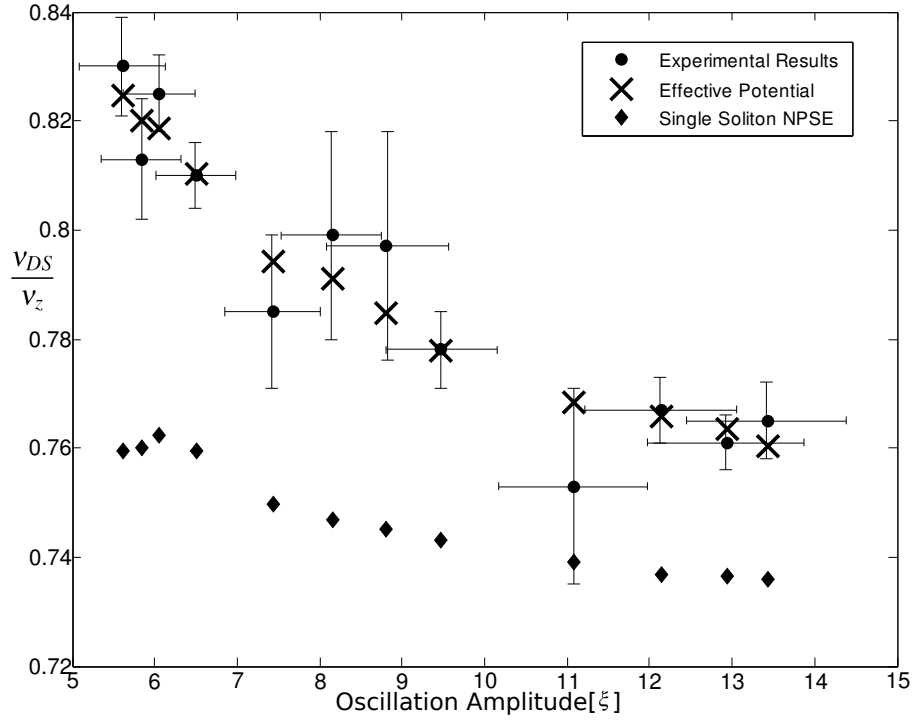


Figure 5.4: The experimentally observed oscillation frequencies (dots with error bars), the corresponding oscillation frequencies obtained from the effective interaction potential (crosses) and the corresponding single soliton frequencies from the numerical time evolution of the NPSE. The effect of the interaction can be observed as the difference between the experimentally observed two soliton frequencies and the single soliton frequencies.

as the frequencies of the effective harmonic potential.

To ensure the validity of the effective potential, the velocity of the solitons upon collision with each other is required to be smaller than 0.5, scaled in units of the Bogoliubov speed of sound. The maximum velocities the solitons reach during their time evolutions obtained from the equations of motion for the effective potential for the points in figure 5.4 range between 0.26 and 0.33, which is well in the regime of applicability of the effective potential, as discussed in chapter 2.3.3.

The frequencies given by the effective potential show a very good agreement with the experimentally observed frequencies. This graph shows that by measuring the oscillation frequencies of two oscillating solitons for different amplitudes, the interaction between the two solitons manifests itself as the difference between the single soliton frequencies and the experimental results for two solitons. The experimental results are in quantitative agreement with the predictions of the effective interaction potential and thus the interaction between two dark solitons oscillating in a Bose-Einstein condensate is experimentally observed and in quantitative agreement with the theoretical predictions.

## 6 Conclusion and Outlook

To summarize the results: Oscillating dark solitons are created using a method relying on the nonlinear interference of two Bose-Einstein condensate clouds initially prepared in a double well potential. These dark solitons are observed as they move through the condensate cloud and are shown to be stable on timescales longer than several hundreds of milliseconds. Their movement in the harmonically confined condensate is oscillatory and they are observed to be stable after colliding with each other several times. The oscillation frequencies of two solitons are investigated for different oscillation amplitudes and dimensionality regimes. Using an effective potential to model the effects of the interaction and of the effective harmonic potential created by the trapped Bose-Einstein condensate, the amplitude dependence of the soliton oscillation frequencies on the oscillation amplitude can be separated into two parts, one stemming from the dimensionality of the system and one stemming from the interactions between the solitons. This way, the contributions of the interaction between the two solitons can be extracted from the experimentally observed oscillation frequencies and are in quantitative agreement with the predictions given by the effective potential.

The effects of interaction are expected to be even stronger for three oscillating solitons. The possibility of creating three oscillating solitons is investigated and one frequency measurement for this case is conducted. The oscillation amplitude of the solitons in this measurement is too high to observe significant frequency deviations from the corresponding single soliton frequencies. In future experiments, the creation of three solitons will be repeated with a special attention to the creation of small amplitude oscillations to further investigate the stronger effects the interaction has on the soliton oscillation frequencies in this situation. To this end, the effective interaction potential for the dark solitons is generalized to asymmetric collisions of more than two solitons which allows for the unambiguous identification of these interaction effects.

The created solitons were found to exist for more than 1 second in our experiments. The position stability of the solitons between different realizations at the same point in the evolution time dephases on a scale on the order of hundreds of milliseconds. Generally, dark solitons can be observed for a much longer time in single images of the condensate. So far, no quantitative results on the decay of dark solitons have been obtained. The solitons are expected to decay due to a thermodynamic instability (see chapter 3.2.2). This instability causes an increase of the soliton velocities over time which leads to an increased oscillation amplitude. The change of oscillation amplitude can be used to quantitatively investigate this thermodynamic instability in future experiments.



# **A Published Paper: Experimental Observation of Oscillating and Interacting Matter Wave Dark Solitons**

Published in *Physical Review Letters* 101(13), 130401 (09/2009) [66]



# Experimental observation of oscillating and interacting matter wave dark solitons

A. Weller, J.P. Ronzheimer, C. Gross, J. Esteve, and M.K. Oberthaler  
*Kirchhoff Institute for Physics, University of Heidelberg, INF 227, 69120 Heidelberg, Germany*

D.J. Frantzeskakis  
*Department of Physics, University of Athens, Panepistimiopolis, Zografos, Athens 157 84, Greece*

G. Theocharis and P.G. Kevrekidis  
*Department of Mathematics and Statistics, University of Massachusetts, Amherst MA 01003-4515, USA*  
(Dated: August 28, 2008)

We report on the generation, subsequent oscillation and interaction of a pair of matter wave dark solitons. These are created by releasing a Bose-Einstein condensate from a double well potential into a harmonic trap in the crossover regime between one dimension (1D) and three dimensions (3D). Multiple oscillations and collisions of the solitons are observed, in quantitative agreement with simulations of the Gross-Pitaevskii equation. An effective particle picture is developed and confirms that the deviation of the observed oscillation frequencies from the asymptotic prediction  $\nu_z/\sqrt{2}$ , where  $\nu_z$  is the longitudinal trapping frequency, results from the dimensionality of the system and the soliton interactions.

Solitons are one of the most prominent features of nonlinear dynamics emerging in diverse fields extending from hydrodynamics to solid state physics and from nonlinear optics to biophysics. Dark solitons are the fundamental excitations of the defocusing nonlinear Schrödinger equation [1], and have the form of a localized “dip” on a background wave, accompanied by a phase jump [2]. These localized waveforms have been demonstrated experimentally in different contexts, including liquids [3], discrete mechanical systems [4], thin magnetic films [5], optical media [6–8], and, more recently, Bose-Einstein condensates (BECs) [9–15]. The possibility of creating pairs of dark solitons [7] has stimulated considerable interest in the repulsive [16] short-range interactions between them [17, 18]. The resulting collisions, during which the solitons approach within a distance comparable to their width, have a universal character and thus, e.g., optical solitons interact essentially the same way as matter-wave solitons.

In this letter we report on the systematic generation of a pair of matter wave dark solitons which is subsequently oscillating and colliding in a harmonic trap. Our experiment is performed in the crossover regime between 1D and 3D [19], where dark solitons exist and are robust [20]. This allows us to monitor multiple oscillations and collisions of dark solitons, permitting the precise measurement of their oscillation frequency and their mutual repulsive interactions. Previous experiments have been performed in a genuine 3D regime where dark solitons are unstable due to the so-called snaking instability and eventually decay into vortex rings [11, 20]. In these experiments solely their translation in the trap has been shown [9–11]. Only very recently dark solitons have been reported to undergo a single oscillation period in a harmonic trap [15].

Different methods have been explored to create dark

solitons in Bose-Einstein condensates [9–15]. In our experiment, the solitons are generated by merging two coherent condensates initially prepared in a double well potential. This formation process can be regarded as a consequence of matter wave interference of the two condensates [21–24]. The further evolution of the created solitons in the trap is shown in Fig. 1a. Our procedure is very similar to the recently reported generation of vortices out of a triple well potential [25].

Since the two dominant solitons are created with a distance of a few healing lengths  $\xi$  ( $\xi$  is on the order of 250 nm to 400 nm), which defines the range of the repulsive soliton interaction, the collisions between them lead to a significant modification of the oscillation frequency. The measured frequencies deviate up to 16% from the single soliton asymptotic Thomas-Fermi 1D (TF1D) prediction of  $\nu_z/\sqrt{2}$  [26] where  $\nu_z$  is the longitudinal trapping frequency. Our experimental results are in quantitative agreement with numerical simulations of the Gross-Pitaevskii equation (GPE). They reveal that dark solitons can behave very similar to particles. This is confirmed by explaining the essential features of the dynamics within a simple physical picture regarding the dark solitons as particles in an effective potential due to the external trap and their mutually repulsive interactions. Being in the crossover regime, the role of the transverse degrees of freedom has to be included in the effective potential [27].

Before elaborating on the theoretical models and systematic studies we will briefly describe the details of the experimental setup. We prepare a BEC of  $^{87}\text{Rb}$  in the  $|F=2, m_F=2\rangle$  state containing about  $N = 1500$  atoms in a double well potential. This potential is realized by superimposing a far detuned crossed optical dipole trap ( $\lambda = 1064$  nm) and a one dimensional optical lattice ( $\lambda = 843$  nm). The first beam of the dipole trap has

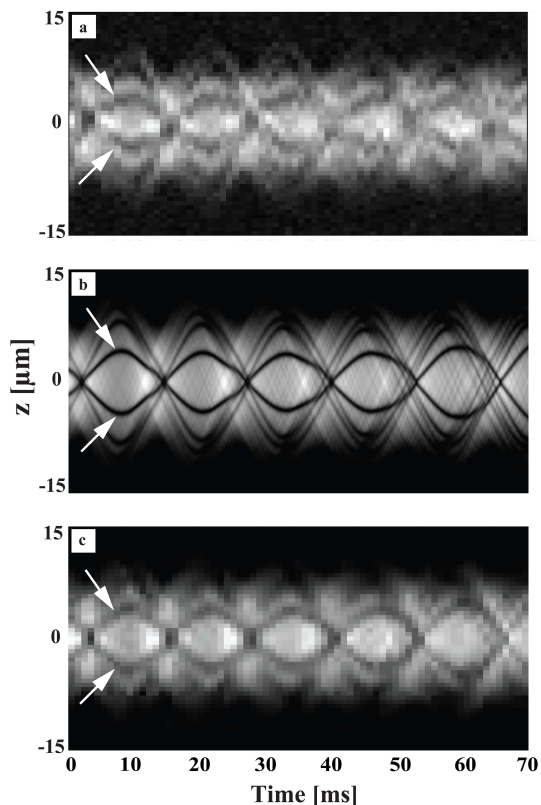


FIG. 1: Observation of the time evolution of dark solitons in a harmonic trap. The dominant soliton pair is indicated by arrows. a) Experimental observation of the dynamics of the longitudinal atomic density. Each longitudinal density profile (vertical lines), corresponding to a given evolution time, is deduced from typically 10 experimental realizations. The obtained absorption images of the condensate at each time step are averaged and integrated over their transverse direction. The number of atoms in the shown case is  $N = 1700$  and the trapping frequencies are  $(\nu_z, \nu_\perp) = (53 \text{ Hz}, 890 \text{ Hz})$ . b) Result of the numerical integration of the 3D GPE taking into account the full preparation process of the solitons. c) Same as b), taking into account the finite spatial ( $1 \mu\text{m}$ ) as well as temporal resolution ( $1 \text{ ms}$ ) of the experiment. The loss of contrast due to the convolution process explains the experimentally observed fading out of the solitons with time.

a gaussian waist of  $5 \mu\text{m}$  and results in a strong transverse and weak longitudinal confinement. The second beam orthogonally crosses the first one and has an elliptic shape ( $60 \mu\text{m} \times 230 \mu\text{m}$  waist) leading to an extra adjustable confinement only in the longitudinal direction of the trap. We start our experiments with a transverse frequency of the total harmonic trap of  $\nu_\perp = 408 \text{ Hz}$  and a longitudinal one of  $\nu_z = 63 \text{ Hz}$ . The barrier height of the optical lattice is chosen to be approximately  $1 \text{ kHz}$  and the lattice spacing is  $5.7 \mu\text{m}$ . This results in a double well potential with a well distance of  $5.4 \mu\text{m}$ .

In order to start with a well defined phase between the two condensates, the barrier height is chosen to be low enough such that thermal phase fluctuations are negligi-

ble for the measured temperature of  $T \approx 10 \text{ nK}$  [28] (the critical temperature for condensation is  $T_c \approx 110 \text{ nK}$ ) and high enough so that high contrast solitons are formed. The solitons are created by switching off the optical lattice and merging the two condensates in the remaining harmonic potential. After the switching off, the trap frequencies are ramped to the parameters of interest  $(\nu_z, \nu_\perp)$ . The distance between the formed solitons is adjusted by choosing different sets of final frequencies and different atom numbers. For each parameter set, the ramping time is empirically optimized to minimize the excitation of the quadrupole mode (e.g. from  $(\nu_z, \nu_\perp) = (63 \text{ Hz}, 408 \text{ Hz})$  to  $(53 \text{ Hz}, 890 \text{ Hz})$  within  $10 \text{ ms}$  for  $N = 1700$  atoms, or to  $(58 \text{ Hz}, 408 \text{ Hz})$  within  $3 \text{ ms}$  for  $N = 950$ ). The atomic density after a certain evolution time in the harmonic trap is obtained using standard absorption imaging with an optical resolution of approximately  $1 \mu\text{m}$ . We use a short time of flight between  $0.6$  and  $0.9 \text{ ms}$  to enhance the contrast.

In our experiment, the initial distance  $D = 5.4 \mu\text{m}$  between the two colliding condensates is well within the regime where the interaction energy exceeds the kinetic energy and thus the formation of dark solitons is expected due to nonlinear interference. This regime is reached if  $D$  is smaller than the critical distance  $D_c = \pi(6 \frac{N\hbar a_s}{\nu_z m})^{1/3} = 25.8 \mu\text{m}$  with  $a_s$  being the s-wave scattering length,  $\nu_z$  the longitudinal trap frequency and  $m$  the atomic mass [22]. The formation of dark solitons for our experimental parameters is confirmed by 3D GPE simulations as shown in Fig. 1. Including the optical and time resolution, the experimentally observed density profile evolution is well reproduced. A dominant pair of solitons oscillates close to the center of the cloud and we can also distinguish additional pairs of solitons with much lower contrast. In the following, we focus on the dynamics of the dominant central pair and show that its oscillation frequency is well described within a two soliton approximation.

We experimentally investigate the oscillation frequency of the dominant soliton pair for different trap parameters and different inter-soliton distances. A typical data set consists of 50 time steps and 10 pictures per time step. The numerical simulations predict, that the solitons do not cross each other at the collision points (see inset of Fig. 3c), but our finite resolution does not allow us to distinguish whether this is actually the case in the experiment. In order to extract the oscillation frequency of the solitons, we fit the time evolution of the inter-soliton distance as shown in the inset of Fig. 2. The obtained frequency is divided by two in order to compare it to the oscillation frequency expected for a single trapped soliton. The shot to shot reproducibility of the soliton dynamics up to  $100 \text{ ms}$  allows the observation of up to 7 oscillation periods. The typical statistical experimental error in the frequency measurement is  $\pm 1.5\%$ . Fig. 2 shows the results of our frequency measurements and their comparison with numerical simulations for the

motion of two trapped solitons using the Nonpolynomial Schrödinger equation (NPSE) [29], which is an excellent approximation to the 3D GPE in the dimensionality crossover regime [27].

In order to capture the essentials of the dynamics of the experimentally realized soliton pairs in the simulations, we initialize the condensate with two solitons such that the rms amplitude of their oscillating motion matches the one observed experimentally. The good agreement between numerics and experiments shows that the dynamics produced by our experimental method is well described within a two soliton approximation even though extra solitons are produced. From our experiment and the NPSE simulations, we observe an upshift up to 16% from the  $\nu_z/\sqrt{2}$  prediction which was the first value theoretically derived for the oscillation frequency of a single trapped soliton [26]. It is expected to be valid in a 1D trap in the asymptotic Thomas-Fermi limit ( $N\Omega a_s/a_\perp \ll 1$  and  $((N/\sqrt{\Omega})a_s/a_\perp)^{1/3} \gg 1$ ) [19], where  $\Omega = \nu_z/\nu_\perp \ll 1$  is the aspect ratio of the trap and  $a_\perp$  the transverse harmonic oscillator length. Our experimental parameter range is:  $\Omega \approx 0.06-0.14$ ,  $N\Omega a_s/a_\perp \approx 1.2-1.8$  and  $((N/\sqrt{\Omega})a_s/a_\perp)^{1/3} \approx 2.8-4.4$ , which sets us out of the validity domain of the  $\nu_z/\sqrt{2}$  prediction.

We now give a theoretical description of the different effects leading to the observed upshift. We consider the two solitons as particles moving in an effective potential which arises from the combination of a harmonic potential due to the trap [26] (see Fig. 3a) and a repulsive potential due to the interaction between the solitons [30]. Because of the spatially symmetric preparation, the effective potential is a symmetric double well potential which is depicted in Fig. 3b. This potential can be expressed as a function of the distance  $z$  of each of the solitons from the trap center and its time derivative  $\dot{z}$ :

$$V(z, \dot{z}) = (2\pi\nu_{1s})^2 \frac{z^2}{2} + \frac{\mu B^2}{2m \cosh^2(2Bz/\xi)} \quad (1)$$

where  $B = \sqrt{1 - (\dot{z}/\xi)^2}(\hbar/\mu)^2$  denotes the darkness of the solitons,  $\mu$  is a typical interaction energy on the order of the chemical potential,  $\xi = \sqrt{\hbar/(m\mu)}$  the associated healing length and  $\nu_{1s}$  the oscillation frequency of a single trapped soliton. The frequency of the motion is obtained by solving the Euler-Lagrange equation associated with the Lagrangian  $\mathcal{L}(z, \dot{z}) = \dot{z}^2/2 - V(z, \dot{z})$ . To obtain quantitative agreement, the model has to take into account correctly both the free propagation of the solitons in the trap when they are far away from each other ( $z \gg \xi$ ) and the repulsive interaction when they approach.

Good estimates for the single soliton frequency  $\nu_{1s}$  are obtained by numerical integration of the NPSE describing a single soliton. Because our experimental parameters are both in the crossover regime and slightly out of the Thomas-Fermi limit, corrections to the asymptotic value  $\nu_z/\sqrt{2}$  are expected. Therefore the oscillation frequency

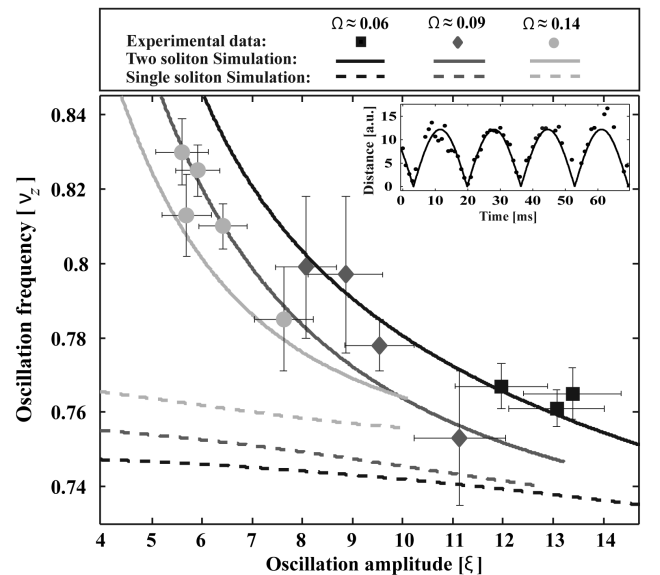


FIG. 2: Comparison between experimentally obtained soliton oscillation frequencies and NPSE simulation for one and two solitons. Each frequency point is deduced from the temporal evolution of the soliton distance as shown in the inset. Different symbols correspond to different aspect ratios  $\Omega$  of the trap. For each aspect ratio the oscillation amplitude is varied as explained in the text. NPSE simulations are represented by solid lines for the two soliton case, and by dashed lines for the respective single soliton oscillations. The error bars on the measured frequencies account for statistical errors on the measured soliton and trap frequencies and systematic errors on the atom number used to calculate the healing length.

of a single dark soliton is upshifted by a few percent from the asymptotic value as discussed in detail using the Bogoliubov-de Gennes analysis of the NPSE in [27] (see Fig. 3a). The simulation results for the three different parameter sets used in the experiment are shown in Fig. 2. This upshift for the single soliton case can be decomposed into two contributions. For example, considering one specific parameter set with  $\Omega \approx 0.06$ , the upshift is 5% (see Fig. 3c). Predictions using the 1D GPE already give a value approximately 2% higher than the asymptotic limit because the Thomas-Fermi limit is not reached [31]. The effect of dimensionality, *i.e.* the role of the transverse degrees of freedom which is captured only by the NPSE or the 3D GPE, accounts for the remaining 3%. Fig. 3c shows the comparison between the  $\nu_z/\sqrt{2}$  prediction and the single soliton NPSE simulation for the considered parameter set.

As also shown in Fig. 3c, the repulsive interaction between the solitons results in an additional upshift of the oscillation frequency compared to the single soliton case that strongly depends on the oscillation amplitude. Our effective particle model accurately reproduces the upshift if the interaction parameter  $\mu$  is set to be the chemical potential of the condensate obtained from the 3D GPE

equation. In our experimentally accessible parameter range, the agreement of the model with NPSE simulations is better than 5%. This allows us to clearly identify the significant role of the repulsive interactions and shows that the effective repulsive potential in Eqn. (1) obtained in the 1D homogeneous case is a good approximation to our complex situation.

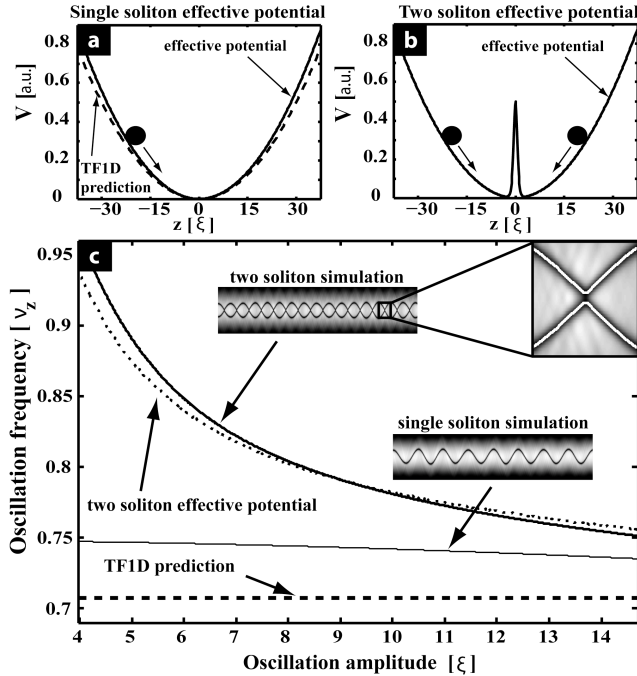


FIG. 3: The oscillation dynamics of dark solitons in a trapped BEC is well captured in an effective particle picture. a) For one soliton, the particle moves in a harmonic trap. b) For two solitons, an additional barrier due to the repulsive interaction appears. c) For the one and two soliton case, the dependence of the oscillation frequencies on the oscillation amplitude from the trap center is shown for one experimental parameter set with  $\Omega = 0.06$ . The dashed line shows the TF1D prediction ( $\nu_z/\sqrt{2}$ ). The thin solid line indicates the upshift of the single soliton frequency mainly due to dimensionality. For the case of two solitons, the thick solid line also includes the upshift due to the inter-soliton interaction deduced from the NPSE. The dotted line represents the result of the simple effective particle model from Eqn. (1). Density profile evolutions obtained from the NPSE are shown in the insets. A collision between the two solitons is also shown in detail, demonstrating that they do not cross each other. The white lines correspond to the trajectories of the density minima.

In conclusion we controllably create pairs of dark solitons by colliding two atomic clouds released from a double well potential in a harmonic trap. The full dynamics of multiple dark soliton oscillations and collisions is observed, allowing for precise frequency measurements and showing that dark solitons are still stable after several collisions. The experimentally observed total upshifts from the TF1D frequency prediction are up to 16%. A simple effective particle picture confirms that the oscil-

lation frequency of two solitons in a harmonic trap is affected by two effects namely the single soliton frequency upshift and the inter-soliton interaction. The presented robust method for preparing solitonic excitations will be a starting point for further studies towards multi-soliton interactions and perhaps even dark soliton gases.

We thank P. Schmelcher for useful discussions as well as B. Hemmerling, R. Gati and T. Ottenstein. We acknowledge support from NSF, DFG and AHF. J.E. acknowledges support from the EC MC-EIF program.

- 
- [1] V. E. Zakharov and A. B. Shabat, *Sov. Phys. JETP* **37**, 823 (1973).
  - [2] Y. S. Kivshar and B. Luther-Davies, *Phys. Rep.* **298**, 81 (1998).
  - [3] B. Denardo and S. Wright, W. and Putterman, *Phys. Rev. Lett.* **64**, 1518 (1990).
  - [4] B. Denardo et al., *Phys. Rev. Lett.* **68**, 1730 (1992).
  - [5] M. Chen et al., *Phys. Rev. Lett.* **70**, 1707 (1993).
  - [6] P. Emplit et al., *Opt. Comm.* **62**, 374 (1987).
  - [7] D. Krökel et al., *Phys. Rev. Lett.* **60**, 29 (1988).
  - [8] A. M. Weiner et al., *Phys. Rev. Lett.* **61**, 2445 (1988).
  - [9] S. Burger et al., *Phys. Rev. Lett.* **83**, 5198 (1999).
  - [10] J. Denschlag et al., *Science* **287**, 97 (2000).
  - [11] B. P. Anderson et al., *Phys. Rev. Lett.* **86**, 2926 (2001).
  - [12] Z. Dutton et al., *Science* **293**, 663 (2001).
  - [13] P. Engels and C. Atherton, *Phys. Rev. Lett.* **99**, 160405 (2007).
  - [14] G.-B. Jo et al., *Phys. Rev. Lett.* **98**, 180401 (2007).
  - [15] C. Becker et al., *Nature Physics* **4**, 496 (2008).
  - [16] K. J. Blow and N. J. Doran, *Phys. Lett. A* **107**, 55 (1985).
  - [17] D. Foursa and P. Emplit, *Phys. Rev. Lett.* **77**, 4011 (1996).
  - [18] A. Dreischuh et al., *Phys. Rev. Lett.* **96**, 043901 (2006).
  - [19] C. Menotti and S. Stringari, *Phys. Rev. A* **66**, 043610 (2002).
  - [20] A. E. Muryshev, H. B. van Linden van den Heuvell, and G. V. Shlyapnikov, *Phys. Rev. A* **60**, R2665 (1999).
  - [21] W. P. Reinhardt and C. W. Clark, *J. Phys. B At. Mol. Opt.* **30**, L785 (1997).
  - [22] T. F. Scott, R. J. Ballagh, and K. Burnett, *J. Phys. B At. Mol. Opt.* **31**, L329 (1998).
  - [23] C. Lee, E. A. Ostrovskaya, and Y. S. Kivshar, *J. Phys. B At. Mol. Opt.* **40**, 4235 (2007).
  - [24] Since the submission of the manuscript we learned about a related experiment: I. Shomroni et al., arXiv:0805.3263v1 (2008).
  - [25] D. R. Scherer et al., *Phys. Rev. Lett.* **98**, 110402 (2007).
  - [26] T. Busch and J. R. Anglin, *Phys. Rev. Lett.* **84**, 2298 (2000).
  - [27] G. Theocharis et al., *Phys. Rev. A* **76**, 045601 (2007).
  - [28] R. Gati et al., *Phys. Rev. Lett.* **96**, 130404 (2006).
  - [29] L. Salasnich, A. Parola, and L. Reatto, *Phys. Rev. A* **65**, 043614 (2002).
  - [30] Y. S. Kivshar and W. Królikowski, *Opt. Comm.* **114**, 353 (1995). This potential is valid provided that the solitons do not overlap.
  - [31] V. A. Brazhnyi and V. V. Konotop, *Phys. Rev. A* **68**, 043613 (2003).

# Bibliography

- [1] John Scott Russel. Report on waves. In *Forteenth meeting of the British Association for the Advancement of Science*, 1844.
- [2] D. J. Korteweg and Gustav de Vries. On the change of form of long waves advancing in a rectangular canal and on a new type of long stationary waves. *Philosophical Magazine*, 39:422–443, 1895.
- [3] Bruce Denardo, William Wright, Seth Putterman, and Andrés Larraza. Observation of a kink soliton on the surface of a liquid. *Phys. Rev. Lett.*, 64(13):1518–, March 1990.
- [4] Bruce Denardo, Brian Galvin, Alan Greenfield, Andrés Larraza, Seth Putterman, and William Wright. Observations of localized structures in nonlinear lattices: Domain walls and kinks. *Phys. Rev. Lett.*, 68(11):1730–, March 1992.
- [5] Ming Chen, Mincho A. Tsankov, Jon M. Nash, and Carl E. Patton. Microwave magnetic-envelope dark solitons in yttrium iron garnet thin films. *Phys. Rev. Lett.*, 70(11):1707–, March 1993.
- [6] T. Tsuzuki. Nonlinear waves in the pitaevskii-gross equation. *Journal of Low Temperature Physics*, 4:441–457, April 1971.
- [7] V. E. Zakharov and A. B. Shabat. Interaction between solitons in a stable medium. *Soviet Journal of Experimental and Theoretical Physics*, 37:823–828, November 1973.
- [8] P. Emplit, J. P. Hamaide, F. Reynaud, C. Froehly, and A. Barthelemy. Picosecond steps and dark pulses through nonlinear single mode fibers. *Optics Communications*, 62(6):374–379, June 1987.
- [9] D. Krökel, N. J. Halas, G. Giuliani, and D. Grischkowsky. Dark-pulse propagation in optical fibers. *Phys. Rev. Lett.*, 60(1):29–, January 1988.
- [10] A. M. Weiner, J. P. Heritage, R. J. Hawkins, R. N. Thurston, E. M. Kirschner, D. E. Leaird, and W. J. Tomlinson. Experimental observation of the fundamental dark soliton in optical fibers. *Phys. Rev. Lett.*, 61(21):2445–, November 1988.
- [11] K.J. Blow and N.J. Doran. Multiple dark soliton solutions of the nonlinear schroedinger equation. *Physics Letters A*, 107(2):55–58, January 1985.
- [12] Nail Akhmediev and Adrian Ankiewicz. First-order exact solutions of the nonlinear schrödinger equation in the normal-dispersion regime. *Phys. Rev. A*, 47(4):3213–, April 1993.
- [13] Dmitri Foursa and Philippe Emplit. Investigation of black-gray soliton interaction. *Phys. Rev. Lett.*, 77(19):4011–, November 1996.

## Bibliography

- [14] Alexander Dreischuh, Dragomir N. Neshev, Dan E. Petersen, Ole Bang, and Wieslaw Krolikowski. Observation of attraction between dark solitons. *Physical Review Letters*, 96(4):043901, 2006.
- [15] M. H. Anderson, J. R. Ensher, M. R. Matthews, C. E. Wieman, and E. A. Cornell. Observation of bose-einstein condensation in a dilute atomic vapor. *Science*, 269(5221):198–201, 1995.
- [16] K. B. Davis, M. O. Mewes, M. R. Andrews, N. J. van Druten, D. S. Durfee, D. M. Kurn, and W. Ketterle. Bose-einstein condensation in a gas of sodium atoms. *Phys. Rev. Lett.*, 75(22):3969–, November 1995.
- [17] C. C. Bradley, C. A. Sackett, J. J. Tollett, and R. G. Hulet. Evidence of bose-einstein condensation in an atomic gas with attractive interactions. *Phys. Rev. Lett.*, 75(9):1687–, August 1995.
- [18] S. Burger, K. Bongs, S. Dettmer, W. Ertmer, K. Sengstock, A. Sanpera, G. V. Shlyapnikov, and M. Lewenstein. Dark solitons in bose-einstein condensates. *Phys. Rev. Lett.*, 83(25):5198–, December 1999.
- [19] J. Denschlag, J. E. Simsarian, D. L. Feder, Charles W. Clark, L. A. Collins, J. Cubizolles, L. Deng, E. W. Hagley, K. Helmerson, W. P. Reinhardt, S. L. Rolston, B. I. Schneider, and W. D. Phillips. Generating solitons by phase engineering of a bose-einstein condensate. *Science*, 287(5450):97–101, January 2000.
- [20] B. P. Anderson, P. C. Haljan, C. A. Regal, D. L. Feder, L. A. Collins, C. W. Clark, and E. A. Cornell. Watching dark solitons decay into vortex rings in a bose-einstein condensate. *Phys. Rev. Lett.*, 86(14):2926–, April 2001.
- [21] Zachary Dutton, Michael Budde, Christopher Slowe, and Lene Vestergaard Hau. Observation of quantum shock waves created with ultra-compressed slow light pulses in a bose-einstein condensate. *Science*, 293(5530):663–668, July 2001.
- [22] E.A. Kuznetsov and S.K. Turitsyn. Instability and collapse of solitons in media with a defocusing nonlinearity. *Sov. Phys. JETP*, 67:1583–1588, 1988.
- [23] Christoph Becker, Simon Stellmer, Parvis Soltan-Panahi, Soren Dorscher, Mathis Baumert, Eva-Maria Richter, Jochen Kronjager, Kai Bongs, and Klaus Sengstock. Oscillations and interactions of dark and dark-bright solitons in bose-einstein condensates. *Nat Phys*, advanced online publication:–, May 2008.
- [24] Th. Busch and J. R. Anglin. Motion of dark solitons in trapped bose-einstein condensates. *Phys. Rev. Lett.*, 84(11):2298–, March 2000.
- [25] S. Stellmer, C. Becker, P. Soltan-Panahi, E.-M. Richter, S. Dorscher, M. Baumert, J. Kronjager, K. Bongs, and K. Sengstock. Collisions of dark solitons in elongated bose-einstein condensates. *Phys. Rev. Lett.*, 101(12):120406–4, September 2008.
- [26] A.C. Scott, F.Y.F. Chu, and D.W. McLaughlin. The soliton: A new concept in applied science. *Proceedings of the IEEE*, 61(10):1443– 1483, October 1973.
- [27] N. P. Proukakis, N. G. Parker, D. J. Frantzeskakis, and C. S. Adams. Analogies between dark solitons in atomic bose-einstein condensates and optical systems. *Journal of Optics B: Quantum and Semiclassical Optics*, 6(5):S380–S391, 2004.

- [28] V. E. Zakharov. Kinetic equation for solitons. *Soviet Journal of Experimental and Theoretical Physics*, 33(3):538–541, September 1971.
- [29] Yuri S. Kivshar and Wieslaw Królikowski. Lagrangian approach for dark solitons. *Optics Communications*, 114(3-4):353–362, February 1995.
- [30] P. G. Kevrekidis and G. Theocharis. private communication. University of Massachusetts, Amherst, MA, USA, 2008.
- [31] C. J. Pethick and H. Smith. *Bose-Einstein condensation in dilute gases*. Cambridge University Press, Cambridge, UK, 2002.
- [32] N. N. Bogoliubov. On the theory of superfluidity. *J. Phys. USSR*, 11(23), 1947.
- [33] L. P. Pitaevskii. Vortex lines in an imperfect bose gas. *Sov. Phys. JETP*, 13(2):451, 1961.
- [34] Eugene P. Gross. Structure of a quantized vortex in boson systems. *Nuovo Cimento*, 20(3):454–477, 1961.
- [35] L. D. Carr, Charles W. Clark, and W. P. Reinhardt. Stationary solutions of the one-dimensional nonlinear schrödinger equation. i. case of repulsive nonlinearity. *Phys. Rev. A*, 62(6):063610–, November 2000.
- [36] N. G. Parker, N. P. Proukakis, M. Leadbeater, and C. S. Adams. Soliton-sound interactions in quasi-one-dimensional bose-einstein condensates. *Phys. Rev. Lett.*, 90(22):220401–, June 2003.
- [37] S. Gupta, K. W. Murch, K. L. Moore, T. P. Purdy, and D. M. Stamper-Kurn. Bose-einstein condensation in a circular waveguide. *Physical Review Letters*, 95(14):143201, 2005.
- [38] Chiara Menotti and Sandro Stringari. Collective oscillations of a one-dimensional trapped bose-einstein gas. *Phys. Rev. A*, 66(4):043610–, October 2002.
- [39] V. Dunjko, V. Lorent, and M. Olshanii. Bosons in cigar-shaped traps: Thomas-fermi regime, tonks-girardeau regime, and in between. *Phys. Rev. Lett.*, 86(24):5413–, June 2001.
- [40] L. Salasnich, A. Parola, and L. Reatto. Effective wave equations for the dynamics of cigar-shaped and disk-shaped bose condensates. *Phys. Rev. A*, 65(4):043614–, April 2002.
- [41] G. Theocharis, P. G. Kevrekidis, M. K. Oberthaler, and D. J. Frantzeskakis. Dark matter-wave solitons in the dimensionality crossover. *Phys. Rev. A*, 76(4):045601–4, October 2007.
- [42] M.D Feit, J.A Fleck Jr., and A Steiger. Solution of the schrödinger equation by a spectral method. *Journal of Computational Physics*, 47(3):412–433, September 1982.
- [43] Juha Javanainen and Janne Ruostekoski. Symbolic calculation in development of algorithms: split-step methods for the gross-pitaevskii equation. *Journal of Physics A: Mathematical and General*, 39(12):L179–L184, 2006.

## Bibliography

- [44] D. L. Feder, M. S. Pindzola, L. A. Collins, B. I. Schneider, and C. W. Clark. Dark-soliton states of bose-einstein condensates in anisotropic traps. *Phys. Rev. A*, 62(5):053606–, October 2000.
- [45] Yuri S. Kivshar and Barry Luther-Davies. Dark optical solitons: physics and applications. *Physics Reports*, 298(2-3):81–197, May 1998.
- [46] A. E. Muryshev, H. B. van Linden van den Heuvell, and G. V. Shlyapnikov. Stability of standing matter waves in a trap. *Phys. Rev. A*, 60(4):R2665–, October 1999.
- [47] A. Muryshev, G. V. Shlyapnikov, W. Ertmer, K. Sengstock, and M. Lewenstein. Dynamics of dark solitons in elongated bose-einstein condensates. *Phys. Rev. Lett.*, 89(11):110401–, August 2002.
- [48] P. O. Fedichev, A. E. Muryshev, and G. V. Shlyapnikov. Dissipative dynamics of a kink state in a bose-condensed gas. *Phys. Rev. A*, 60(4):3220–, October 1999.
- [49] V. A. Brazhnyi and V. V. Konotop. Evolution of a dark soliton in a parabolic potential: Application to bose-einstein condensates. *Phys. Rev. A*, 68(4):043613–, October 2003.
- [50] V. A. Brazhnyi, V. V. Konotop, and L. P. Pitaevskii. Dark solitons as quasiparticles in trapped condensates. *Phys. Rev. A*, 73(5):053601–14, May 2006.
- [51] S. Burger, L. D. Carr, P. Öhberg, K. Sengstock, and A. Sanpera. Generation and interaction of solitons in bose-einstein condensates. *Phys. Rev. A*, 65(4):043611–, April 2002.
- [52] Dimitri J. Frantzeskakis Panayotis G. Kevrekidis and Ricardo Carretero-Gonzales, editors. *Emergent Nonlinear Phenomena in Bose-Einstein Condensates*. Springer-Verlag Berlin Heidelberg, 2008.
- [53] M. R. Andrews, C. G. Townsend, H.-J. Miesner, D. S. Durfee, D. M. Kurn, and W. Ketterle. Observation of interference between two bose condensates. *Science*, 275(5300):637–641, January 1997.
- [54] A. Röhrl, M. Naraschewski, A. Schenzle, and H. Wallis. Transition from phase locking to the interference of independent bose condensates: Theory versus experiment. *Phys. Rev. Lett.*, 78(22):4143–, June 1997.
- [55] William P. Reinhardt and Charles W. Clark. Soliton dynamics in the collisions of bose - einstein condensates: an analogue of the josephson effect. *Journal of Physics B: Atomic, Molecular and Optical Physics*, 30(22):L785–L789, 1997.
- [56] T. F. Scott, R. J. Ballagh, and K. Burnett. Formation of fundamental structures in bose - einstein condensates. *Journal of Physics B: Atomic, Molecular and Optical Physics*, 31(8):L329–L335, 1998.
- [57] Rudolf Gati, Borge Hemmerling, Jonas Fölling, Michael Albiez, and Markus K. Oberthaler. Noise thermometry with two weakly coupled bose-einstein condensates. *Phys. Rev. Lett.*, 96(13):130404–4, April 2006.
- [58] K. Dieckmann, R. J. C. Spreeuw, M. Weidemüller, and J. T. M. Walraven. Two-dimensional magneto-optical trap as a source of slow atoms. *Phys. Rev. A*, 58(5):3891–, November 1998.

- [59] E. L. Raab, M. Prentiss, Alex Cable, Steven Chu, and D. E. Pritchard. Trapping of neutral sodium atoms with radiation pressure. *Phys. Rev. Lett.*, 59(23):2631–, December 1987.
- [60] Wolfgang Petrich, Michael H. Anderson, Jason R. Ensher, and Eric A. Cornell. Stable, tightly confining magnetic trap for evaporative cooling of neutral atoms. *Phys. Rev. Lett.*, 74(17):3352–, April 1995.
- [61] Bernd Eiermann. *Kohärente nichtlineare Materiewellendynamik - Helle atomare Solitonen* -. PhD thesis, Faculty of Physics and Astronomy, University of Heidelberg, 2004.
- [62] J. Appmeier. Bose-einstein condensates in a double well potential: A route to quantum interferometry. Diploma thesis, Faculty of Physics and Astronomy, University of Heidelberg, 2007.
- [63] R. T. Gati. *Bose-Einstein Condensates in a Single Double-Well Potential*. PhD thesis, Faculty of Physics and Astronomy, University of Heidelberg, 2006.
- [64] T. B. Ottenstein. A new objective for high resolution imaging of bose-einstein condensates. Diploma thesis, Faculty of Physics and Astronomy, University of Heidelberg, 2006.
- [65] R. Gati, J. Esteve, B. Hemmerling, T. B. Ottenstein, J. Appmeier, A. Weller, and M. K. Oberthaler. A primary noise thermometer for ultracold bose gases. *New Journal of Physics*, 8(9):189–189, 2006.
- [66] A. Weller, J. P. Ronzheimer, C. Gross, J. Esteve, M. K. Oberthaler, D. J. Frantzeskakis, G. Theocharis, and P. G. Kevrekidis. Experimental observation of oscillating and interacting matter wave dark solitons. *Phys. Rev. Lett.*, 101(13):130401–4, September 2008.



## Acknowledgements

I would like to thank Prof. Dr. Markus K. Oberthaler for giving me the opportunity to work on this interesting experiment, for his ability to motivate people and the relaxed and productive environment he has created. Working on this diploma thesis has been a great experience.

I would also like to thank Prof. Dr. Peter Schmelcher for agreeing to conduct the second evaluation of this thesis.

This work would not exist in the present form without the huge contributions Andreas Weller made. We shared all the work on this, which makes it simply our project. Thank you for this great work and for the enjoyable and productive atmosphere in which we worked together.

I would like to thank Jérôme Estève and Christian Gross for all their help during my time here, be it at the experiment or regarding any other question, and Tilman Zibold and Eike Nicklas for the spirit of collaboration that made working at the BEC experiment the great experience it was. Also I would like to thank everybody who worked on this experiment in the past and helped making it as stable and reliable as it was when I joined the group.

It was a pleasure to work in the matterwaves group, owing to the air of cooperation and collegiality to which everyone contributes. Thank you all, this is how it should be.

I would like to thank Panos G. Kevrekidis and Georgios Theocharis for their contributions to this work from the theoretical side as well as for their help on any kind of questions and their shared interest and numerous suggestions concerning the dark solitons.

These years in Heidelberg would not have been the same without all the people that made my life here so much better. I would like to thank Alex, Richard, Diana, Michi, Simon, Line, Ninja, Claudio, Carlus and so many others for making Heidelberg what it was. We had a great time, and I hope to see you all again as often as possible.

Finally, I would like to thank my parents for all their support throughout these years. There are so many ways in which I would not be who and where I am today without you and I am most grateful for all that you've done for me. Thank you.



## Erklärung:

Ich versichere, dass ich diese Arbeit selbständig verfasst und keine anderen als die angegebenen Quellen und Hilfsmittel benutzt habe.

Heidelberg, den 14. November 2008

.....  
(Unterschrift)